Journal of Rock Mechanics and Geotechnical Engineering xxx (xxxx) xxx

Contents lists available at ScienceDirect

Journal of Rock Mechanics and Geotechnical Engineering

journal homepage: www.jrmge.cn

Review

Particle transport in fractured geo-energy reservoirs considering the effect of fluid inertia and turbulent flow: A review

E.A.A.V. Edirisinghe [a], M.S.A. Perera [a, *], D. Elsworth [b], S.K. Matthai [a], E. Goudeli [c]

[a] Department of Infrastructure Engineering, The University of Melbourne, Engineering Block B, Grattan Street, Parkville, Victoria, 3010, Australia
[b] Energy and Mineral Engineering, G3 Centre and EMS Energy Institute, Pennsylvania State University, University Park, PA, 16801, USA
[c] Department of Chemical Engineering, The University of Melbourne, Grattan Street, Parkville, Victoria, 3010, Australia

ARTICLE INFO

Article history:
Received 27 November 2023
Received in revised form
24 March 2024
Accepted 14 April 2024
Available online xxx

Keywords:
Two-phase flows
Rock fractures
Proppant transport
Fluid inertia
Turbulent flows
Hydraulic fracturing

ABSTRACT

Particle-fluid two-phase flows in rock fractures and fracture networks play a pivotal role in determining the efficiency and effectiveness of hydraulic fracturing operations, a vital component in unconventional oil and gas extraction. Central to this phenomenon is the transport of proppants, tiny solid particles injected into the fractures to prevent them from closing once the injection is stopped. However, effective transport and deposition of proppant is critical in keeping fracture pathways open, especially in low-permeability reservoirs. This review explores, then quantifies, the important role of fluid inertia and turbulent flows in governing proppant transport. While traditional models predominantly assume and then characterise flow as laminar, this may not accurately capture the complexities inherent in real-world hydraulic fracturing and proppant emplacement. Recent investigations highlight the paramount importance of fluid inertia, especially at the high Reynolds numbers typically associated with fracturing operations. Fluid inertia, often overlooked, introduces crucial forces that influence particle settling velocities, particle-particle interactions, and the eventual deposition of proppants within fractures. With their inherent eddies and transient and chaotic nature, turbulent flows introduce additional complexities to proppant transport, crucially altering proppant settling velocities and dispersion patterns. The following comprehensive survey of experimental, numerical, and analytical studies elucidates controls on the intricate dynamics of proppant transport under fluid inertia and turbulence - towards providing a holistic understanding of the current state-of-the-art, guiding future research directions, and optimising hydraulic fracturing practices.

1. Introduction

Particle-fluid flows are commonly encountered in various industrial (chemical, petroleum) and environmental processes (Yan and Koplik, 2009; Qu et al., 2021b), including fluidisation beds (Sahu et al., 2013), sediment movement in rivers and lakes (Chalov et al., 2015), wastewater treatment, pipeline transportation, and proppant transport during hydraulic fracturing in geological formations (Tong and Mohanty, 2016; Osiptsov, 2017; Sahai and Moghanloo, 2019). Particle fluid flows are typically classified by mixture concentration — from dilute to dense — and with regard to the ability to retain the entrained suspension as “slurries” if the particles settle quickly and as ‘dispersions” if the particles remain suspended for extended periods. Suspensions are typically regarded as flows where the particles remain adequately dispersed throughout the carrier phase, maintaining a relatively even distribution (Morris, 2020). Particle-laden suspension flow is a two-phase flow (solid particle-dispersed phase, fluid-carrier phase) in which the momentum exchange between particles and fluid occurs frequently. However, it is challenging to understand and predict the dynamics of particle-laden flows since various parameters affect the suspension flow. The behaviour of the dispersed and carrier phases can differ significantly based on particle characteristics such as shape, size, stiffness, relative density and volume fraction, as well as the constitutive relations of the liquid phase and the flow regime (e.g. laminar or turbulent, Newtonian or non-Newtonian). Two primary mechanisms that govern particle dynamics are fluid drag and particle settling. Fluid drag forces acting on particles control their transport velocity, with feedbacks on fluid flow. Moreover,

* Corresponding author.
E-mail address: samintha.perera@unimelb.edu.au (M.S.A. Perera).
Peer review under responsibility of Institute of Rock and Soil Mechanics, Chinese Academy of Sciences.

https://doi.org/10.1016/j.jrmge.2024.04.006

inter-particle forces and fluid flows play a significant role in dense particle flows (Tomac and Gutierrez, 2014), which can dominate particle movement, leading to increased flow field disturbance. Particle-fluid flow becomes even more complicated due to interactions between particles and static features such as walls, especially where roughness is high (Guo et al., 2014).

Hydraulic fracturing is a widely applied technique to increase the permeability of tight-rock formations for the recovery of geothermal fluids and hydrocarbons from the subsurface (Tomac and Gutierrez, 2013; Fernández et al., 2019; Fjaestad and Tomac, 2019; Qu et al., 2021b) for the production of energy and fuels. This involves the injection of highly pressurized fracturing fluid from the wellbore into the underground formation, resulting in the initiation and then propagation of a hydraulic fracture (Boronin and Osiptsov, 2014; Zhang et al., 2020c; Wang et al., 2022b). However, in situ rock stresses conspire to close the fracture once the fluid pressure drops and the fracturing treatment is complete. Proppants, introduced into the fluid propagating the fracture, saltate and jam in the stalled fracture to prevent closure (Adachi et al., 2007; Economides et al., 2007; Tomac and Gutierrez, 2013; Xu et al., 2020; Yan et al., 2020; Wang et al., 2021). The long-term permeability and production efficiency of the reservoir depend on successful proppant placement (Tomac and Gutierrez, 2013; Fjaestad and Tomac, 2019; Qu et al., 2021b). Apart from proppant transport, the mobilization and migration of fine particles (fines) is another common phenomenon impacting remnant fracture flow following hydraulic fracturing. When extracting hydrocarbons, the pore pressure drops and the effective stress within the rock matrix rises, potentially causing the formation to fail and generating small particles that mix with the fluids in the formation (Mays, 2005; Bai et al., 2017; Fan and Chen, 2020). The migration of fine particles is dominated by different mechanisms depending on their size. The transport of small fines (0.001 μm) is mainly governed by Brownian motion, while larger fines (10 μm) are primarily influenced by gravitational settling (Fan and Chen, 2020).

High-velocity flows are often employed in hydraulic fracturing stimulations to transport proppants deep into the fracture network formed within the subsurface reservoirs, with flows potentially reaching many m^3/min (6–14 m^3/min) (Zhang et al., 2020c). Such conditions necessarily develop unsteady inertial and turbulent flows where the impact of the fluid inertia cannot be neglected. In addition, turbulent vortices developed in the carrier fluid play a critical role in determining the penetration of the particle-laden slurry flow into the evolving fracture system (Gadde et al., 2004). Inertial resistance results from spatial and temporal changes in acceleration and related changes in momentum (Zimmerman and Yeo, 2000; Zimmerman, 2003; Zimmerman et al., 2004; Fourar et al., 2005; Panfilov and Fourar, 2006; Belhaj, 2023). However, the mechanisms and impacts of inertial and turbulent effects remain not fully understood (Tomac and Tartakovsky, 2018). In conventional reservoir engineering applications, it has been considered that viscous forces primarily control the fluid flow at low flow velocities (Matthäi et al., 2007; Blyton et al., 2015; Hu et al., 2018b; Huang et al., 2023) and the impact of fluid inertia is typically regarded as only relevant at high flow velocities rates when turbulent flow occurs. However, the presence of complex geometries, including fracture intersections (Liu et al., 2018, 2020), rough wall boundaries (Cunningham et al., 2020; Rong et al., 2021), shear displacement (Dang et al., 2019, 2021) and spatial variations in aperture (Zimmerman et al., 2004; Cardenas et al., 2009; Guo et al., 2022) within fracture networks result in sudden spatial changes in the velocity field. As a result, fluid inertia may become significant even at low flow rates. This behaviour is expected since fluid inertia resists changes in flow speed and direction, manifest and quantifiable as temporal and spatial accelerations. Understanding such phenomena is crucial when studying fluid flow and particle transport in such complex systems. While traditional models have often emphasized the influence of gravitational settling and fluid viscosity, recent investigations highlight the paramount importance of fluid inertia, especially at the high Reynolds numbers associated with contemporary massive hydraulic fracturing operations (Manoorkar et al., 2018; Wang et al., 2022b; Zhang et al., 2022b). Turbulent phenomena remain difficult but important to characterise due to their unpredictable nature and practical significance. Even in single-phase systems, understanding turbulent flows remains challenging because of the simultaneous evolution of small flow structures nested within larger and more flows. Particle-laden turbulent flows are even more complex since they involve the interaction between particles and turbulent structures, introducing additional length and time scales that must be considered (Fornari et al., 2016c; Capecelatro et al., 2018; Brandt and Coletti, 2022). There are two principal mechanisms of particle/proppant transport within fractures that evolve during hydraulic fracturing: suspended load transport and bed-load transport (Mack et al., 2014; Chang et al., 2017; Barboza et al., 2021). This review focuses on the suspended load transport process and related mechanisms that are vital for the optimisation of fracture treatments and the efficient delivery of proppants to the created fractures.

Several studies review experiments and numerical approaches examining particle transport in fracture flows, especially considering the role of proppant transport in hydraulic fracturing (McLennan et al., 2008; Sahai and Moghanloo, 2019; Roostaei et al., 2020b; Isah et al., 2021). Comprehensive reviews of recent numerical and experimental observations of proppant transport in complex fracture networks are reported in (Isah et al., 2021; Roostaei et al., 2020b; Sahai and Moghanloo, 2019). Recent reviews address key issues in the fluid mechanics of hydraulic fracturing (Osiptsov, 2017), bed load proppant transport (McClure, 2018), experimental studies of proppant settling (Yao et al., 2022), fines migration (Miri et al., 2021) and advances and challenges remaining in characterizing these impacts in hydraulic fracturing (Wu et al., 2022), including numerical modelling of proppant-transport (Barboza et al., 2021; Wen et al., 2022).

While several reviews have been published on particle-fluid flows, especially considering those of proppant transport in hydraulic fractures, few explicitly focus on mechanisms controlling particle transport in the complex evolving fracture networks. Although many reviews address recent experimental and numerical findings, mechanisms of particle transport in complex hydraulic fractures, including the impacts of inertial and turbulent flows on particle suspension, have not been adequately discussed. Also, numerous valuable and insightful studies addressing particle suspension flows in inertial and turbulent regimes cannot be directly extrapolated to the dense particle dynamics in in-fracture flows. Thus, the focus of this review is to bridge the gap between experimental and numerical observations that relate to the particle dynamics of flows specifically confined within fractures – as related to proppant transport in hydraulic fracturing. Recent experimental and numerical findings related to particle suspension flows are extracted from the literature and set within an appropriate framework. More importantly, the impact of fluid inertia (inertia-driven flows) and turbulent flow on particle/proppant transport within hydraulic fractures is discussed in detail. Finally, a suite of considerations is suggested for future research studies to more fully characterise the impacts of inertia and turbulence on particle suspension flows in fractures.

2. Mechanism of hydraulic fracturing

Hydraulic fractures are a type of tensile fracture propagating under existing compressive forces, driven by the pressure from an injected fluid (Detournay, 2016). The crack propagation mechanism is a multifaceted process that integrates the principles of stress concentration, fracture mechanics, interaction with natural fractures, and proppant placement in impermeable rock formations (Cheng et al., 2023). Initially, the injection of high-pressure fracturing fluid into a wellbore induces stress concentration around the wellbore, leading to the initiation of a fracture when the local stress exceeds the tensile strength of the rock. Proppant injection into the fractures ensures they remain open post-pressure reduction, a critical aspect of fracturing (Cheng et al., 2023). The crack opening displacement (COD) or the width of a hydraulic fracture is vital as it ensures an adequate pathway for the proppant to enter the fractures (Abdollahipour et al., 2016; Moradi et al., 2017). Fluctuations in fluid pressure result in alterations in both stress and deformation of the matrix, subsequently impacting fluid volume and pressure. These alterations can affect fractures at various points, leading to their deformation (Abdollahipour et al., 2015, 2016). Similarly, temperature fluctuations also significantly influence the mechanical deformation of geological media, leading to fracture propagation (Abdollahipour and Marji, 2020). The existence of natural fractures modifies the stress fields, thereby influencing the advancement of hydraulic fractures. Depending on the orientation of hydraulic and natural fractures, the impact of natural fractures can either vanish or significantly alter the direction of propagation (Moradi et al., 2017). The dynamics between hydraulic fractures (HFs) and natural fractures (NFs) can lead to a range of consequences, including the stopping or redirection of HFs, in addition to the initiation or development of new fractures (Guo et al., 2015; Zhou et al., 2016). Moreover, variations in the alignment and differences in the spacing and lengths of NFs and HFs influence their propagation routes under specific circumstances. The impact of NFs became more pronounced when they were nearer to the initial HFs and had lesser spacing between them (Moradi et al., 2017).

Crack branching (bifurcation) is often approached from a dynamic perspective, where cracks tend to diverge as they propagate at high speeds (Meyers, 1994). Crack branching can occur even at lower velocities due to the role of microcracks forming ahead of the primary crack. The dynamics between these microcracks and the main crack are crucial in branching (Ravi-Chandar and Knauss, 1984). Under various loading scenarios, the original cracks, which may be straight or curved, are subjected to either tensile or compressive forces, and these cracks may kink, leading to the initiation of secondary cracks from the kinked sections. Secondary cracks are more likely to form under compressive loads due to predominant shear stresses, offering insights into the quasi-static crack branching phenomenon (Manouchehrian and Marji, 2012; Marji, 2014). The original crack propagation is primarily driven by the extension of wing cracks, either towards compressive forces or away from tensile forces. While secondary cracks may not initially form during the early stages of crack growth, their propagation becomes more likely as the crack extends. In scenarios involving curved cracks, wing crack development is significant, with crack branching occurring especially under compressive loading. Under tensile stress, secondary cracks may emerge but tend to merge with wing cracks, potentially facilitating further wing crack extension perpendicular to the applied forces (Marji, 2014).

3. Particle-fluid interactions

In the complex environment of fracture flow, the dynamics of proppant particle transport is profoundly influenced by their interactions with the carrying fluid (Osiptsov, 2017). These particle-fluid interactions are central to understanding the settling velocity of particles, their suspension, and their horizontal conveyance through the fracture network (Barboza et al., 2021). These interactions become increasingly complex under varying regimes of fluid inertia and turbulence, significantly altering non-linear flow behaviours and transport phenomena. Fluid inertia affects the settling rate of particles and distribution, potentially leading to inertial migration where proppants may concentrate at specific locations within the flow field (Gadde et al., 2004; Osiptsov and Asmolov, 2008; Osiptsov, 2017). Turbulence, characterized by chaotic fluid flow, can impede or augment the settling process, facilitate horizontal conveyance, and enhance proppant dispersion by forming vortices in fracture flow (Fornari et al., 2016c; Tomac and Tartakovsky, 2018; Fernández et al., 2019). The resulting patterns of proppant deposition and transport are critical in determining the fracture conductivity and homogeneity. Therefore, a nuanced understanding of these interactions is vital to maximise fracture performance and, consequently, hydrocarbon production. The following section will explore such fluid-particle interactions by considering the impact of fluid inertia and flow turbulence on particle settling and transport in fracture flow.

3.1. Particle migration along the flow and lateral migration

Suspensions in Newtonian fluids exhibit two distinct types of primary particle movement: shear-induced migration and inertial migration (Morris, 2020). Shear-induced migration, driven by the rheological properties of the suspension, occurs at high solid volume fractions and low bulk Reynolds numbers and is commonly observed in suspension flows (Morris, 2020). In contrast, inertial migration is observed in the dilute limit at finite particle Reynolds numbers, where the effects of inertia are dominant and can be described at the level of individual particles (Di Carlo, 2009). When a particle remains stationary within a moving fluid, it experiences a drag force, accelerates, and begins to move. The magnitude of the drag force depends on the difference in velocity between the fluid and the particle. As the particle accelerates, this difference in velocity reduces, causing the acceleration of the particle to slow down until its speed stabilizes. However, due to the energy loss, particles cannot match the exact velocity of the fluid. This difference in velocities is termed the slippage velocity.

The magnitude of this slippage velocity is influenced by factors such as the size of the particle and the fluid's viscosity (Zhang et al., 2019). In most of the proppant flow modelling approaches, it has been oversimplified by assuming that the horizontal velocity of the proppant is equal to the average local fluid velocity (Blyton et al., 2018) (i.e. tends to follow the fracture tip with the same velocity as the fracturing fluid) (Novotny, 1977; Barree and Conway, 1994; Belyadi et al., 2019). Also, it is usually assumed that the proppant concentration across the fracture width is constant (Novotny, 1977; Barree and Conway, 1994, 1995). In several models, the slip between particles and the carrier fluid is assumed to be induced only by gravity, and thus no-slip occurs along the flow direction (Gadde et al., 2004; Adachi et al., 2007; Kumar et al., 2019). However, experimental observations have shown that the particle velocity component in the flow direction could be either locally retarded or accelerated relative to the carrying fluid (Huang et al., 2023). As noted in previous studies, the relative velocity between particle and fluid depends on particle concentration and the proximity and characteristics of the fracture wall (Barree and Conway, 1995; Liu and Sharma, 2005; Osiptsov, 2017). The horizontal distance a particle travels within a fracture before settling is governed by the horizontal and vertical velocities of the particles. The horizontal velocity of sand slurry flow is ~70%–90% of fluid velocity in laminar

flow (Clark et al., 1977). However, two-phase particulate flow modelling using coupled Computational Fluid Dynamics Discrete Element Method (CFD-DEM) has revealed a much lower ratio of fluid velocity to particle velocity (0.2−0.8) in narrow fractures (Tomac and Gutierrez, 2014). Visual observations of proppant transport in experiments (Barree and Conway, 1995) showed that particles tend to flow fastest along the fracture centreline, where unimpeded Newtonian fluid flows are a maximum at low proppant concentrations (0−10% by volume). However, maximum proppant flow velocity tends to decrease at high proppant concentrations (greater than 10% by volume), resulting in a blunted flow profile (uniform velocity across the fracture width). For a uniform distribution of particles, the average particle velocity is higher than the average fluid velocity (Staben et al., 2003). This phenomenon can be primarily attributed to the exclusion of particles from the slowest fluid velocity region near the walls (Staben et al., 2003). The outcomes from CFD-DEM simulations unambiguously show that the average velocity of the proppant phase tends to be slower than that of the fluid phase.

Moreover, there is a linear correlation between the decrease in velocity and the volume concentration of the proppant. However, an exception emerges when there are minimal proppant concentrations and a high ratio of proppant size to fracture width. Nonetheless, this scenario is rarely observed in hydraulic fracturing practice (Blyton et al., 2015). Apart from these findings, the ratio of the proppant diameter to fracture width plays a crucial role in determining the relative average velocity of the proppant and fluid velocity (Blyton et al., 2018). Due to viscous drag, proppants move with the flowing fluid and accumulate in the centre of the fracture aperture (away from the fracture walls), where the velocity is highest, allowing proppants to flow at a higher superficial velocity than the carrying fluid (Barree and Conway, 1995; Dontsov and Peirce, 2014b, 2015). In this case, the velocity profile deviates from the classical parabolic profile due to the high particle concentration in the centre of the channel (Dontsov and Peirce, 2014b). However, the vertical velocity of proppants, the settling velocity, differs from the fluid vertical velocity due to the impact of gravitational forces, viscous forces, and slippage between proppant particles and fluid. Due to the scale of the system, proppant movement across the fracture width is commonly neglected (fracture width is comparatively much smaller than fracture length and height (for vertical fractures)) (Belyadi et al., 2019).

In hydraulic fracturing operations, both dilute and dense particle suspensions are utilized, making both mechanisms of particle migration relevant, as the particle volume fraction can vary widely from dilute (in slick-water fracturing of low-permeability rocks for shale gas recovery) to concentrated, dense slurries (standard hydraulic fracturing in sandstone) (Boronin and Osiptsov, 2014; Osiptsov, 2017). In dilute particle suspensions, it is crucial to consider four distinct physical phenomena: (1) the buoyancy of the particles, which is generally negative, induces settling; (2) particle inertia results in the slip between the particles and the surrounding fluid; (3) interactions between the particles and the walls, and (4) inertial effects of carrier fluid (Osiptsov, 2017). The lift force acting on a particle can be described as the drag force experienced by the particle in response to developing a lateral component of the fluid flow. This lateral migration arises from the disruption caused by the presence of particles that alter the surrounding fluid velocity field (Boronin and Osiptsov, 2014; Osiptsov, 2017). This lateral migration of particles is governed by different mechanisms that depend on the volume fraction of the particles. In the case of dilute suspensions, the transverse motion of particles is induced by an inertial lateral force, which arises from fluid inertia, particle settling and the local nature of the shear flow around the particle (Boronin and Osiptsov, 2014). Two fundamentally different scenarios are documented for the motion of particles in a Poiseuille flow through a plane vertical channel (Adachi et al., 2007; Osiptsov, 2017). The first scenario involves a neutrally buoyant particle that moves with no slip relative to the main flow but experiences rotation due to the shear flow and velocity gradient. The second scenario involves a negatively buoyant heavy particle that moves with a certain slip velocity relative to the carrier fluid, which is particularly relevant in proppant transport (Osiptsov, 2017).

The motion of a neutrally buoyant particle in a Poiseuille flow through a plane vertical channel has been extensively studied (Poiseuille, 1836; Segre and Silberberg, 1962) and found that particles aggregate at an equilibrium radius of 0.62R, known as the “pinch effect”. Several theoretical studies have analysed the lift force on a particle in this configuration, which has extended the applicability of this analysis in terms of the channel Reynolds number from order unity to large values (Schonberg and Hinch, 1989; Asmolov, 1999; Matas et al., 2004). An analytical expression is available (Saffman, 1965) for the lift force applied to a small sphere moving with slip relative to a linear shear flow (in the plane of the velocity and its gradient) (Fig. 1). In this configuration, the migration of a particle with non-zero slip velocity in a shear flow of a viscous fluid results in an "inertial lift" force due to the inertia of the fluid, not that of the particle inertia (Boronin and Osiptsov, 2014). The lift force is negligible at the vanishing channel Reynolds number in Poiseuille flow. Compared to the lift force on a neutrally buoyant force-free particle rotating in a shear flow, the lift force in the presence of the inter-phase velocity slip (the Saffman lift force) is larger by one order of magnitude. Therefore, when there is a slip, the contribution of rotation to the lift can be neglected (Boronin and Osiptsov, 2014; Boronin et al., 2015). When the particle radius to tube radius (a/R) ratio is 0.06, and the initial volume fraction is 0.1, no significant radial migration of particles towards the centre is observed (Hampton et al., 1997). This was attributed to the effect of inertia, which tends to move particles midway between the fracture centreline and wall, and the impact of particle-particle interaction, which tends to concentrate particles at the centre. These two effects appear to counter each other, resulting in the observed outcome. Confirming these observations, it was suggested that fluid inertia cannot be disregarded even in the flow of highly concentrated suspensions when the Reynolds number (Re_p) is greater than ~0.1 (Han et al., 1999). Additionally, it is crucial to consider both inertia and particle-particle interaction even for the low volume fraction of two-phase flow.

In previous studies, researchers have derived expressions for the inertial lateral force exerted on settling particles in horizontal viscous flow in a channel with plane vertical walls (Asmolov and Osiptsov, 2009). The inertial migration of particles in dilute suspension flow through the initial sections of a plane channel (circular tube), neglecting particle settling, has been investigated (Osiptsov and Asmolov, 2008). This investigation showed that the particles migrate towards two planes (rings) at a certain distance from the channel (pipe) walls, with regions devoid of particles forming near the walls. In the case of a concentrated suspension, this migration is diffusive and is attributable to the flow shear and transverse gradient of particle concentration. This results in the formation of a non-uniform concentration profile that peaks on the channel axis (Asmolov et al., 2009) (Fig. 1a). Numerical simulations by Yan and Koplik (2009) also revealed particle migration towards the centreline due to inertial effects and the formation of weak concentration peaks at the walls (Fig. 2). The fluid velocity profiles are approximately parabolic at low particle concentrations but flatten systematically and become more uniform as concentration increases. Particle velocity profiles range from V-shaped to parabolic as the particle Reynolds number increases (Yan and Koplik, 2009).

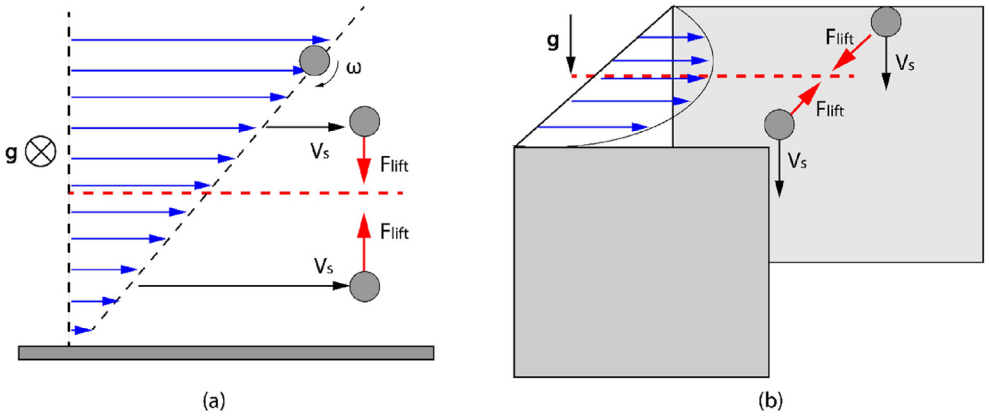

Fig. 1. Lift force on a (a) neutrally buoyant particle when slip is in the plane (Saffman, 1965; Asmolov et al., 2009), (b) and when slip is normal to the plane of fluid velocity under vertical settling (Asmolov and Osiptsov, 2009). Recreated from Osiptsov (2017).

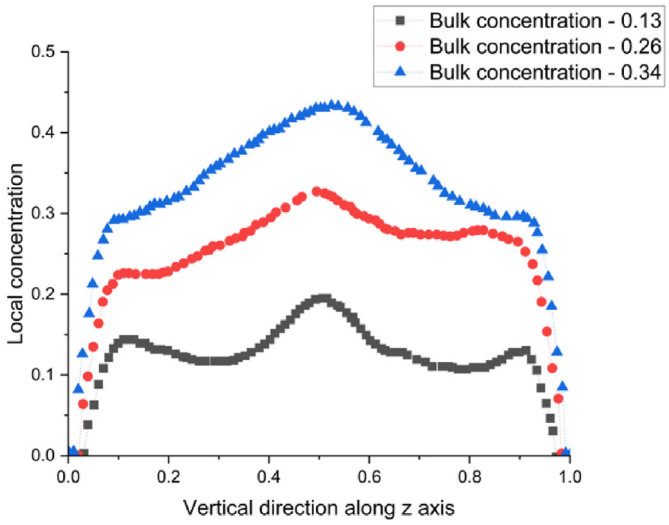

Fig. 2. Average particle concentration for various bulk concentrations in the case of neutrally buoyant particles. Recreated from Yan and Koplik (2009).

However, in actual hydraulic fracturing treatments, the flow behaviour differs from Poiseuille flow, and a more complex turbulent flow appears (Li et al., 2022). For single-phase fluids, it is widely acknowledged that as the Reynolds number increases, there is a marked shift from laminar flow behaviour to the chaotic dynamics observed in transitional and turbulent flows (Picano et al., 2015). Numerous experimental and computational studies have illustrated a dual-mode particle distribution with a clear peak near the wall and a broader peak at the channel/fracture centreline (Picano et al., 2015; Fornari et al., 2016a; Lashgari et al., 2016; Costa et al., 2018; Zade et al., 2018). The peak proximate to the wall has been attributed by Picano et al. (2015) to the stabilization of particle movements stemming from the lubrication between the particle and the wall — a phenomenon previously seen in laminar flows (Hampton et al., 1997). Layered particle concentrations have also been recorded in turbulent suspensions with large beads having a density slightly greater than water (Baker and Coletti, 2019). This lubrication relates to the pressure-driven force observed between the particle and the wall (Ahmadi et al., 2021). Data suggest that particle movements are fundamentally due to particle collisions for larger particles in semi-dense flows (volumetric fraction 10%–20%). These collisions are most common in high-shear zones where the particle concentration tends to be at its lowest (Fornari et al., 2016a). It has been observed that the peak concentration near the wall increases with both fluid and particle inertia (Ardekani et al., 2018). The overall drag tends to increase with the volume fraction, exceeding predictions based on viscosity increases from the presence of particles alone. For the highest volume fractions, there is a noted decline in velocity fluctuation intensities and Reynolds shear stress. Stresses induced by particles govern high *Re* dynamics and primarily contribute to the increase in drag (Picano et al., 2015). Thus, reduced turbulence and increased stresses are caused by the presence of particles in dense environments. As the volumetric fraction of particles increases, migration to the centreline also increases, possibly due to enhanced collision frequencies. Although this increases with particle inertia (i.e. increased particle diameter and density), this migration diminishes with increasing *Re*, which is attributable to intensified turbulent mixing (Brandt and Coletti, 2022).

The motion of non-neutrally buoyant particles significantly impacts the transport of proppants in the fracturing process (Fig. 1b), where particles settle and translate within a pressure-driven Newtonian fluid flowing within a vertical fracture. The particle experiences slip perpendicular to the plane defined by the maximum fluid velocity and gradient. In this configuration, the lift force acting on the particle can be defined (Asmolov and Osiptsov, 2009) as a generalization of the Saffman force. This force accounts for three specific effects: the influence of the walls, particle settling and local shear within the Poiseuille flow. As a result, the force acts from the fracture walls towards the fracture centreline plane, causing settling particles to aggregate on this fracture central plane, while particle-free layers form near the walls. Consequently, these effects give rise to a non-uniform concentration profile of proppants across the fracture, which deviates from the conventional models assuming a uniform distribution (Asmolov et al., 2009; Boronin and Osiptsov, 2014; Osiptsov, 2017). Theoretical and numerical approaches show (Boronin and Osiptsov, 2014) that particle migration towards the centre of the fracture leads to an increase in particle penetration depth and a reduction in gravitational convection at the leading front (Boronin and Osiptsov, 2014).

Heavy particles with higher densities than the carrier fluid have the potential to detach from the fluid. This can lead to clustering, preferential sampling and large collision velocities (Bec et al., 2023). Suspension mechanisms for heavy particles depend on gravity, turbulence, flow shear and inter-particle collisions. In typical channel flows, the lower section of the channel has a higher particle concentration since gravity acts perpendicular to the bulk

motion of the particle flow direction. However, turbulence in the carrier phase diffuses the particles within the flow similarly to acting against the gravitational force (Ahmadi et al., 2021). Experimental investigations of heavy-dilute particle flow in a turbulent channel showed the impact of *Re* and particle volumetric concentration on the wall-peaking particle distribution in horizontal flows (Ahmadi et al., 2021). A bimodal particle distribution was observed with increasing *Re* for lower particle concentrations since turbulent vortices carry some particles away from the wall. In contrast to this behaviour for higher particle concentrations, near-wall particle accumulation becomes more stable with increasing *Re* without forming a bimodal distribution. The effect of varying the mass and volume fraction of a suspension of rigid spheres dispersed in a turbulent channel flow has been studied numerically (Fornari et al., 2016a) to show that the particle volumetric fraction has a greater impact on the increase of overall drag than the effect caused by the density ratio between particle and fluid. Further, shear-induced migration of particles towards the channel centreline becomes more intense with the increase of particle density in the turbulent channel flows.

According to the available literature, most current models used for proppant transport in fractures assume a uniformly distributed particle concentration across the fracture channel. However, this assumption has been challenged in a few recent studies (Boronin and Osiptsov, 2014; Dontsov and Peirce, 2014b, 2015; Lecampion and Garagash, 2014). Ignoring this crossflow migration of the proppant results in an underestimation of penetration length and sedimentation rate, which affects estimates of propped fracture area – an important factor controlling the efficiency of fluid recovery from the fracture wall during subsequent hydrocarbon production. As a result, existing models tend to underestimate the propped length and overestimate the propped height due to the higher longitudinal velocity of the proppant sheet as compared to the average flow velocity and more rapid settling due to gravitational convection effects. In suspension channel flows, the formation of low-concentration layers near the wall (or pure-fluid layers in cases of low initial particle concentration) and a high-concentration core flow are common features of particle migration, regardless of the particle volume fraction (Boronin and Osiptsov, 2014).

In conclusion, previous research on suspension dynamics in fracture flow has primarily focused on the Stokes regime and neglected fluid inertial effects, except for a few studies. There are numerous studies on neutrally buoyant particle suspensions in turbulent channel flows, but only a few studies are reported on dense particle dynamics in turbulent channel flows. The results obtained for neutrally buoyant particles cannot be directly extrapolated to cases of dense (particle density > fluid density) particle flows. Thus, these findings cannot be directly applied to the transport of proppant particles due to fundamental distinctions in the lift forces experienced in different scenarios. Specifically, when proppant particles settle and move within a fracture, the lift force they encounter is significantly greater in magnitude and consistently directed from the fracture walls toward the fracture centreline plane. Additionally, unlike neutrally buoyant particles transported in channels or tubes, proppant particles lack an equilibrium position except at the centreline of the fracture/tube. As a result, they continually migrate from the walls toward the centreline until they form a concentrated suspension near the middle plane. Consequently, this establishes a non-uniform concentration profile and other forces specific to dense suspensions become influential.

3.2. Gravitational settling

Particle settling in hydraulic fractures is a widely researched subject in proppant transport due to its experimental accessibility and the availability of a specific analytical formula (Osiptsov, 2017). Theoretical solutions for steady-state settling, assuming a slow flow regime and disregarding inertia, provide the Stokes settling velocity for a single particle in an infinite fluid. Various complexities are associated with this phenomenon which impacts the settling velocity of particles which include: flow inertia, non-Newtonian rheology of the carrier fluid, hindered settling and particle agglomeration (clustering) effects (which arise due to the finite volume fraction of particles in dense suspensions), effects due to wall retardation and the innate complexity of the evolving fracture network. Experiments examining longitudinal transport and vertical sedimentation in rough-walled fractures have shown that roughness impedes settling and causes proppant retardation during horizontal transport (Liu and Sharma, 2005; Liu, 2006). The "Boycott effect," which leads to enhanced sedimentation in inclined fracture channels, has also been studied (McCaffery et al., 1998; Nevskii and Osiptsov, 2011). This section discusses the impact of particle-fluid interactions on particle settling considering the effects of fluid inertia and turbulent flow.

3.2.1. Hydrodynamic drag

Particle settling out of the suspension is controlled by the combined effects of gravitational, buoyancy and fluid drag forces (Barboza et al., 2021). When a particle settles in a fluid, the fluid retards its movement by exerting a hydrodynamic drag on its surface, with this drag force dependent on the flow regime. According to the Reynolds number, three different flow regimes have been identified: Stokes flow, an intermediate regime, and the Newtonian regime (Clift et al., 1978). Several theoretical, empirical, and numerical models have been proposed in the literature to represent drag forces or drag coefficients exerted on particles for different ranges of Reynolds numbers. However, the theoretical drag coefficient models only exist in the Stokes regime (Clift et al., 1978; Khan and Richardson, 1987) with other correlations based on empirical models. Certain assumptions are applied to the Navier-Stokes equations to obtain the analytical solution. These assumptions are based on the fluid flow regime and the dominance of the viscous or inertial forces on particle movement (Roostaei et al., 2020b). The creeping flow estimation is the most logical assumption to simplify the Navier-Stokes equations, which is only valid for low Reynolds number flows. In this case, the convective term of the Navier-Stokes equation is negligible, and the effect of fluid inertia is completely neglected compared with the viscous forces (Clift et al., 1978).

The drag force expresses the interaction between the carrier fluid and a particle, which acts in the opposite direction of the fluid flow (Barboza et al., 2021; Yao et al., 2022). The drag force (F_D) can be defined as

$$F_D = \frac{1}{2}\rho v^2 A C_D \tag{1}$$

where ρ is the fluid density, v is the velocity of the particle relative to the fluid, A is often the area defined by an orthographic projection of the particle on a plane perpendicular to the direction of flow, and C_D is the drag coefficient. The drag coefficient for a spherical particle can be expressed as

$$C_D = \frac{24}{Re} \tag{2}$$

with this valid only within the Stokes regime ($Re < 0.2$) (Clift et al., 1978), where the particle Reynolds number is

$$Re_p = \frac{\rho v d_p}{\mu} \tag{3}$$

where d_p is the particle diameter and μ is the dynamic fluid viscosity. For the viscous regime, the corresponding terminal velocity for a single particle induced by gravity within a fluid of infinite extent is given as (Novotny, 1977):

$$v_t = \frac{g{d_p}^2\left(\rho_p - \rho_f\right)}{18\mu} \tag{4}$$

However, Stokes flow requires certain assumptions that are typically violated during the conditions of proppant transport in hydraulic fracturing and therefore cannot be used to predict the settling of proppants in a two-phase confined slurry flow (Gadde et al., 2004; Liu and Sharma, 2005; Palisch et al., 2008; Dayan et al., 2009; King, 2010) due to the following reasons:

(1) Particles are assumed to be perfectly spherical, typically violated in actual conditions.
(2) Stokes law is only valid for predicting the terminal velocity of a single particle and spatial variations in flow velocity may render the flow non-steady.
(3) For proppant settling within slurry flow, the settling of one particle is affected by the presence of other particles, which Stokes settling does not quantify.
(4) Hydraulic fracturing is a dynamic process, and the Stokes law is only valid for static fluid or creeping flow. Thus, this is only applicable to predict the proppant settling during fracture closure after fracture propagation. (i.e. after pumping ceases after fracture treatment).
(5) In the hydraulic fracturing process, the settling velocities of particles are significantly influenced by the presence of the fracture walls. The reduction in settling velocity caused by wall roughness cannot be incorporated into proppant settling via the infinite fluid assumption for Stokes law.
(6) High fluid injection rates in hydraulic fracturing generate non-Darcian/turbulent flows. At high flow rates, inertial effects dominate over viscous effects. Thus, turbulent and inertial effects further complicate the quantification of proppant settling, and Stokes law is no longer valid for such non-creeping flow conditions.

A particle subject to free-settling within a fluid typically transits two stages. The first stage is acceleration, where the settling velocity increases with the increasing drag force. The second and later stage is the equilibrium stage, where the particle achieves terminal velocity (the maximum settling velocity) with a constant drag force. In this stage, the drag force is equal to the buoyant weight of the particle. The standard drag coefficient curve (Fig. 3), recovered from experimental data, identifies four regimes: laminar flow (or Stokes' regime) $Re_p < 1$, an intermediate regime in $1 < Re_p < 1000$, a turbulent regime (or Newton's regime) in $1000 < Re_p < 2 \times 10^5$, and a boundary-layer-separation regime within $Re_p > 2 \times 10^5$ (Dey et al., 2019; Yao et al., 2022). Many cases of proppant settling during hydraulic fracturing occur within the intermediate regime (Mack et al., 2014), and analytical solutions are unavailable. Efforts have concentrated on deriving empirical correlations linking Re to drag coefficient C_D from experimental data.

3.2.2. Effect of fluid inertia on hydrodynamic drag

Fluid inertia is one of the key factors influencing the settling of particles (Sahai, 2012; McClure and Kang, 2017; Roostaei et al., 2020b). Analytical solutions to Stokes flow have advanced to investigating the impact of inertial effects from experimental observations, which involve changes in particle speed and drag force at finite particle Reynolds numbers and the collective dynamics that arise in suspensions (Roostaei et al., 2020b; Brandt and Coletti, 2022). Except for very low Re flows (creeping laminar flow), fluid inertial effects cannot be neglected, and their impact on the drag force on a particle becomes significant. Additional drag forces are applied to particles in addition to those representative of the Stokes regime (Di Vaira et al., 2020; Roostaei et al., 2020a; Brandt and Coletti, 2022). In individual particle motion, the viscous drag force ensures that the particle follows the fluid flow path or streamline. Conversely, inertial lift forces can divert the particles, making them veer away from the fluid streamlines that they would otherwise follow (Manoorkar and Morris, 2021). Far away from the particle, the fluid inertial force may not be trivial relative to the viscous force, and the viscous force can be predominant only if the disturbance decays exponentially (Oseen, 1910) - with this suggesting a correlation by linearizing the inertial term in the Navier-Stokes equation rather than ignoring it. Table 1 shows some theoretical approaches after Oseen (1910), with Table 2 identifying some proposed empirical correlations for the drag coefficient beyond the Stokes regime.

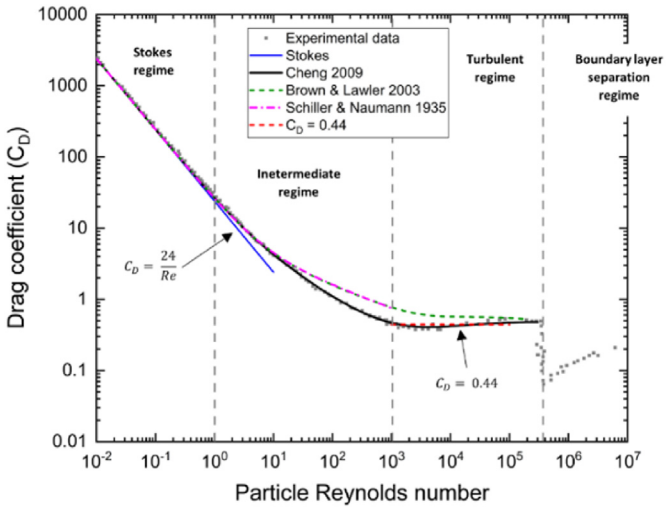

Fig. 3. Experimental data linking drag coefficient C_D to particle Reynolds number Re (Yao et al., 2022). Experimental data points from Brown and Lawler (2003).

Proppant transportation and settling models have been developed, incorporating such inertial effects, using the three-dimensional (3D) hydraulic fracture simulator (UTFRAC-3D) (Gadde et al., 2004). This model was developed to account for the effect of fluid inertia associated with high relative velocities between the fluid and the moving proppant within a fracture, on the settling velocity of the proppant. The simulations showed that inertial effects become significant at high settling velocities for particle Reynolds numbers greater than two ($Re_p > 2$). Fig. 4 shows a graphical representation contrasting settling rates according to the Stokes equation and the corrected correlation for terminal velocity. At higher particle Reynolds numbers, settling rates of the proppants are significantly reduced due to the inertial effect (Gadde et al., 2004). The following correlation, proposed by (Happel and Brenner, 1983), was used to account for the fluid inertial effect on proppant settling at higher Reynolds numbers ($2 < Re_p < 500$). The corrected drag coefficient and settling velocity are given as

Table 1
Theoretical correlations for drag coefficient C_D of a spherical particle settling in Newtonian fluids for intermediate Reynolds numbers.

Source	Correlation	Reynolds number (Re) range
Oseen (1910)	$C_D = \frac{24}{Re}\left(1 + \frac{3}{16}Re\right)$	$Re < 10$
Goldstein (1929)	$C_D = \frac{24}{Re}\left(1 + \frac{3}{16}Re - \frac{19}{1280}Re^2 + \frac{71}{20408}Re^3 - \frac{30179}{34406400}Re^4 + \frac{122519}{550502400}Re^5\right)$	$Re < 2$
Proudman and Pearson (1957)	$C_D = \frac{24}{Re}\left(1 + \frac{3}{16}Re + \frac{9}{160}Re^2 \log_{10}\frac{Re}{2}\right)$	
Abraham (1970)	$C_D = \left(\sqrt{\frac{24}{Re_p}} + 0.5407\right)^2$	$Re_p \leq 6000$
Mikhailov and Freire (2013)	$C_D = \frac{1920\,(3696 + 1665\,Re_p + 136\,{Re_p}^2)}{Re_p(295680 + 77760\,Re_p + 689\,{Re_p}^2)}$	$Re_p \leq 10$

Table 2
Empirical correlations for the drag coefficient of a spherical particle settling in Newtonian fluids for intermediate Reynolds numbers.

Source	Correlation	Re_p range
Schiller and Naumann (1935)	$C_D = \frac{24}{Re_p}\,(1 + 0.15\,{Re_p}^{0.687})$	$Re_p \leq 800$
Roos and Willmarth (1971)	$C_D = \frac{1.2028}{Re_p}\;\frac{765.4926 + 99.5463\,Re_p + 0.5123{Re_p}^2}{34.5236 + 1.4370Re_p + 2.5926\times10^{-6}{Re_p}^2}$	$Re_p \leq 2 \times 10^4$
Clift et al. (1978)	$C_D = \frac{24}{Re_p}\,(1 + 0.1315\,{Re_p}^{0.82-0.05\,\log Re_p})$	$0.01 \leq Re_p \leq 20$
	$\log_{10}C_D = 1.6435 - 1.1242\log_{10}Re_p + 0.1558(\log_{10}Re_p)^2$	$20 \leq Re_p \leq 260$
	$\log_{10}C_D = -2.4571 + 2.5558\log_{10}Re_p - 0.9295(\log_{10}Re_p)^2 + 0.1049(\log_{10}Re_p)^3$	$260 \leq Re_p \leq 1500$
	$\log_{10}C_D = -4.3390 + 1.5809\log_{10}Re_p - 0.1546\,(\log_{10}Re_p)^2$	$1500 \leq Re_p \leq 1.2 \times 10^4$
		$4.4 \times 10^4 \leq Re_p \leq 3.38 \times 10^5$
Khan and Richardson (1987)	$C_D = (2.25\,{Re_p}^{-0.31} + 0.36\,{Re_p}^{0.06})^{3.45}$	$0.01 \leq Re_p \leq 3 \times 10^5$
Brown and Lawler (2003)	$C_D = \frac{24}{Re_p}\,(1 + 0.15\,{Re_p}^{0.681}) + \frac{0.407}{1 + 8710/Re_p}$	$Re_p \leq 2 \times 10^5$
Cheng (2009)	$C_D = \frac{24}{Re_p}\,(1 + 0.27Re_p)^{0.43} + 0.47(1 - e^{-0.04{Re_p}^{0.38}})$	$Re_p \leq 3 \times 10^5$
Morrison (2013)	$C_D = \frac{24}{Re_p} + \frac{2.6Re_p/5.0}{1 + (Re_p/5.0)^{1.52}} + \frac{0.411(Re_p/2.63\times10^5)^{-7.94}}{1 + (Re_p/2.63\times10^5)^{-8.0}} + \frac{0.25Re_p/10^6}{1 + Re_p/10^6}$	
Terfous et al. (2013)	$C_D = 2.689 + \frac{21.683}{Re_p} + \frac{0.131}{{Re_p}^2} - \frac{10.616}{{Re_p}^{0.1}} + \frac{12.216}{{Re_p}^{0.2}}$	$Re_p \leq 2 \times 10^5$

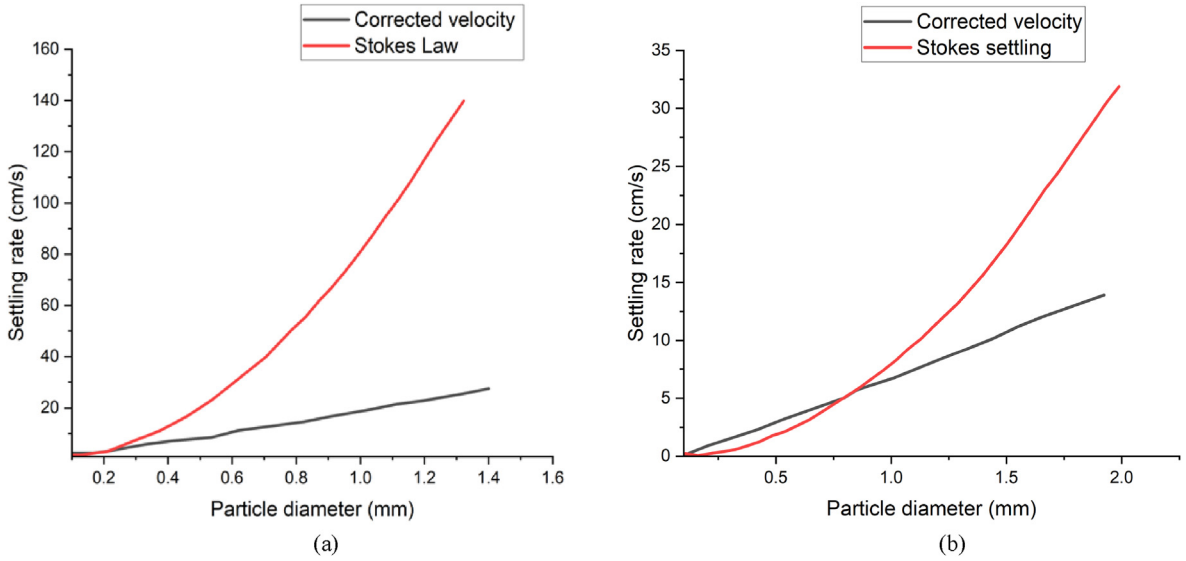

Fig. 4. Terminal velocities of different size particles predicted by Stokes settling and corrected for inertial effect for (a) fluid viscosity 1 cP and (b) fluid viscosity 10 cP (1 cP = 0.001 Pa s) (replotted from Gadde et al. (2004)).

$$C_D = \frac{18.5}{Re_p^{0.6}} \tag{5}$$

$$V_{Re} = \frac{20.34\left(\rho_p - \rho_f\right)^{0.71} d_p^{1.14}}{\rho_f^{0.29}\mu^{0.43}} \tag{6}$$

where v_{Re} is the settling velocity, ρ_p is the particle density, ρ_f is the fluid density, μ is the fluid viscosity, d_p is the particle diameter, and g is the gravitational acceleration.

Inertial effects associated with high relative velocities between the proppants and the fluid significantly reduce the settling rates of the particles, with the settling velocities of the proppants reduced by a factor of 2–6 (Liu, 2006) - in agreement with previous findings (Gadde et al., 2004). The motion of small groups of solid spheres settling under constant gravitational forces is affected by the inertia of the surrounding fluid at low Reynolds numbers with significant fluid inertia causing small clusters of solid spheres to approach each other along the line connecting their centres (Leshansky et al., 2003). Recent investigations examine the effect of fluid inertia and other hydrodynamic forces on the motion of small spherical solid particles in a turbulent flow using direct numerical simulation (DNS) (Zhang et al., 2021). The hydrodynamic force is decomposed into several component forces, including stationary drag, force history, lift forces, added-mass effect and a fluid inertial force. Based on the results, the fluid inertia effect dominates in controlling the motion of light particles ($\rho_p/\rho_f < 1$) but can be neglected for heavy particles ($\rho_p/\rho_f > 10$). Zhang et al. (2021) confirmed that the fluid inertial force is negligible compared to the drag force for particles of very small diameters (typically Stokes numbers <1, Eq. (7)) when the density ratio (ρ_p/ρ_f) is of order one or larger. However, with the increase of particle Stokes number, the density ratio also needs to be increased if the fluid inertial effect is to be neglected on the motion of particles (Zhang et al., 2021).

Moreover, accommodating the particle fluid interaction force is vital in the numerical modelling of two-phase flows in fractures and other channels. Generally, this interaction force is divided into several components, and interphase drag force is one component among them (other components are pressure gradient force, lift force, virtual mass force and turbulent dispersive force) (Liu et al., 2022). Several drag models have been introduced to model the interphase drag force to describe the momentum exchange between solid and fluid phases. The most commonly used drag models are given in Table 3 with some of these models based on empirical correlations. The Wen and Yu model (Wen and Yu, 1966) is most suitable for dilute particle suspensions among these models. Likewise, Syamlal-O'Brien, Gidaspow, and modified Gidaspow models are efficient for low and high solid concentrations (Liu et al., 2022). Even though the same drag coefficient (C_D) is used in several models, the interphase momentum exchange (β) is typically calculated in different ways, which is not included in this table.

3.2.3. Effect of turbulent flow on particle settling

The turbulent flow of the suspending fluid affects the settling velocity of particles in a suspension (Gadde et al., 2004). Even at low particle concentrations, the velocity fluctuations of suspended particles are highly attenuated in a slurry flow (Bareš et al., 2014). The interaction between the fluid phase and the particulate phase is bidirectional, meaning that the turbulence of the fluid phase (carrier-phase) impacts the dispersion and preferential accumulation of the solid phase (particulate phase), which in turn modulates fluid turbulence (Bagchi and Balachandar, 2003). Characterization using Stokes law (viscous regime absent inertia) becomes invalid and loses accuracy at large Reynolds number flows since the turbulent flow can apply lift and drag to particles (Fjaestad and Tomac, 2019). Small particles in a turbulent environment assume turbulent behaviour due to their response to fluid velocity fluctuations (Mei et al., 1997). In fracture flow, smaller particles tend to react more effectively to higher flow rates and are carried along by turbulent vortices above the bed of the proppant. This phenomenon causes the formation of a smaller proppant bed, enabling the slurry, composed of smaller sand particles, to travel further along the fracture system (Tomac and Tartakovsky, 2018).

The dynamics of particle settling in turbulent flow depend on the density ratio between solid and fluid, solid volume fraction, and Galileo number (Ga, the ratio between buoyancy and viscous forces), with this dynamic behaviour further complicated by the interaction between solid particles and eddies created in the turbulent flow (Fornari et al., 2016c). The Stokes number (S) defines the impact of small-scale turbulence on particle movement. It is the ratio between particle relaxation time ($t_p = [d^2(\rho_p - \rho_f)/(18\mu)]$) to Kolmogorov time scale (fluid response time) t_k $[(\nu/\varepsilon)^{1/2}]$. It is a characteristic time scale at which the smallest turbulent eddies dissipate their energy through viscous forces. The Stokes number (S) is expressed as (Bec et al., 2014):

$$S = \frac{t_p}{t_k} = \frac{\Delta}{18}\left(\frac{d}{\eta}\right)^2 \tag{7}$$

where ε is the turbulent kinetic energy dissipation rate, and η is the Kolmogorov length scale $[(\nu^3/\varepsilon)^{1/4}]$, where the Kolmogorov length scale is the length scale at which the smallest turbulent eddies dissipate their energy through viscous forces (Bec et al., 2014). Certain conditions must be met to prevent particles from significantly influencing turbulence (one-way coupling). These include having a small volume and mass fraction and ensuring that the particle size is smaller than the Kolmogorov scales (Balachandar and Eaton, 2010). However, as the number density of particles increases, it becomes necessary to consider the impact of the suspended phase on the flow. When individual or agglomerated particles grow larger than the smallest flow structures, called finite-size particles, the geometric effects associated with the local deformation of the fluid flow become notable (Brandt and Coletti, 2022).

There are four mechanisms by which a turbulent velocity field with zero mean velocity (homogeneous, isotropic turbulence) impacts the settling or rising velocity (terminal velocity) of a single particle (Nielsen, 1993). These delaying effects are the nonlinear drag on large particles, trapping inside eddies (vortex trapping), fast tracking and the loitering effect (Dey et al., 2019). The reduction of terminal settling velocity caused by nonlinear drag is expected to be significant for the settling of coarser particles. In vortex tapping, forced vortices can capture particles, decreasing their terminal settling velocity. The fast-tracking mechanism enhances the terminal fall velocity by directing the particles towards a preferred trajectory (Fig. 5). Strong and persistent eddies tend to fast-track the small, heavy particles, eventually causing a substantial increase in settling velocity (Maxey and Corrsin, 1986). The key idea behind the effects of loitering is when a particle falls through a non-uniform velocity predominantly in the opposite direction of the particle motion – then the particle velocity is retarded, and the particle loiters. As a result, coarser particles experience a retarding effect, such as particles falling along a vertical line of symmetry. However, in homogeneous and isotropic turbulence, loitering exerts a negligible impact (Fornari et al., 2016c). The impact of turbulence on particle settling is controversial, and turbulence can

Table 3
Common drag models for fluid-particle two-phase flow numerical modelling and relevant proppant transport modelling approaches.

Model	Drag coefficient/Reynolds number	Proppant transport modelling approach
Schiller-Naumann model (Schiller and Naumann, 1935)	$C_D = \begin{cases} \frac{24}{Re_p}(1+0.15\,Re_p^{0.687}) & (Re_p<1000) \\ 0.44 & (Re_p \geq 1000) \end{cases}$	
Wen-Yu model (Wen and Yu, 1966)	$C_D = \begin{cases} \frac{24}{Re_p}(1+0.15\,Re_p^{0.687}) & (Re_p<1000) \\ 0.44 & (Re_p \geq 1000) \end{cases}$	CFD-DEM (Zeng et al., 2016; Zhang et al., 2017b, 2020b; Wang et al., 2019); MP-PIC (multiphase particle in cell) (Mao et al., 2021)
Gidaspow model (Gidaspow, 1994)	Ergun model for $\varphi > 0.2$ (Dense flow) Wen-Yu model for $\varphi < 0.2$ (Dilute flow)	CFD-DEM (Tomac and Gutierrez, 2014; Zhang et al., 2017a, 2017c, 2022b, 2022c; Lu et al., 2020; Hu et al., 2021; Liu et al., 2021; Wang et al., 2022a);
Huilin-Gidaspow model (Huilin and Gidaspow, 2003)	$C_D = \begin{cases} \frac{24}{\varphi Re_p}(1+0.15\,\varphi Re_p^{0.687}) & (Re_p<1000) \\ 0.44 & (Re_p \geq 1000) \end{cases}$ φ is the particle volumetric fraction	TFM two-fluid model (Li et al., 2018; Yang et al., 2019; Gong et al., 2020; Zhou et al., 2023); DDPM (Tong and Mohanty, 2016; Zhang et al., 2020c); Hybrid model (CFD-DEM and Eulerian Granular) (Suri et al., 2019)
Syamlal–O'Brien model (Syamlal and O'Brien, 1989)	$C_D = \left(0.63+\frac{4.8}{\sqrt{Re/V_r}}\right)^2$	EGM (Eulerian granular model) (Han et al., 2016)
Helland model (Helland et al., 2007)	$C_D = \begin{cases} \frac{24}{Re_p}(1+0.15\,Re_p^{0.687}) & (Re_p<1000) \\ 0.44 & (Re_p \geq 1000) \end{cases}$	
Di Felice model (Di Felice, 1994)	$C_D = \left(0.63+\frac{4.8}{\sqrt{Re_p}}\right)^2$	CFD-DEM (Kou et al., 2018; Wu and Sharma, 2019; Yamashiro and Tomac, 2020a; Qu et al., 2022; Zhang et al., 2022a; Pu et al., 2023 Zhu et al., 2023)

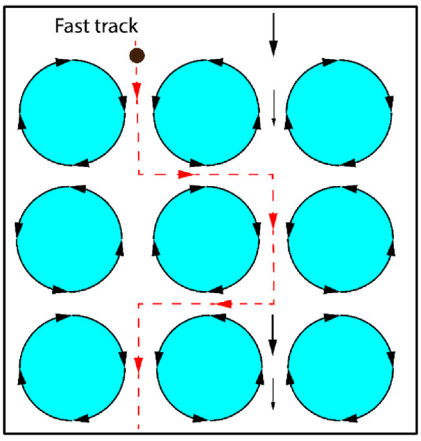

Fig. 5. Small heavy particles subjected to fast-tracking and larger particles subjected to delay during settling (Nielsen, 1993).

either enhance, reduce or inhibit the settling of particles (Fornari et al., 2016c).

Particles with low inertia tend to be expelled from the core of eddies, and these particles accumulate within areas with low vorticity and high strain rates (Squires and Eaton, 1991). Due to both this effect and gravitational settling, particles tend to be swept into downdraft areas (preferential sweeping or fast-tracking). Therefore, the mean settling velocities of the particles increase. This dynamic behaviour is observed in simulations of random flows (Maxey, 1987) and turbulent flows (Wang and Maxey, 1993) and is experimentally confirmed (Nielsen, 1993; Aliseda et al., 2002; Yang and Shy, 2003, 2005). This effect of increased settling has been attributed to inertial bias, with it concluded that small-scale (Kolmogorov) fluctuations are more critical in determining the increase of settling velocity (Maxey, 1987; Wang and Maxey, 1993). According to some studies, particle settling rates in a turbulent flow are mainly affected by two mechanisms (Bagchi and Balachandar, 2003). The first mechanism is the non-linear dependency of drag on the relative velocity. The mean settling velocity in turbulent flow is less than that in stagnant flow, resulting in a greater drag force than in stagnant flow (Bagchi and Balachandar, 2003). This effect decreases with decreasing Reynolds number and completely vanishes in viscous Stokes flow. The second and more complex mechanism is the formation of preferential trajectories by freely falling particles. The mean fluid velocity experienced by a particle is not uniform throughout the entire region. Due to this effect, the mean settling velocity of a particle increases and the drag force is reduced (Bagchi and Balachandar, 2003). Also, particles undergoing settling in turbulent flows tend to preferentially accumulate in areas where the vertical fluid velocity is in alignment with gravitational forces (Bec et al., 2014). This phenomenon increases their average settling rate, congruent with previous experimental and numerical observations (Maxey, 1987; Wang and Maxey, 1993; Bagchi and Balachandar, 2003). One of the most important results of numerical analysis is that the settling velocity of particles increases to a maximum when the ratio of particle relaxation time and Kolmogorov time scale approaches a value of unity (Wang and Maxey, 1993). These numerical results show a variation of settling velocity compared to settling in a quiescent fluid as a function of the ratio of the two-time scales (Wang and Maxey, 1993). The results are normalized by the Kolmogorov velocity, which is equivalent to the Stokes settling velocity. Also, as shown in Fig. 6, these results indicate a variation in maximum settling velocity with Reynolds number (with increasing Reynolds number, the change in settling velocity increases) (Mack et al., 2014).

In contrast, a reduction in mean settling velocity has been reported in experimental observations (Yang and Shy, 2003; Kawanisi and Shiozaki, 2008) and numerical simulations (Wang and Maxey, 1993; Good et al., 2014). However, the reduced settling velocity can only be investigated by DNS if the drag force imparted by nonlinear effects is considered (i.e. for a finite particle Reynolds number) (Good et al., 2014; Fornari et al., 2016c). The non-linear drag force attenuates the increased settling velocity caused by turbulence in the suspending fluid (Mei et al., 1997). It has been shown experimentally (Tooby et al., 1977) that forced vortices with horizontal axes can trap heavy particles and thus eliminate their settling velocity. Also observed is that vortex-trapping effects are unrelated to the nonlinearity of the drag force (Nielsen, 1993). The mean settling velocity of a particle is reduced when the particle terminal velocity is greater than the turbulent velocity fluctuations (when the ratio $\tau_p g/u'$ is greater than 1, where $\tau_p = 2(\rho_p/\rho_f)a^2/(9\nu)$ is particle relaxation time with the particle radius, ν is the fluid kinematic

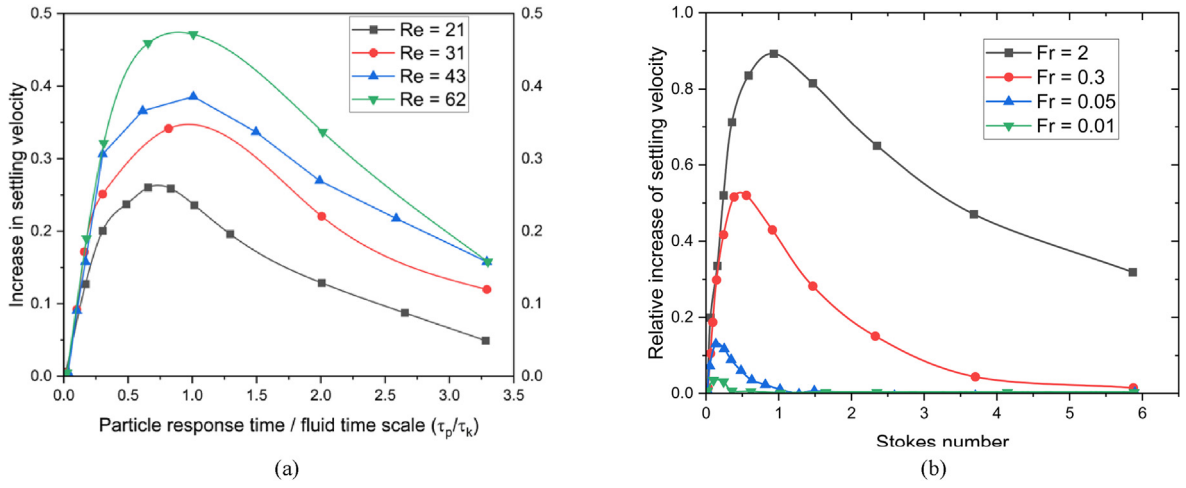

Fig. 6. (a) Relative increase of settling velocity as a function of Stokes number for various Reynolds numbers (Wang and Maxey, 1993) (replotted from Mack et al. (2014)), and (b) Relative increase of settling velocity for different Froude numbers (replotted from Bec et al. (2014)).

viscosity and u' is the turbulent velocity fluctuations) (Good et al., 2014). It can be concluded that when the Stokes settling velocity of a particle is sufficiently high, these particles follow a straight vertical path during freefall and cannot sidestep the turbulent eddies due to their weak horizontal velocity fluctuations. Thus, the effect of fast-tracking is suppressed, and the mean settling velocities are reduced due to an increment of drag related to the Finite Reynolds number (Fornari et al., 2016c). An empirical correlation between the terminal velocity of a particle settling in a turbulent flow (Clark and Quadir, 1981) shows an increased drag (decreased settling velocity) of particles in a turbulent flow ($750 < Re < 3.5 \times 10^5$, $C_D = 0.445$ (constant)) as (Clift et al., 1978):

$$v_t = 1.74\left[\frac{2a\left(\rho_p - \rho_f\right)}{\rho_f}\right]^{\frac{1}{2}} \tag{8}$$

The mean settling velocity progressively decreases as the density ratio between the particle and the fluid (ρ_p/ρ_f) decreases in homogeneous isotropic turbulence (HIT) (Fornari et al., 2016b, c). Also, the interactions between particles and turbulent eddies further complicate the settling process. Thus, the reduced settling speed of the particle is attributed to the increase in the nonlinear drag force caused by large fluctuations in relative velocities. Within HIT, the mean settling velocity of particles is reduced when compared to those in the quiescent fluid - this reduction can be of 6%–60% when compared to the terminal settling velocity of an isolated particle in quiescent fluid (Fornari et al., 2016c). The most striking result of this study is a significant reduction of mean settling velocity compared to the terminal settling velocity of a single particle in a still/quiescent fluid with decreasing Galileo number *Ga* (the ratio between buoyancy and viscous forces) (Fig. 7). Also, when the turbulent fluctuations are larger than the characteristic reference velocity of the particle settling process (terminal settling velocity of an isolated particle), the overall drag force on a particle increases considerably (Fornari et al., 2016c). This behaviour is attributed to the increment of variance of particle velocity and the increased intensity of the particle relative motion. These results (Fornari et al., 2016c) are consistent with other recent findings (Homann et al., 2013; Chouippe and Uhlmann, 2015), which suggest a higher nonlinear drag in turbulent flow when compared to laminar flow. In addition, at low-volume fractions, the settling rate is strongly affected by the interaction with turbulence (Fornari et al., 2019). The hindering effect at high-volume fractions becomes the dominant factor determining settling rates, while particle velocity variations in the direction of gravity are consistently influenced by turbulence (Fornari et al., 2019).

In conclusion, fluid inertia plays a significant role in determining the settling velocity of particles within fracture flow by altering the fluid drag experienced by the particles, resulting in significant deviations from predictions based solely on Stokes law. Furthermore, at even higher *Re* flows (high inertia flow), flow turbulence within fractures can further complicate the settling dynamics of particles. Additionally, the turbulent dynamics are altered by the interactions between particles and turbulent eddies. Sizes of these eddies range from largest (channel scale) to smallest (Kolmogorov scale) scales; thus, in such situations, additional parameters, including the ratio between particle diameter and a characteristic length-scale of the turbulence, the ratio of the particle relaxation time to a turbulent time scale, and the relative turbulence intensity (defined as the ratio between the root-mean-square turbulent velocity and the terminal settling speed of the particle) should be considered. Overall, the reduction in mean settling velocity is due to the unsteady effects and nonlinearity of the drag forces. Since a comparatively large number of parameters and complex feedbacks are involved, the particle settling phenomenon remains incompletely understood. Also, detailed studies of the dense concentrations of particles (i.e. proppant, sand particle) settling in fractures under turbulent flow conditions are limited - with most experimental and numerical studies focusing on low-density concentrations of solid suspensions. Thus, such observations in fluid dynamics cannot be directly extrapolated to the case of proppant transport, where the suspensions are not dilute. Turbulent fluctuations in velocity and pressure exert additional forces on the particles, causing them to experience enhanced dispersion and altered settling. Understanding the interplay between fluid inertia, flow turbulence, and particle settling is crucial for accurately predicting particle behaviour and resulting transport within fracture flow environments.

3.3. *Effect of temperature-dependent fluid viscosity on particle fluid interactions*

Turbulent flows feature eddies of various sizes, with the size of the largest eddies constrained by the flow boundaries of the system (Doran, 2013). At elevated Reynolds numbers, the turbulence experienced by large-scale eddies is not influenced by fluid

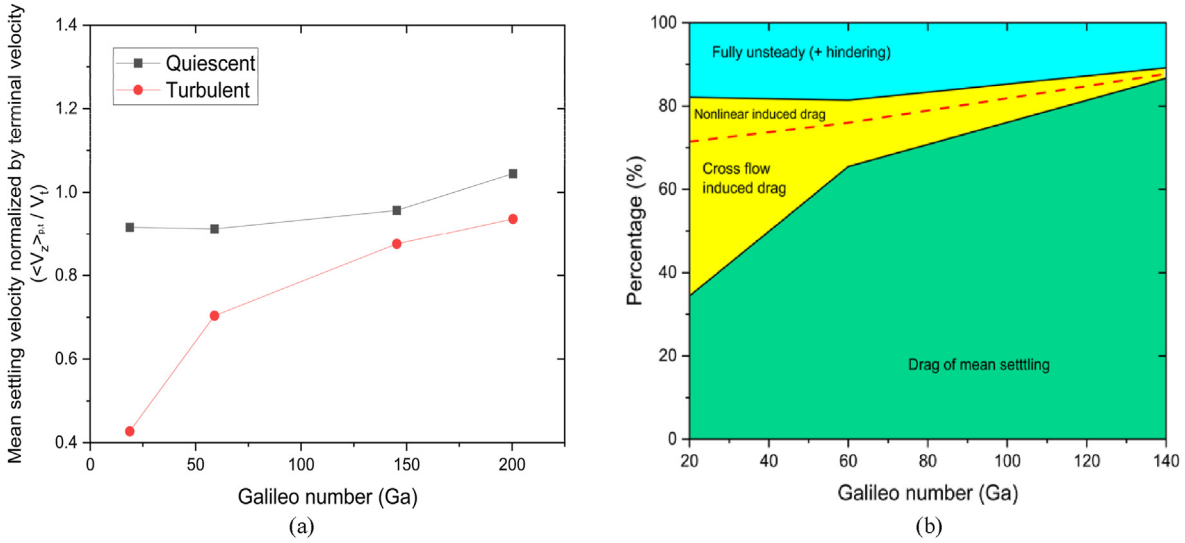

Fig. 7. (a) Mean settling velocity as a function of Galileo number (*Ga*) for quiescent and turbulent settling, and (b) Relative contribution to the overall mean drag in a turbulent flow (replotted from Fornari et al. (2016c)).

viscosity. These large eddies are inherently unstable within turbulent flows, forming smaller eddies and generating even more minor eddies. This hierarchy of turbulence scales exists simultaneously and overlays the average flow, with smaller eddies nested within larger ones. As the Reynolds number grows, the spectrum of eddy sizes expands due to the smallest eddies becoming smaller with increased fluid velocity or reduced viscosity (Doran, 2013; Ting, 2016). The large eddies, which also hold most of the Turbulent Kinetic Energy (TKE), are the primary contributors to momentum transport in turbulent flows. Conversely, the motion at more minor scales is linked to significant velocity gradients and high shear stresses. At the scale of the smallest eddies, the energy they receive is dissipated as heat due to viscosity and fluid friction, which breaks down the eddy structure and velocity gradients (Ting, 2016). The fluid viscosity and the intensity of the velocity gradient determine the efficiency of viscous energy dissipation by the smallest eddies. Thus, even in high Reynolds number flows where inertial forces generally outweigh viscous forces, viscosity remains crucial at the smallest scales of turbulence. The elevated shear stresses at these minor scales result in higher energy dissipation rates in turbulent flow than in laminar flow (Doran, 2013). The relationship between fluid viscosity and turbulence is nuanced and can appear contradictory at first glance. The statement that turbulence decreases with decreasing fluid viscosity might seem counterintuitive since lower viscosity typically leads to higher Reynolds numbers associated with increased turbulence. However, the context in which viscosity decreases can significantly affect turbulence differently.

Unlike viscosity, for most standard heat transfer fluids, properties such as density, specific heat, and thermal conductivity largely remain unaffected by temperature changes. Compared to models assuming constant viscosity, analyses incorporating temperature-dependent viscosity reveal marked disparities in fluid velocity statistics across the channel, especially near the walls (Marchioli et al., 2012). Studies on turbulent flows through heated-wall pipes and channels have detected notable changes in flow dynamics due to temperature-dependent viscosity. The secondary flows close to the heated wall become larger and more vigorous. The fluid layer affected by viscosity near the heated wall also becomes considerably thicker than when heating is applied (Métais and Vázquez, 2002). Contrary to expectations, the colder sections of the channel, characterised by higher viscosity, show an increase in turbulence, while the warmer sections, where viscosity is lower, exhibit reduced turbulence (Métais and Vázquez, 2002; Marchioli et al., 2012). The heightened viscosity near the cold wall notably boosts TKE and diminishes the average velocity gradient. Conversely, at the warmer wall, reduced viscosity leads to subdued turbulence due to increased viscous dissipation, and velocity fluctuations become more sporadic. This pattern of intermittent fluctuations is also observed beyond the buffer zone on the colder side of the channel (Marchioli et al., 2012). Thus, while the fundamental principle that lower viscosity should lead to more turbulence holds under many conditions, the relationship is complex and influenced by various factors, including flow geometry, temperature gradients, and the specific energy transfer dynamics within the turbulent flow.

The impact of temperature-dependent viscosity on particle dynamics in turbulent flows is a complex interplay that significantly influences particle behaviour, distribution, and transport. However, studies regarding the impact of temperature-dependent viscosity on particle-laden turbulent flows are rarely found in literature in the context of dense particle dynamics. Particles within turbulent flows often form clusters and voids rather than remaining evenly dispersed (Toschi and Bodenschatz, 2009; Banko et al., 2020). This non-uniform distribution of particles in turbulent flows is primarily due to the centrifugal forces generated by eddies, which drive particles from areas of high vorticity to areas of high strain rate, a process known as preferential concentration (Squires and Eaton, 1991; McLaughlin, 1994; Banko et al., 2020). This phenomenon of preferential concentration is observed at the Kolmogorov scale for Stokes numbers near unity. It extends to larger scales of turbulence, such as the inertial or integral length scales. Hence, particle clustering is common across a wide range of turbulent flow conditions (Bragg et al., 2015). Temperature-dependent viscosity alters the preferential concentration of particles, affecting their clustering within the flow and the regions where particles preferentially concentrate can shift, leading to changes in particle distribution and clustering patterns (Squires and Eaton, 1991; Eaton and Fessler, 1994). Here, the decrease in viscosity leads to lower drag on the particles, making them less prone to being carried by the fluid phase. Consequently, particles are more likely to stay within clusters, even though the decay of TKE occurs at a slower rate. Particle clusters form regardless of the Stokes number, but the clustering

characteristics vary according to the functional behaviour of temperature-dependent viscosity (Saieed et al., 2022).

Some studies have highlighted that, as the temperature changes viscosity, it directly impacts the settling behaviour of particles within two-phase flows (McCullough et al., 2020) and the thermophoretic effect (Reeks, 1983), which causes particles to migrate towards regions of lower turbulence intensity. However, most of these studies are limited to low Reynolds number flows or highly temperature-sensitive fluids (like polymers), gases different from the Newtonian fluids focused on in this review, and studies related to dense particle-laden turbulent flows are rarely reported.

4. Particle-particle interactions

Particle settling unaffected by the presence of other particles or adjacent walls or boundaries is known as free settling (McMechan and Shah, 1991b). In a classification by Tesuji (Tsuji, 2007), the dominant mechanism for the particle-particle interactions has been considered, and two-phase flows have been classified into three categories:

(1) Collision-free flow: Particle-particle interactions can be neglected.
(2) Collision-dominated flow: With an increase in particle concentration within the fluid, particles collide with each other but still become dispersed in the flow field.
(3) Contact-dominated flow: As the particle concentration increases, particles tend to contact each other rather than become dispersed.

The collision-free flows require dilute suspensions, and collision-dominated and contact-dominated flows are a consequence of dense suspensions. According to this classification and these definitions, a proppant-fluid two-phase flow can be considered a dense suspension (Crowe et al., 2011). A particle concentration within a solid-liquid two-phase flow can be used as an index to identify the dilute or dense nature of the flow. Typically, a low particle concentration causes dilute two-phase flow, and high particle concentrations cause dense two-phase flows. Generally, a flow field can contain multiple and heterogeneous regions of dilute and dense flows. Particle settling within a dilute flow depends on the drag force exerted by the fluid. In the case of dense flow, it also depends on the inter-particle collision (particle-particle interaction) (Crowe et al., 2011). The presence of multiple particles and fluids within a system increases the effective viscosity of the flowing media, which is represented as a slurry viscosity. Also, it accounts for a return flow, which changes the drag forces and terminal velocities of each particle within the system (Roostaei et al., 2020b). This phenomenon is the same as with proppant transport, and when a large number of particles are flowing or settling within a single-flow region, the drag force acting on a proppant by the fluid will differ from the drag force exerted on a single isolated particle (Yao et al., 2022). Particle-particle collisions enhance the dispersion of particles within the flow, although the impact is somewhat less noticeable when compared with the impact of rough walls (Mallouppas and van Wachem, 2013). Particle clustering and hindered settling have been identified as cumulatively affecting particle settling velocity for concentrated slurries of proppants/particles (Wen et al., 2022). The contributions of these mechanisms vary significantly with proppant/particle concentrations (McMechan and Shah, 1991a; Mack et al., 2014; Huang et al., 2023).

4.1. Hindering effect

In the context of Stokes flows, the decrease in the average settling speed of particles in suspensions is attributed to a hindrance effect. This effect arises from an upstream fluid flow on average, which can be explained by the principle of mass conservation (Guazzelli and Morris, 2011; Fornari et al., 2019; Morris, 2020). Hindered settling is significantly different from free settling since the terminal velocity of a particle is affected and hindered by surrounding particles when the particles within a slurry flow are sufficiently close (Clark and Quadir, 1981; Barboza et al., 2021). As a result, the mean settling speed of the suspension decreases with increasing volume fraction and becomes smaller than the terminal settling speed of an isolated particle (Fornari et al., 2019). The setting velocities monotonically decrease with incremented particle concentrations - in the absence of interparticle aggregations (Liu and Sharma, 2005). Even though the hindrance can be neglected in dilute slurries, the effect becomes significant at high particle concentrations (Mack et al., 2014; Sahai et al., 2014). In the case of particles settling in narrow slots and pipes, a uniform spatial distribution of particles within the flow is generally assumed and most existing experimental correlations relate average slurry settling velocity to the velocity of a single particle (Novotny, 1977; Harrington et al., 1979; Hannah and Harrington, 1981; Shah and Lord, 1990; Shah et al., 2007). The drag coefficient of a particle settling within a clustering environment is affected by several factors, including the number of surrounding particles, the relative position of the particles, the distance between particles, the particle Reynolds number and the presence of the boundary to the fluid medium (in this experiment a pipe wall) (Liang et al., 1996). Both increments and decrements of the drag coefficient were observed when compared with the drag coefficient on an isolated particle. Hindered settling occurs above the settled bank at elevated proppant concentrations, especially considering proppant movement in the more concentrated saltation layer (Barree and Conway, 1995; Mack et al., 2014). Therefore, hindered settling effects should be included in the modelling of hydraulic fracturing operations, given typical proppant concentrations (Mack et al., 2014; Hu et al., 2019). Due to proppant settling, proppant concentration typically increases downwards, which can rapidly develop a vertical concentration gradient with an effective fluid low-viscosity (McMechan and Shah, 1991a). As a result, hindered settling effects evolve with location and time, affecting proppant settling velocity differentially across the medium (Huang et al., 2023).

Correlations for hindered settling of particles have been previously reported (Burgers, 1942; Maude and Whitmore, 1958; Barnea and Mizrahi, 1973; Zigrang and Sylvester, 1981; Richardson and Zaki, 1997). The hindered settling velocity is quantified by the (terminal) velocity of the hindered particle over its free (terminal) settling velocity. Table 4 summarizes the available correlations correlating the hindered settling with particle concentration and particle Reynolds number.

4.2. Clustering effect (particle agglomeration)

When particles are sparsely distributed in the dilute flow regime, collisions are rare and fluid drag is the dominant force affecting their motion. However, as particle concentrations increase and the separation between particles decreases, collisions occur more frequently (Luo and Tomac, 2018a), impacting how the slurry flows (Tomac and Gutierrez, 2014). Previous studies have shown that dense particle slurries can experience particle clustering, enhancing settling in still (quiescent) suspensions, and these findings have been supported by several studies (McMechan and Shah, 1991a; Economides and Nolte, 2000; Liu and Sharma, 2005; Luo and Tomac, 2018a). Some experimental studies have shown that in dilute slurry transport flows, proppants move together but

Table 4
Correlations for hindered settling velocity of particles and their applicable conditions, where v_{hs} is the hindered settling velocity, v_s is the Stokes settling velocity, c_v is the particle volumetric concentration, and α and β are the empirical coefficients.

Source	Correlation	Particle	Applicable condition
Burgers (1942)	$v_{hs} = v_s(1 + 6.88c_v)^{-1}$		
Richardson and Zaki (1954)	$v_{hs} = v_s(1 - c_v)^{4.65}$	Identical spheres	
Maude and Whitmore (1958)	$v_{hs} = v_s(1 - c_v)^{\beta}$	Identical spheres	For any Re; $\beta = 5$ for mono-dispersed spheres in creeping flow; β is between 2 and 4 in turbulent flow
Aziz (1972)	$v_{hs} = v_s e^{-5.9c_v}$		
Batchelor and Green (1972)	$v_{hs} = v_s(1 - \alpha c_v)$	Identical spheres	$Re_p < 1$, $c_v < 0.05$
	$\alpha = 6.55$ (Batchelor and Green, 1972)		
	$\alpha = 5.5$ (Batchelor and Wen, 1982)		
	$\alpha = 7.5$ (Al-Naafa and Selim, 1992)		
	$\frac{6.5 - \alpha}{\alpha - 3} = 0.1Re_p^{0.74}$ (Di Felice, 1999)		
Barnea and Mizrahi (1973)	$v_{hs} = \frac{v_s(1 - c_v)^2}{1 + c_v\sqrt{\frac{1}{3}e^{\frac{5C_v}{3(1 - C_v)}}}}$	Spheres of common specific gravity with a relatively narrow size distribution	$Re_p < 3500$
Novotny (1977)	$v_{hs} = v_s\left(1 - \frac{c_v}{\rho_p}\right)^{\alpha}$		
	$\alpha = 5.5$		$Re_p < 2$
	$\alpha = 3.5$		$2 < Re_p < 500$
	$\alpha = 2$		$Re_p > 500$
Daneshy (1978)	$v_{hs} = \frac{v_s c_v^2}{10^{1.82}(1 - c_v)}$		$Re_p < 1$
Zigrang and Sylvester (1981)	$v_{hs} = \gamma - \sqrt{\gamma^2 - \alpha^2}$		
	$\gamma = \frac{2\alpha + \delta^2}{2}$		
	$\alpha = \frac{2}{0.63\sqrt{3}}\left[\frac{(\rho_f - \rho_p)gd_p(1 - c_v)}{\rho_f(1 - c_v)^{1/3}}\right]^{1/2}$		
	$\delta = \frac{4.8}{0.63}\left\{\mu \exp\left[\frac{5c_v}{3(1 - c_v)}\right] \Big/ \rho_f d_p\right\}^{1/2}$		
Richardson and Zaki (1997)	$v_{hs} = v_s(1 - c_v)^{\alpha}$	Identical spheres	$0.05 < c_v < 0.5$
	$\alpha = 4.65 + 19.5\,\lambda$		$Re_p \le 0.2$
	$\alpha = (4.35 + 17.5\,\lambda)Re_p^{-0.03}$		$0.2 \le Re_p < 1$
	$\alpha = (4.45 + 18\lambda)Re_p^{-0.1}$		$1 \le Re_p < 200$
	$\alpha = 4.45Re_p^{-0.1}$		$200 \le Re_p < 500$
	$\alpha = 2.4$		$500 \le Re_p$
	$\frac{4.7 - \alpha}{\alpha - 2.35} = 0.175Re_p^{0.75}$ (Rowe, 1987)		$0.2 \le Re_p < 500$
Gadde et al. (2004)	$v_{hs} = v_s(2.37c_v^2 - 3.08\,c_v + 1)$		
Liu (2006)	$v_{hs} = v_s(1 - 4.7892\,c_v + 8.84777c_v^2 - 5.918c_v^3)$	Identical spheres	$Re_p < 1000$

remain adjacent without collision nor rebound, eventually forming particle clusters (i.e. agglomeration) (Davis et al., 1986; Tomac and Gutierrez, 2014; Yamashiro and Tomac, 2021). However, strong and smooth particles tend to collide and rebound from each other and settle as individual particles by separating from each other (Mack et al., 2014). Clustering can be significant even at low proppant concentrations (McMechan and Shah, 1991a). However, most studies have assumed that proppant-laden slurry flows are of homogeneous composition – generally an invalid assumption (Yamashiro and Tomac, 2020a). Further, simplified assumptions based on Stokes law are considered for proppant settling behaviour, and these simplified assumptions are even used in commercial-level hydraulic fracturing software (Sahai and Moghanloo, 2019). These simplifications ignore the tendency of concentrated particles to form clusters and their resulting impact on particle transport and settling (Yamashiro and Tomac, 2020a).

The earliest experimental studies showed that particle clustering could lead to higher average setting velocities than that for a single particle in either Newtonian or non-Newtonian fluids (Clark et al., 1977; Kirkby and Rockefeller, 1985; Roodhart, 1985). Within a particle cluster, particles agglomerate or remain very close to each other - essentially acting as a single structure. In this, the volume-to-surface area ratio reduces relative to that of separate particles, thus accelerating the settling of particles (Mack et al., 2014;

Yamashiro and Tomac, 2020a). Previous experiments of concentrated particles in quiescent flows have indicated that particle settling is enhanced by the formation clusters (McMechan and Shah, 1991a; Economides and Nolte, 2000; Luo and Tomac, 2018a). Settling velocities of agglomerated sand have been observed to increase with the increment in the size of the agglomerate (Luo and Tomac, 2018b). Further, these experimental observations indicate that an increase in slurry viscosity promotes the formation of particle agglomerates and, thus, increases the settling velocities of particles within narrow slots (Luo and Tomac, 2018b). Recently, the static settling velocity has shown to be several times larger than the dynamic settling velocity. This behaviour is attributed to particle clustering, which dominates the static settling process (Hu et al., 2019).

Although the behaviour of concentrated particle slurries with significant particle clustering has been observed, its prevalence and influence in flowing slurries are not fully understood. For example, in some studies, particle clustering is observed only in concentrated slurries settling in still fluids, and researchers have concluded that particle clustering is not vital for flowing slurries (Liu and Sharma, 2005). Notably, this study did not specify the concentrations of flowing slurries evaluated for this clustering. In contrast, particle clustering in flowing slurries has been observed in other vertical fracture slot experiments. Proppant clustering is observed during the initial injection stage into a vertical slot (Kadhim et al., 2017), with particles transported in clusters for concentrations >0.5 lb/gal in Newtonian and non-Newtonian fluids (Clark et al., 1977). Earlier experiments (Sievert et al., 1981) have shown that particles tended to flow more as clusters than as individual particles in proppant slurries with non-Newtonian fluids. These studies suggest that particle clustering in flowing slurries is significant and should be considered when evaluating the behaviour of concentrated particle slurries.

Particle-particle and particle-wall interactions can result in agglomeration or clustering between particles (Zhang et al., 2019). Some recent numerical studies show that the shape of clustering is influenced by the Froude number (ratio of inertial to gravitational forces) and the Stokes number (ratio of particle momentum response time to the flow-field time scale) (Farhan et al., 2015). Differences in these values result in different types of clustering, such as “chain-like” and “curtain-like” shapes (Peker and Helvaci, 2011; Farhan et al., 2015). Also, particle clustering occurs in flowing conditions and significantly affects particle conveyance behaviour (Yamashiro and Tomac, 2020a). The cluster shape and the clustering prevalence depend on the flow rate and particle concentration. Further, particle-level evaluation of two-dimensional (2D) cluster structures reveals a lifting effect (upward drag) in some clustered groupings (Yamashiro and Tomac, 2020a). Compared to the classical Stokes law-based evaluation, this lifting effect further contributes to the conveyance of particles. However, this effect does not persist at higher proppant concentrations, indicating a limited range for the uplifting of clustering (Yamashiro and Tomac, 2020a). Furthermore, cluster shape and spatial distribution depend not only on the injection rate and particle concentration but also on particle settling (Yamashiro and Tomac, 2021). The formation of one-dimensional chain-like clusters at low particle concentrations and the development of 2D curtain-like clusters with increased concentration were also observed.

The importance of the lubrication effect on particle transport and settling results in particle agglomeration and channel clogging (Tomac and Gutierrez, 2013, 2014). A thin fluid layer is formed between particles approaching each other within a viscous fluid. This thin lubrication layer acts as a nonlinear damper that dissipates the kinetic energy of the particles and affects post-collision behaviour (Davis et al., 1986; Barnocky and Davis, 1988). Due to this lubrication effect, particles slow down and sometimes stay adjacent without rebounding. Further, particle accumulations tend to occur when the lubrication effect dominates over other forces (Tomac and Gutierrez, 2015). Due to the formation of irregular proppant agglomerates, the proppant-fluid slurry mixture cannot be considered a uniform slurry flow. The micromechanical particle interactions, fluid counterflows and erratic upward flows that occur during proppant settling lead to proppant trajectories that do not always act in the direction of gravity. These erratic particle trajectories (paths) are formed due to the combined effect of downward particle settling and upward fluid Stokes drag (Tomac and Gutierrez, 2015). This effect can lead to the clogging of fractures or the formation of particle agglomerates, which cause faster settling. Numerical results of particle settling have been compared (Tomac and Gutierrez, 2015) with the correlation proposed by Gadde et al. (2004), Clark and Quadir (1981) and Daneshy (1978) and show how the average proppant settling velocity increases instead of decreases at relatively high particle volumetric concentrations due to agglomeration (Fig. 8). Also, fluid viscosity promotes the lubrication effect, and an increased number of agglomerates are observed in high-viscosity fluids. Therefore, slurry settling rates increase relatively at higher fluid viscosities (Luo and Tomac, 2018a).

In addition to studies on proppant transport in fractures, many studies on turbulent particle dynamics in wall-bounded flows have revealed cluster-induced turbulence (CIT) in solid-liquid two-phase flows. This CIT was first observed for particle flow simulations in a two-dimensional vertical channel (Tsuji et al., 1994). With an increase in particle volumetric fraction within the flow, the impact of the particle phase on the fluid phase can no longer be ignored (Alletto and Breuer, 2012). At significantly higher particle concentrations, the self-organization of particles in dense clusters is observed, known as CIT (Capecelatro et al., 2014, 2015). When exposed to turbulence, the dispersed phase can be driven out of high-vorticity areas and accumulate in high-strain regions (Balachandar and Eaton, 2010). Furthermore, when gravitational effects are significant, the momentum exchange between the different phases can spontaneously form concentrated clusters (Agrawal et al., 2001; Capecelatro et al., 2015). However, the fundamental understanding of the characteristics of clusters and their impact on the carrier phase remains unclear. This behaviour is rarely reported for proppant transport or particle flow in fractures. According to a most recent study on proppant transport in a tortuous fracture, the impact of proppant concentration on proppant velocity is not straightforward (Ma et al., 2022). However, fracture intersection angle significantly impacts this effect. Finally, elevated proppant concentrations account for more particle collisions, clustering and the formation of eddies (Ma et al., 2022). Thus, further studies are required to understand the evolution of particle clusters and cluster-induced characteristics in flows comprehensively.

Moreover, particle shape can significantly affect the turbulence structures and turbulent modulation of the carrier fluid (Gupta et al., 2018) and particle agglomeration (Mortimer and Fairweather, 2019). There are two important aspects regarding the impact of the shape of the particles in turbulent flows: the impact of particles on the turbulent modulation and the impact of orientation and rotation of the particles on particle-fluid interactions (Voth and Soldati, 2017; Gupta et al., 2018). Small finite-sized particles tend to dampen turbulence in the carrier phase (but amplify velocity fluctuations near walls), while larger particles can enhance it (Eaton et al., 1994). Non-spherical particles with a greater mass significantly reduce the streamwise velocity of the fluid compared to a single-phase flow. While turbulence is

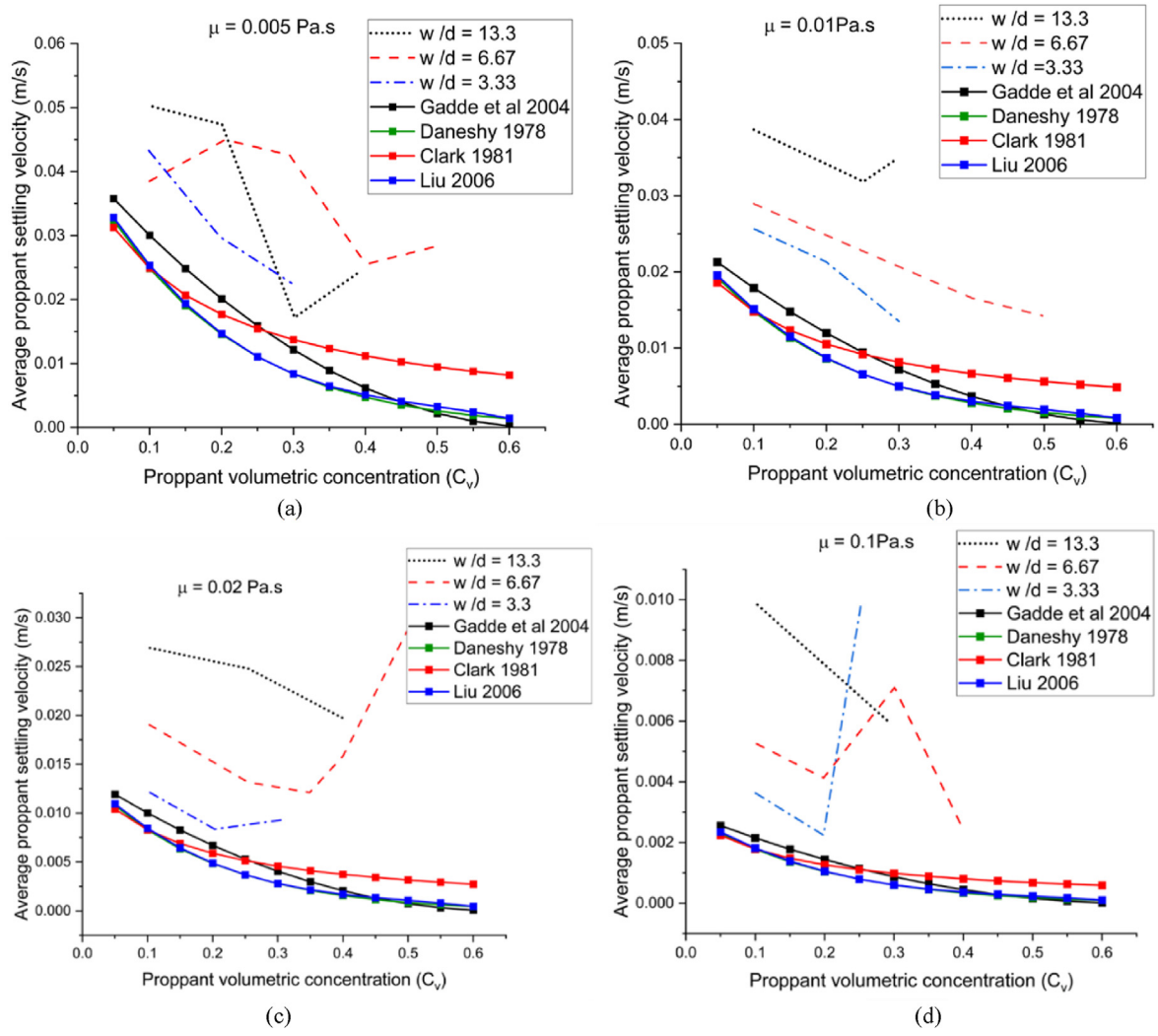

Fig. 8. Comparison of average particle settling velocity with particle volumetric concentration based on previous theoretical and experimental approaches. Dashed and dotted lines are from Tomac and Gutierrez (2015). The ratio of fracture width w and particle diameter d (d = 0.6 mm) is w/d = 3.3–13.3.

diminished by the presence of both types of particles, this effect is more pronounced with heavier particles than neutrally buoyant particles (Eshghinejadfard et al., 2019). For particles smaller than the Kolmogorov length scale (point-particles), even relatively low volume fractions (greater than 0.01%) can significantly influence turbulence within the fluid phase (Elghobashi and Ferrante, 2004). Some studies have observed reductions in Turbulent Kinetic Energy (TKE) by 3% and 15% for prolate ellipsoidal and spherical particles. Spherical particles were observed to remove energy from large scales and reinsert it at small scales. In contrast, ellipsoids removed relatively less TKE from large scales and reinserted relatively more at small scales (Bellani et al., 2012).

It was also noted that an increase in particle aspect ratio tends to decrease the average particle rotation rate (Andersson et al., 2015). Spheroidal particles, compared to spherical ones, exhibit significantly lower rotational velocities near the wall and tend to align more parallel to it (Gupta et al., 2018). While turbulence is dampened in the streamwise direction for both particle types, this effect is more marked in spherical particles. In the radial and tangential directions, turbulence fluctuations for spheroids more closely resemble those of a single-phase flow, unlike spheres, which demonstrate a local concentration peak near the wall. This preferential alignment and rotation are more pronounced near the walls and escalate with the particle's aspect ratio (Gupta et al., 2018). Further, the influence of particle size and inertia becomes distinct when the particle diameter surpasses a certain threshold, altering the local velocity field due to no-slip and impermeability constraints at the particle surface (Elghobashi et al., 2010). The efficiency of particle clustering diminishes with an increase in particle size, leading to a slower agglomeration pace over more extended periods as particles begin to form clusters and the average size of the agglomerates grows. Smaller particles are shown to have a higher propensity for collisions. Moreover, the likelihood of agglomeration following a collision is greater near the centreline of the channel, where the movement of particles tends to result in collisions at lower relative velocities (Eshghinejadfard et al., 2018; Mortimer and Fairweather, 2019).

In conclusion, the settling behaviour of particles in fluid systems, particularly in proppant-fluid two-phase flows, exhibits distinct characteristics influenced by particle-particle interactions and concentration. It is worth noting that a flow field can consist of multiple regions with varying degrees of dilute and dense flows. Two mechanisms, hindered settling and particle clustering, affect the settling velocity of concentrated proppant slurries. Hindered settling becomes more significant at higher proppant concentrations, while clustering can affect settling even at low

concentrations. The lubrication effect becomes more pronounced in narrow channels where particles frequently interact. Future research should focus on addressing several gaps in understanding. Firstly, a deeper understanding of hindered settling and clustering effects on settling velocity in different particle configurations and environments is needed. The influence of factors such as the number of surrounding particles, their relative positions and the presence of boundaries requires further elucidation. Developing accurate correlations for hindered settling in proppant-fluid systems, considering particle concentration and Reynolds number, would also be valuable. Also, studying the evolution of hindered settling effects over time and location is crucial, as proppant settling can lead to concentration gradients and affect settling velocities across the medium. Further research should explore the dynamics of these effects and their implications for proppant distribution and fracture conductivity. While many studies have focused on clustering in quiescent flows, the behaviour of particle clusters in flowing slurries is not yet fully understood under inertial and turbulent flow conditions.

5. Particle-fracture wall interactions

The transport dynamics of particles within fractures is governed by the confluence of complex mechanisms, with particle-wall interactions playing a pivotal role in determining their ultimate distribution (Barboza et al., 2021; Yamashiro and Tomac, 2022). These interactions, crucial for settling particles under the influence of gravity and their horizontal transport amid fluid flow, are markedly influenced by the high-velocity flows within fracture networks (Wu et al., 2016; Zhou et al., 2022; Hangyu et al., 2023). Unlike other dense solid-liquid flows, particle-fracture wall interactions significantly affect proppant transport in hydraulic fractures since apertures are generally small (Wu et al., 2016; Zhou et al., 2022). Understanding the nuances of this behaviour is critical in optimising particle conveyance and elucidating the conditions under which proppant bridging (a phenomenon where particles aggregate, jam, then bridge and block across fractures) occurs. This section discusses particle-wall interactions on particle dynamics within fractures by considering settling, horizontal conveyance, and bridging effects.

5.1. Wall retardation effect on settling

The proximity of fracture walls confining proppant flows retards both the movement of particles and particle settling (Yao et al., 2022). Counterflow of the liquid phase increases the hydrodynamic drag exerted on particles during settling through the gap between particles and the confining wall (Luo and Tomac, 2018a; Roostaei et al., 2020b). As the gap between walls is reduced, the exerted drag force concomitantly increases. Due to this effect, the settling velocities of particles flowing within a confined flow are lower than those in an unconfined flow (Roostaei et al., 2020b; Barboza et al., 2021). The impact of a wall on the settling of particles is known as the wall factor effect or wall retardation effect. The wall retardation effect is defined to quantify the impact of bounding walls on the settling of particles, and this can be expressed in terms of drag force (Latto et al., 1973), velocity change (Duduković and Končar-Djurdjević, 1981) or equivalent viscosity change (Iwaoka and Ishii, 1979). Defining the wall factor (f_w) in terms of the ratio of velocity to terminal settling velocity is most relevant in quantifying wall effects for proppant transport in hydraulic fractures as (Roostaei et al., 2020b; Yao et al., 2022):

$$f_w = \frac{v_w}{v_t} \tag{9}$$

where v_w is the terminal settling velocity of a particle in a fluid flow bounded by walls (corrected settling velocity for the wall effect), and v_t is the terminal settling velocity of the particle in the same but unbounded conditions. Dimensional analysis has shown that the wall effect is negligible for particles settling in a long container, and this assumption is also valid in the case of particles settling in hydraulic fractures. Therefore, the wall effect is only a function of Reynolds number (Re) and ratio (λ) between particle diameter (d_p) and the diameter of the container (D_c) (Roostaei et al., 2020b). Numerous experimental studies on wall retardation effects beyond the creeping flow regime exist, although analytical studies are limited. These studies have shown that under very low and very high Reynolds number flows, wall retardation only depends on the particle diameter to channel diameter ratio (λ) (Clift et al., 1978; Di Felice, 1996; Chhabra et al., 2003).

Numerous empirical correlations have been proposed regarding the wall retardation factor based on particle settling within tubes and cylinders (Munroe, 1889; Francis, 1933; Fidleris and Whitmore, 1961; Di Felice, 1996; Delidis and Stamatoudis, 2009). Apart from tubes and cylinders, many experimental studies have been conducted between parallel plates and in rectangular columns to study particle settling behaviour. By considering the bridging and clogging of proppant in a fracture due to the wall retardation effect, correlations have been defined for the wall retardation factor (Novotny, 1977). Also, the wall factor in a deep, square column is higher than that in a cylinder with a diameter equal to the column width (Balaramakrishna and Chhabra, 1992). Empirical correlations have been developed for wall factors by considering the impact of four bounding walls (Machac and Lecjaks, 1995) and incorporating the influence of fluid viscosity (Liu and Sharma, 2005) (Table 5). Most previous correlations are based on particles settling in quiescent fluids. However, proppant settling during hydraulic fracturing occurs in a dynamic flow environment together with a forward motion of the particles carried by the fluid. Furthermore, horizontal flow does not significantly impact proppant settling in a Newtonian fluid (Liu and Sharma, 2005). An empirical correlation for wall factor representing particle settling in a viscoelastic fluid has been developed by non-linear regression (Malhotra and Sharma, 2012). The correlation for wall factor developed by Song et al. (2019) showed a small increase in wall factor at relatively small Reynolds numbers, followed by a sharp increase at medium Re and then a slowly increasing wall factor at high Re − similar to the trend proposed by Di Felice (1996) (Fig. 9).

Most of the correlations proposed for the wall retardation effect are modified power-law functions accommodating the ratio λ, except those proposed by Liu and Sharma (2005) and Song et al. (2019). Thus, these correlations suggest that wall retardation depends on factors other than the size ratio (λ). Also, few studies transform the wall effect in settling velocity into a correlation factor for the drag coefficient (Zhou et al., 2022). Updating the drag coefficient by incorporating the wall retardation effect is essential in improving the accuracy of numerical modelling in proppant transport simulations.

5.2. Wall effect on the horizontal conveyance of particles

When particles move between two parallel, smooth plates, the flat surfaces create additional hydrodynamic resistance, decreasing particle transport velocity as the gap between the plates narrows (Zhou et al., 2022). Conversely, as particles move between rough-walled plates, the consistent interactions among the particles

Table 5
Correlations for wall retardation factor.

Source	Wall retardation factor	Condition
Francis (1933)	$f_w = \left(\frac{1-\lambda}{1-0.475\lambda}\right)^4$	$Re < 1$ $0.09 < \lambda < 0.83$
Novotny (1977)	$f_w = 1 - 0.6526\lambda + 0.147\lambda^3 - 0.131\lambda^4 - 0.0644\lambda^5$	$Re < 1$
	$f_w = 1 - \lambda^{3/2}$	$Re > 100$
Munroe (1889)	$f_w = 1 - \lambda^{3/2}$	$1000 < Re < 3000$ $0.11 < \lambda < 0.83$
Di Felice (1996)	$f_w = \left(\frac{1-\lambda}{1-0.33\lambda}\right)^{2.7}$	Viscous regime
	$f_w = \left(\frac{1-\lambda}{1-0.33\lambda}\right)^{\alpha}$	Intermediate regime $Re < 200$ $0.08 < \lambda < 0.7$
	$\frac{3.3-\alpha}{\alpha-0.85} = \frac{Re}{10}$	
	$f_w = \left(\frac{1-\lambda}{1-0.33\lambda}\right)^{0.85}$	Turbulent regime $Re > 200$
Machac and Lecjaks (1995)	$f_w = \frac{1}{1+k_1\lambda^* + k_2(\lambda^*)^2}$	$0.00014 < Re < 0.5$ $0.083 < \lambda < 0.343$
	$\lambda^* = \frac{d}{d_e} d_e = \frac{2ab}{a+b} - \frac{2db}{d+b}$	
	d_e is the column effective diameter, a is the column width, b is the column length, coefficients k_1 and k_2 depend on the fluid rheological properties	
Gadde et al. (2004)	$f_w = 1 - 1.563\lambda + 0.563\lambda^2$	$\lambda < 1$
Liu and Sharma (2005)	$f_w = 1 - (0.16\mu^{0.28})\lambda \quad (\lambda < 0.9)$	$Re < 700$ $0.05 < \lambda < 0.94$
	$f_w = (8.26e^{-0.0061\mu})(1-\lambda) \quad (\lambda > 0.9)$	
	μ is the viscosity of a Newtonian fluid	
Malhotra and Sharma (2012)	$f_w = (1-\lambda)^{\alpha}$	$0.0005 < Re < 2.63$ $0.125 < \lambda < 1$
	$\alpha = 0.37\left(\frac{\beta}{1+\beta}\right)^{0.81} Re^{-0.24} n^{0.17}, \beta = \frac{2tv_t}{d_p}, Re = \frac{\rho v_t d_p}{\mu}$	
	t is the relaxation time, n is the flow behaviour index of a power-law fluid, Re refers to the Reynolds number based on the terminal velocity v_t in an unbounded fluid	
Zhang et al. (2016)	$\frac{f_w - 0.001}{0.999} = \left[1 + \left(\frac{\lambda}{0.64}\right)^2\right]^{-0.98}$	$0.0011 < Re < 9.75$ $0.02 < \lambda < 0.83$
Song et al. (2019)	$\frac{f_w - f_\infty}{f_0 - f_\infty} = (1 + 0.165Re^{0.89})^{-2.546}$	$0.0001 < Re < 144.25$ $0.1 < \lambda < 0.9$
	$f_\infty = -0.259\lambda^2 - 0.0608\lambda + 1.0079$	
	$f_0 = -0.7861\lambda + 1.0449$	
Zhang et al. (2019)	$f_w = e^{-25.372\frac{\lambda}{Re}}$	$19.64 < Re < 1261.98$

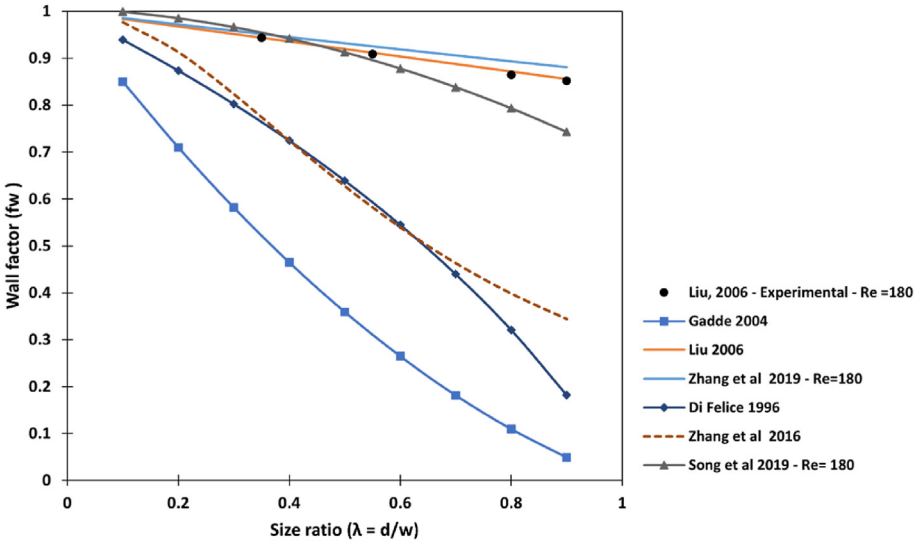

Fig. 9. Wall factor vs size ratio curves. Plotted from the empirical correlations in Table 5.

introduce retardation due to mechanical interference, further reducing velocity. As the particle Reynolds number increases, the impact of this mechanical resistance becomes progressively more pronounced, eventually becoming the primary influencing factor (Zhang et al., 2019). The width of a hydraulic fracture varies from zero near the tip of the fracture to a maximum width towards the initiating wellbore. Thus, the ratio of the proppant diameter to the fracture width varies for different locations along the fracture. Significant velocity differences between the fluid and proppant horizontal velocity may be expected in regions where the fracture width is comparable to the proppant diameter. The retardation effect caused by the fracture walls can significantly hinder proppant transport (Liu and Sharma, 2005; Zhou et al., 2022). Under some circumstances, proppants tend to flow at a velocity higher than the average fluid velocity when the proppant concentration is significantly elevated near the centreline of the fracture. However, if the retarding impact of the wall becomes dominant, proppant velocity can saltate in the finite fluid velocity (Liu and Sharma, 2005).

The average particle velocity is higher than the average fluid velocity for a uniform distribution of particles (Staben et al., 2003). This phenomenon can be primarily attributed to the exclusion of particles from the slowest fluid region near the walls. The maximum average particle velocity may exceed the average fluid velocity by 18% for particles with diameters equal to 42% of the channel height. However, for particles with diameters greater than 82% of the channel height, their average velocities are lower than that of the fluid due to the retarding effect of the walls. Recent numerical studies have identified a notable difference in proppant conveyance in roughed-walled fractures compared to smooth walls (Yamashiro and Tomac, 2020b). The conveyance velocity, both in the case of single-particle and multi-particle systems, is enhanced by the rough walls (Yamashiro and Tomac, 2020b). Experimental studies define the effect of the walls on proppant transport for both smooth- and roughed-walled fractures (Liu, 2006; Liu and Sharma, 2005). These experimental results conclude that the rough-wall configurations substantially reduce the velocity of particles. Empirical correlations define this response (Liu and Sharma, 2005) to modify the horizontal particle conveyance velocity accounting for the wall effect in smooth wall fractures as

$$\frac{v_p}{v_{af}} = -0.862\left(\frac{D}{w}\right)^2 + 0.0475\left(\frac{D}{w}\right) + 1.2713 \quad \left(\frac{D}{w} < 0.93\right) \tag{10}$$

$$\frac{v_p}{v_{af}} = -7.71\left(\frac{D}{w}\right) + 7.71 \quad \left(\frac{D}{w} \geq 0.93\right) \tag{11}$$

where v_p is the particle flow rate, v_{af} is the average fluid flow rate, d is the particle diameter, and w is the fracture width. Regarding the impact of wall retardation on particle horizontal transport in laminar flow for Newtonian fluids, it can be inferred that the effect remains constant regardless of the fluid viscosity. However, the magnitude of wall retardation is influenced solely by the ratio of particle size to cell width (Liu and Sharma, 2005).

When multiple particles move horizontally between parallel plates, the particles shift from regions of high shear (closer to the walls) to areas of low shear (towards the centre of the channel). As a result, their horizontal velocity increases, often exceeding the initial injection velocity. The flat walls of the plates introduce a notable hydrodynamic resistance, which impacts the slippage velocity of the particles. This slippage velocity diminishes as the ratio of the particle diameter to the gap between the plates increases (Liu and Sharma, 2005; Zhang et al., 2019). Furthermore, when particles are confined between two rough parallel plates, there is a significant enhancement in the mechanical interactions among particles and between particles and the walls. This intensifies the forward movement of the particles and inhibits their lateral movement. Generally, hydrodynamic resistance is the primary factor influencing particle motion for low particle Reynolds numbers. However, as the particle Reynolds number increases, particles are more likely to interact with each other and the walls. This increases the effects of mechanical interactions, causing these interactions to gradually become the primary determinant of particle movement (Zhang et al., 2019).

The mechanical retardation caused by rough walls may be quantified via a rough wall factor (V_{MTR}/V_{MTS}), defined as the ratio of particle average horizontal transport velocity between two parallel rough plates (V_{MTR}) to that for two parallel smooth plates (V_{MTS}) (Zhang et al., 2019). A diamensionless composite parameter, represented as Ar/Re, is useful, where Ar represents the Archimedes number, indicating the balance between buoyant and inertial forces. When the Ar/Re ratio is low, variations in the ratio do not significantly affect the rough wall factor, which remains constant. However, the rough wall factor sharply declines when Ar/Re increases beyond a certain threshold (Fig. 10). Where particles move through high-viscosity liquids, the flow inside the channel remains stable. This results in negligible mechanical slowing from drag and is often overlooked. Conversely, in low-viscosity liquids, the interplay among particles and between particles and the walls intensifies. Consequently, the impact of these mechanical interactions in reducing flow velocity becomes much more dominant, eventually being the primary influence leading to a significant reduction in the horizontal speed of the particles (Zhang et al., 2019).

5.3. Particle jamming and bridging

Proppant transport and placement in the fracture are significantly impacted by proppant bridging (Ray et al., 2017; Golovin et al., 2022) since it can stall the injection of the suspension and cause a screen out in the near well-bore area (Garagash et al., 2019). Primarily, geometric constraints control proppant bridging and arching (Osiptsov, 2017; Garagash et al., 2019). Bridging occurs when there is an equilibrium between the hydrodynamic force of

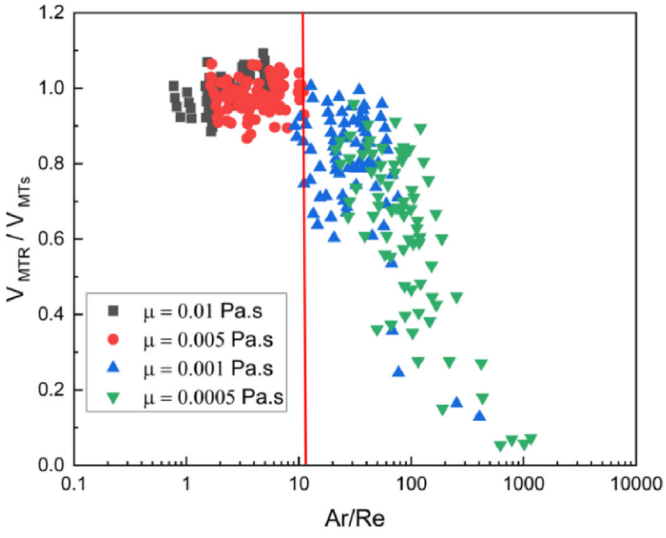

Fig. 10. Variation of average horizontal transport velocity ratio with Ar/Re for particle transport between roughed-walled parallel plates (replotted from Zhang et al. (2019)).

the fluid acting on the particles and the friction force of the walls acting on the particles (Garagash et al., 2019). When a pressure-driven suspension flows through a rough-walled narrow channel, particles lag the flow and slow down due to the interactions between particles and walls of the channel. Eventually, this results in an increase in the mean particle volume fraction. When the fracture is sufficiently narrow to reach the bridging criterion, the concentration reaches the maximum packing limit (Osiptsov, 2017). Since the particles cannot rearrange in the form of a regular train along the fracture, eventually, these particles block the fracture, creating a particle "bridge" or an "arch" between the two adjacent fracture walls. Particle roughness, particle embedment into fracture walls and contact stresses (transmitted through particles) will fix the proppant as a "bridge" that remains stationary where it is formed (Osiptsov, 2017). Such bridges restrict further transport of the suspension upstream from this point. The typical width of a hydraulic fracture is about 1–10 mm (Economides and Nolte, 2000), and this implies that under certain situations, the flow of proppant-fluid slurry can be partially or fully blocked due to the local clogging (bridging) by proppants (Golovin et al., 2022).

In general, the most common method of modelling proppant bridging is to define a threshold width at which particles tend to form a bridge or arch. When any part of the fracture has a width less than or equal to this threshold width (w^*), proppants are prevented from passing beyond this point (Osiptsov, 2017). It has been shown that for low viscosity fluids (1–20 cp) and proppant concentrations up to 0.6 tpm (tonnes of proppant per cubic meter of fluid), proppant bridging occurs when the ratio of fracture width to maximum proppant diameter is ~2 ($w/d \approx 2$) (van der Vlis et al., 1975). But for high viscosity fluids (200 cp) and proppant concentrations up to 1.2 tpm, proppant bridging occurs immediately, even for a larger width-to-diameter ratio ($w/d \approx 4$). By default, in many commercial-level simulation software, the criteria proposed by van der Vlis et al. (1975) are used to determine the critical conditions for proppant bridging (Osiptsov, 2017). It is experimentally determined the bridging factor (b); $b = w^*/d = 2.6$, where d is the particle diameter (van der Vlis et al., 1975). For low proppant concentrations, the bridging factor is 1.8 (Osiptsov, 2017). In industry, a customizable value for the bridging factor is selected from the interval 2.5 to 3 ($w^*/d \in [2.5–3]$) (Gu and Desroches, 2003; Dontsov and Peirce, 2014a).

More sophisticated criteria for proppant bridging following experimental observations have been proposed (Gruesbeck and Collins, 1982). According to these criteria, the critical width depends on the proppant concentration of the suspension upstream of the bridging point. Even though this criterion (Gruesbeck and Collins, 1982) were initially developed for modelling proppant bridging at perforations, a modified version of the proppant bridging criterion is reported (Mack and Warpinski, 2000; Osiptsov, 2017). Where the bridging factor $b = 2.5$ by default, d is the particle diameter, and C_p is the particle volume fraction in the flowing suspension as

$$w^* = \min\left[b, 1 + \frac{C_p}{0.17}(b-1)\right]d \tag{12}$$

Importantly, proppant bridging in slots differs significantly from that in circular openings. Unlike stable multi-particle bridges known to form in circular openings, such bridges are not readily developed in slot geometries (Barree and Conway, 2001). Slot bridging can only occur when particles are too large to fit into the slot and block all available openings. Even when a bridge does form in slots, it is unstable and can be removed by applying any differential pressure when the slot width is slightly above the maximum particle diameter of the proppant pack. Due to this dynamic instability, a fracture cannot be bridged unless the particles forming the pack have a diameter equal to or larger than the slot width ($w/d \approx 1$) (Barree and Conway, 2001) – with this confirmed by several experimental studies (Koivisto and Durian, 2017; Ray et al., 2017). Recently, the occurrence of bridging has been quantified by estimating the corresponding percentage of proppant reaching secondary fractures (Kou et al., 2019). Further, the critical effect of proppant concentration C_p and the ratio between the secondary fracture aperture and proppant diameter (R_{fp}) on the occurrence of proppant bridging has been explored. For a constant value of R_{fp}, continuous transport of proppant can be obtained when proppant concentration (C_p) is lower than a threshold value. Based on these observations, the following bridging criterion is proposed (Kou et al., 2019):

$$C_{\mathrm{p-max}} = \frac{3}{4}R_{fp}^3 - \frac{1}{2} \tag{13}$$

A dynamic criterion for the bridging and arching of proppants in a 3D suspension flow through a channel with plane walls has been developed (Garagash et al., 2019). This dynamic bridging criterion is based on two nondimensional parameters: the particle size to channel width ratio and the normalized flow velocity. A range of critical velocities in which bridging initiates has been identified for each scaled particle diameter. This approach differs from previous approaches based on pure-kinematic criteria formulated in terms of the particle diameter ratio to the channel width, with an effort to consider the dynamics of the bridging process via numerical simulations and solid mechanics considerations. The results show that there is an interval of fluid velocities that supports the formation of bridging ($v_1 \le v \le v_2$) (Garagash et al., 2019); when the flow velocity is below the required velocity range ($v \le v_1$), the bridge forms but slips on the walls. But when the fluid velocity is within the range ($v_1 \le v \le v_2$), then the frictional force exerted on the particles is sufficiently high to withstand the hydrodynamic forces exerted on the particles to keep the proppant bridge immobile (Garagash et al., 2019). Particle bridging is a multistage process (Golovin et al., 2022) with a stochastic nature in which the initial clogging event is arbitrary in terms of time and position. Bridging begins with clogging by two particles and forming a local island of bridged proppants. Arches then form, connecting the previously developed islands of bridged proppants. Finally, the accumulation of proppants continues and complete sand-out of the cell develops (Golovin et al., 2022). Thus, twin-particle bridging is sufficient for triggering proppant bridging with triple-particle clogging rarely occurring, although possible with adequate time with high particle concentrations (Golovin et al., 2022). Within the range of parameters studied, initial clogging is independent of flow velocity (Golovin et al., 2022).

In conclusion, the occurrence of jamming can be reasonably predicted by estimating the maximum volume fraction of solids. Meanwhile, fracture models can anticipate bridging events by examining the ratio of slot width to particle size, typically below 3 to 10, although this number is often adjusted based on experience. Simulations have shown that dynamic proppant bridging criteria are considerably influenced by the size and shape of bridged zones. Furthermore, dynamic bridging creates a much lower pressure drop along the channel, ultimately influencing the final shape of the hydraulic fracture. Thus, it is essential to conduct simulations using coupled geomechanics and fluid mechanics models to understand the dynamic impact and feedback of proppant bridging on the hydraulic fracturing process. The exact position and time of the initial clogging events are arbitrary, although they typically initiate from twin-particle jamming. The formation of arched structures depends on several factors, including local inhomogeneities in the

inlet proppant concentration. When the accumulation of granular material upstream of the blocked region is sufficiently slow, the region blocked by the bridged proppant can be penetrated by the dilute slurry. However, further statistical analysis is required to obtain a probabilistic description of all these processes. Predicting bridging events remains complicated by the physics and complex feedback that govern these phenomena. Bridging is a discrete event influenced by the likelihood of its occurrence, which cannot be adequately resolved by continuum models or accurately predicted by discrete models.

6. Fracture complexity

Complex fracture networks are formed during reservoir stimulation by creating primary, secondary and tertiary hydraulic fractures. The presence of open and healed natural fractures may facilitate the development of these networks. Micro-seismic imaging reveals that shale reservoirs tend to generate more intricate fracture networks than conventional tight gas reservoirs, which typically exhibit simple bi-wing fractures (Sahai and Moghanloo, 2019). The complex geometry of these networks, including step-overs, corners, junctions, and pinch points, can significantly affect proppant placement (Osiptsov, 2017). Recent literature has focused on studying particle transport and distribution in complex fractures through experiments and numerical simulations (Hu et al., 2018b; Li et al., 2018; Zhang et al., 2019; Xiong et al., 2020; Chun et al., 2021). When a fracture propagates, it may temporarily deviate from its original trajectory along interacted joints or natural fractures before returning to its original direction, eventually creating a stepwise and tortuous path (Qu et al., 2021b). Experimental investigations and mine-back evidence have demonstrated the existence of various irregular fracture morphologies, such as branched, T-shaped and curved fractures (Warpinski and Teufel, 1987; Arash Dahi et al., 2013; Lee et al., 2015; Fu et al., 2019). Thus, the interaction between slurry and complex boundaries can significantly affect particle migration and deposition (Lee et al., 2015; Fu et al., 2019; Wang et al., 2019).

6.1. Threshold velocity and transport mechanisms

Dayan et al. (2009) were the first to perform laboratory slot flow experiments to investigate the transport of fracturing fluid into secondary fractures. This study revealed a threshold flow rate below in which fluid flow into the secondary fracture does not occur. Also, a significant proppant build-up within the primary fracture must occur to transport proppants into the secondary fracture. The tendency of proppant to enter secondary fractures decreases when the secondary fracture is distant from the main fracture root due to the loss of velocity and the tendency to follow multiple paths when moving away from the wellbore zone (Dayan et al., 2009). When a secondary fracture is perpendicular to the primary fracture, a minimum velocity is required to transport proppants into that secondary fracture (Chang et al., 2017). Mathematical models define the critical turning velocity at fracture intersections and show that the bulk proppants tend to follow a straight trajectory within the primary fracture and resist turning into orthogonal secondary fractures (Chang et al., 2017). Results further reveal that the fracture intersections also introduce the recirculation of proppants, which is governed by the complex geometry of the fracture. A large-scale laboratory experiment showed a disturbance zone around the fracture intersection due to the large number of vortices in the flow field and the increased flow rate (Li et al., 2022). However, with a further increase in the injection rate, the disturbance zone gets depleted, proppants tend to follow a straight trajectory, and the amount of proppant diverted into the secondary fracture decreases. Thus, an optimal flow rate range maximises proppant transport into secondary fractures (Li et al., 2022).

Previous experimental observations have revealed two mechanisms controlling the migration of proppants/dense particles into subsidiary fractures (secondary and tertiary fractures). These are: (1) suspension effects, where the proppant flows around the intersection corner at a fluid velocity higher than a threshold value; and (2) gravity effects, where the proppant falls from the primary dune and rolls into the secondary fracture from the dune surface formed within the primary fracture (regardless of the flow velocity) (Sahai et al., 2014; Wen et al., 2016; Pan et al., 2018; Sahai and Moghanloo, 2019; Zhang et al., 2022b). Also, a significant build-up of particles within the primary fracture should occur before particles are transported into the secondary fracture, i.e. the proppant bed height should reach a sufficient height (Xiao et al., 2021). In general, particles moving into the secondary fracture by "rolling" will migrate less far in the secondary fracture (Zhang et al., 2022b). Fluid displacement is the most critical factor that controls the form of the proppant distribution within the primary fracture (Pan et al., 2018), which is different in primary and secondary slot configurations (Sahai et al., 2014). Two mechanisms are identified regarding the accumulation of the proppants within the tortuous fracture segment (Qu et al., 2021b). The first mechanism is particle settling promoted by inter-particle collision between suspended particles. The second is that of collision with fracture walls and deposition of the resuspended particles (Qu et al., 2021a, 2021b). Studies of transport in tertiary fracture slots and complex fracture networks have concluded that fracture complexity and turning corners are not the major factors that limit the proppant transport – rather, it appears to primarily depend on the development of dunes within the preceding fractures as a plentiful source of supply (Alotaibi and Miskimins, 2018).

6.2. Impact of fracture intersection angle

Experimental and numerical studies on particle transport in fracture networks with different types of secondary and tertiary fracture networks confirm that particle/proppant placement within the secondary fracture decreases with increasing bypass/

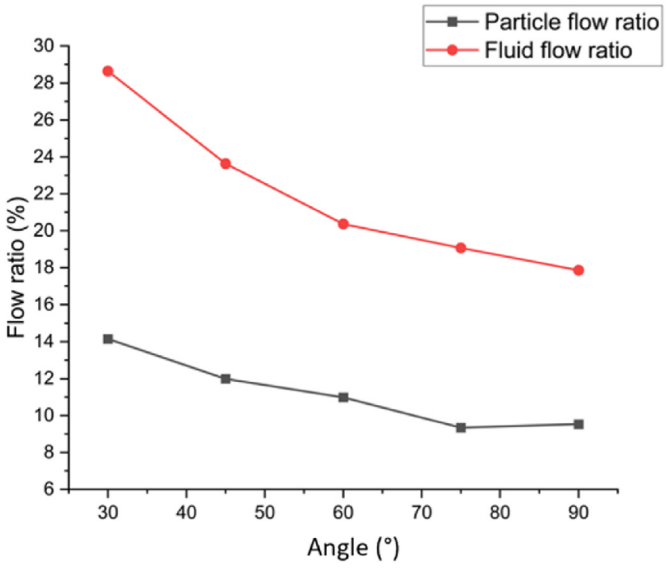

Fig. 11. Flow ratios for proppant transport into secondary fractures at different intersection angles (replotted from Zhang et al. (2022b)).

intersection angle (Tong and Mohanty, 2016; Li et al., 2017, 2018; Pan et al., 2018; Wang et al., 2019). With an increase in the intersection angle between the primary and secondary fracture, the fluid and particle flow rate into the secondary fracture decreases quadratically (Fig. 11) (Zhang et al., 2022b). Further, due to the combined effect of inertial and centrifugal forces, the percentage of particles transported (diverted) into the secondary fracture is reduced when compared to the percentage of the fluid diverted – due to the inertia of the proppants. Both experiments and models show that proppant placement in secondary fractures significantly increases with increasing shear rate (Tong and Mohanty, 2016). Also, depressions in sand beds at fracture intersections are identified with the formation of vortices, which causes significant erosion of the sand bed (Tong and Mohanty, 2016, 2017). The fracture node (turning point) has a significant impact on reducing fracture conductivity and the effective supporting area (Wen et al., 2016). The effect of the secondary fracture is greater when it is closer to the wellbore. Proppant distribution within the secondary fractures close to the wellbore depends on the carrying capacity of the fracturing fluid. Similarly, gravity plays a major role in the secondary fractures distant from the wellbore, where pressure gradients are small (Wen et al., 2016).

Experimental and numerical simulations define the impact of the secondary fracture angle on proppant settling within the primary fracture (Li et al., 2017). When the secondary fracture angle varies, the balanced height within the primary fracture is also susceptible to changes. Thus, with increasing secondary fracture angle from 30 to 90°, the dune height within the secondary slot decreases, but the propped area within the secondary slot increases. When the injection rate and proppant ratio increase, it decreases the balanced height in the primary fracture. The results indicate that secondary fracture balance height decreases with an increasing injection rate of the proppants. Fluid flow gradually transits from laminar to turbulent flow with increasing propped fracture height (Pan et al., 2018). The mass ratio of proppants within the primary fracture is proportional to the secondary fracture angle. The mass ratio of proppants in secondary fractures is proportional to the fluid displacement and inversely proportional to the secondary fracture angle and proppant concentration (Pan et al., 2018). Confirming these results, proppants tend to settle along the length of the secondary fractures with small intersecting angles and settle along the height of the branch with larger intersecting angles (Zhang et al., 2020c). Also, dune development within fractures is categorised into two regimes: (1) dune development within the secondary fracture dependent on the degree of dune development in the primary fracture, and (2) simultaneous development of proppant dunes in the primary and secondary fractures (Zhang et al., 2020c). More importantly, a sensitivity analysis reveals the impact of several different factors on proppant transport, indicating that the sensitivity to proppant transport is defined in the order of fracture geometry, the performance of the proppants, fracking fluid viscosity, fluid displacement within the fracture network and proppant concentration (Peng et al., 2022).

Proppant transport in a tortuous fracture (curved slot) has been studied comprehensively (Qu et al., 2021a, b, 2022). Depressions of particle beds are identified within all proppant beds within the tortuous fracture (Qu et al., 2021b). Due to the hindrance effect caused by bends due to fracture offset, highly turbulent flow is generated above the particle beds, creating vortices, eventually leading to the erosion of beds, which in turn affects depression height. These depressions account for the discontinuous covering of proppants within the tortuous fracture, thus reducing conductivity within the tortuous fracture (Fig. 12). When the height of the proppant bed reaches a threshold value, turbulent flows above the bed generate particle vortices around the bends of tortuous fractures. The results indicate that tortuous fractures enhance the transport capacity of small-diameter proppants – potentially resulting from resuspension (Qu et al., 2021b). In a tortuous fracture, small and light particles tend to be transported long distances within the fracture since they are readily suspended in the fluid (Qu et al., 2021b). Also, the impact of proppant concentration on dune face slopes and proppant velocities is ill-constrained; however, intersection angles impact the activation of this effect. Finally, increased proppant concentrations account for more particle collisions, clustering and the formation of eddies (Ma et al., 2022).

6.3. Fluid inertial effects

Several recent studies have investigated non-deformable particle transport in channels that experience flow-induced stresses. In such conditions, two types of migration phenomena occur. The first is shear-induced migration (Hampton et al., 1997; Koh et al., 1994), primarily relevant to relatively concentrated suspensions and influenced by suspension normal stresses (Morris and Boulay, 1999; Nott and Brady, 1994). The second mechanism is inertial migration, which drives individual particles to specific equilibrium positions in pressure-driven flow in tubes (Han et al., 1999; Matas et al., 2004) and channels (Chun and Ladd, 2006; Matas et al., 2009). Previous studies have examined inertial migration in straight, square channels. Based on these findings, particle-laden flow behaviour within different channel geometries has been studied, with some of these studies motivated by particle transport in hydraulic fracturing (Manoorkar et al., 2016, 2018). Also, several recent studies have highlighted the impact of fluid inertia (inertial forces) on particle transport in cross-intersecting fractures (Zhang et al., 2020a, 2022b; Mao et al., 2021; Wang et al., 2022b).

The manner in which particles and fluid are distributed into the two branches of a T-channel depends on several factors, including flow rate, size and shape of the particles, cannel dimensions and boundary conditions (Morris, 2020). Also, 3D geometry, fluid inertia and sudden changes in flow direction generate secondary circulations in complex spiral streamlines in single-phase Newtonian fluids (Manoorkar and Morris, 2021). Four recirculation regions emerge in T-junctions, with one in each outflow quadrant originating from near the stagnation line at the symmetry plane (Fig. 13). In the case of isolated particles, most follow the fluid streamlines near the junction under dilute concentrations. However, some deviation occurs when the fluid experiences rapid acceleration, such as when a particle is on a streamline that approaches the stagnation line, collides with the wall or enters the central region of an eddy. Despite following similar spiral trajectories to that of the fluid, particles are unable to respond to abrupt changes in the fluid flow direction, due to their finite size (Manoorkar and Morris, 2021). For instance, when particles cannot reach the near-wall streamlines, they avoid the recirculating regions associated with the two separation zones. When particles interact with the boundary in a symmetric T-channel, the strong wall-normal flow can carry the particles into the stagnation zone at the bifurcation (Morris, 2020).

A recent study focused on the flow of pure and particle-laden fluids through a laboratory bifurcation model in a fractured formation (Manoorkar et al., 2016). Flow within the T-shaped geometry exhibits separation at the sharp corner at high Reynolds numbers, forming two separation zones. The first zone occurs in the side branch, while the second occurs in the straight channel opposite the side branch. This study revealed that inertial migration significantly affects the particle distribution in the two channels at different Reynolds numbers (Manoorkar et al., 2016). Suspension flow partitioning at a T-bifurcation under neutrally buoyant conditions was investigated (Manoorkar et al., 2018)

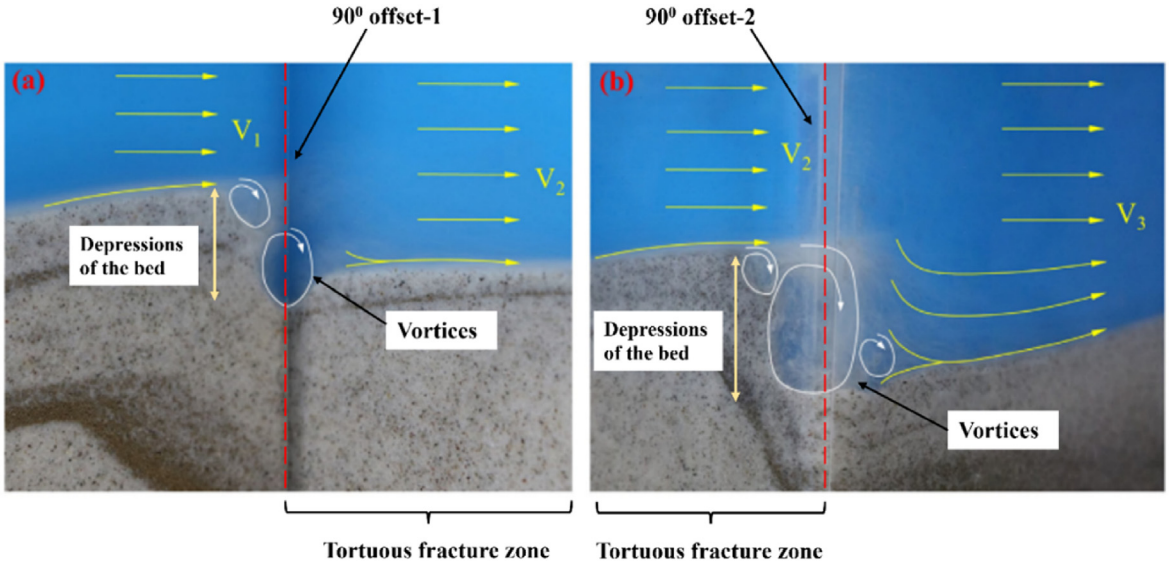

Fig. 12. Experimental observation of particle flow in a tortuous fracture (90° offsets) with the formation of vortices resulting in depressions in the proppant bed (Qu et al., 2021a).

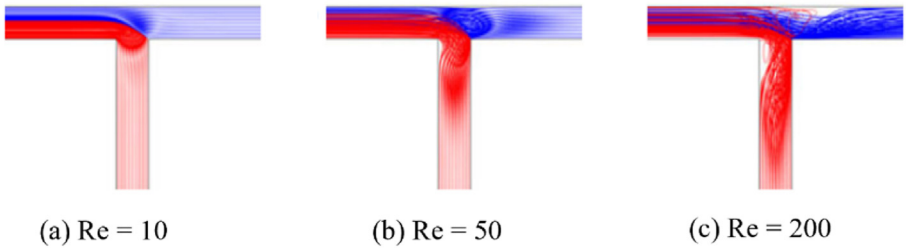

Fig. 13. Flow distribution in a T channel at low *Re* flows (a) and the appearance of separation zones as *Re* is increased, at the corner entering the side branch (b), and on the opposite wall (c) using COMSOL simulations (Manoorkar et al., 2018).

where the volumetric flow rate ratio within the straight outlet branch and inlet branch (β) used to quantify the partitioning of the suspension flow. The analysis revealed fundamental differences between the partitioning behaviour of pure fluids and suspensions at a flow bifurcation. A T-bifurcation created a flow in which inertial effects were significant in partitioning single-phase Newtonian fluid into the two downstream branches. As the Reynolds number (*Re*) increases, the straight branch becomes increasingly favoured as the path for the fluid (Fig. 14). These findings suggest that inertial forces play a critical role in determining the partitioning behaviour of the fluid at the bifurcation and also show good agreement with previous studies (Manoorkar et al., 2016). However, this trend is less pronounced as the solid volume fraction (φ) increases. Notably, for φ values equal to or greater than 0.2, the tendency for more material to exit through the side branch is reduced. This behaviour can be explained by shear-induced migration at higher φ values in the inlet branch and results in a depleted layer of particles near the walls being more easily entrained into the side channel (Morris, 2020).

Particle trajectories approaching the stagnation region were similar to those calculated in Stokes flow (Manoorkar and Morris, 2021). However, under the same conditions, large separation regions are observed at the corners entering the outlet channels, indicating the influence of bulk inertia. A significant challenge in using simple, effective viscosity models in suspension flows with complex geometries was highlighted in this study (Manoorkar and Morris, 2021). This difficulty has also been observed in a previous study of a suspension flowing through an asymmetric T-channel,

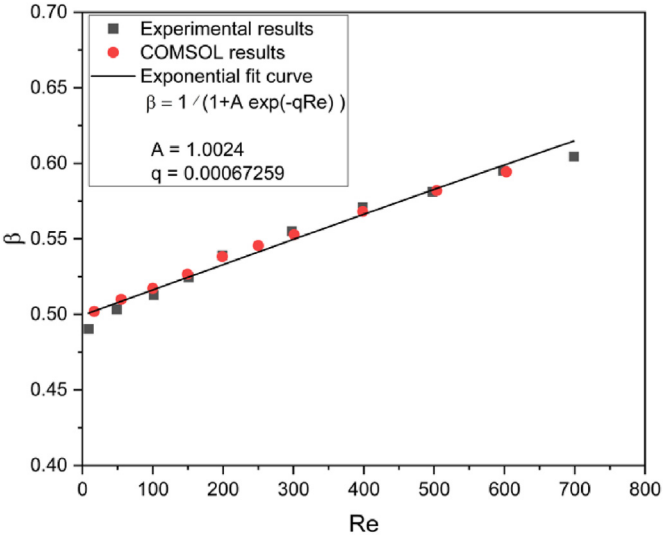

Fig. 14. For a single-phase Newtonian fluid, the flow partitions equally at a small Reynolds number (*Re*) and progressively favours the straight channel as the flow rate increases (replotted from Manoorkar et al. (2018)).

where the lack of a migration model required consideration of extended flow domains (Manoorkar et al., 2018). In this study, the failure of the effective fluid model is attributed to the localized

stagnation line region, and it is suggested that additional dissipation should be considered due to interactions between the particle-laden flow and the boundary in such wall-normal flows (Li et al., 2020a, b). The dependence of particle partitioning in dilute suspensions on Reynolds number (*Re*) may be explained at a semi-quantitative level through a combination of separate analyses of (i) particle migration in pressure-driven suspension flows in straight channels and (ii) single-phase fluid flow in the bifurcation (Manoorkar et al., 2018). However, it is also observed that this decoupled approach becomes invalid at higher concentrations, at least partially because of the influence of particles on the suspension rheology (Manoorkar et al., 2018). Specifically, the partitioning of particles leads to a higher solid fraction in the straight branch, resulting in higher effective viscosity and increased wall shear stress at a given flux in this branch. This phenomenon leads to a higher flux in the side branch for large Reynolds numbers, in contrast to the prediction of an effective fluid model that assumes uniform concentration and yields results similar to those for a single-phase fluid. These findings suggest that upstream particle migration is coupled to the downstream hydraulic relation between axial flux and pressure gradient (Manoorkar et al., 2018).

The migration of particles in the regime of a bisection is due to a combination of shear-induced migration and inertial migration (Manoorkar et al., 2018), consistent with previous work related to tube flow (Hampton et al., 1997; Ahmed and Singh, 2011). Due to this migration, a larger fraction of particles migrate through the straight outlet, increasing the effective viscosity of the suspension and resulting in a higher flow resistance in the straight channel. This effect on the downstream hydraulic relation between flux and pressure gradient has not been previously reported. This result becomes even more apparent when considering the ratio of fluxes, where $\beta_{\text{particle}} > \beta_{\text{fluid}}$ for elevated values of particle volume fraction (φ). This difference in partitioning behaviour is also reflected in the solid volume fraction in the straight outlet branch, as shown in Fig. 15, where an increase in the solid volume fraction is observed in the straight outlet branch. Fig. 16 illustrates the significance of boundary conditions in suspension flows. The inability of particle centres to reach the near-wall streamlines implies that particles seldom encroach into the recirculating regions associated with the two separation regions, highlighting the influence of boundary conditions on the distribution and behaviour of particles in suspension flows (Morris, 2020).

Several recent studies have revealed the impact of fluid inertia on dense particle flows at fracture intersections. Proppant transport in cross fractures has been investigated numerically (Zhang et al., 2020a), and the proppant behaviour is described using mainly two parameters: equilibrium proppant height (EPH) and the ratio of proppant mass (RPM), the RPM in the secondary fracture to the proppant mass in the cross-fracture network. RPM decreases with increasing Reynolds number; thus, the proppant barely enters the secondary fractures of the cross-fracture network when the Reynolds number is large (Fig. 17a) (Zhang et al., 2020a). The outcome of lattice Boltzmann simulations (Wang et al., 2022b) was in agreement with these findings in which the proppant/particle transport into the subsidiary fractures from the primary fracture was characterized by the proppant leak-off ratio (α). This is the ratio between the number of particles existing through the side branch and the total number of particles entering the computational domain. Increasing the Reynolds number decreases the particle (proppants) leak-off ratio (Fig. 17b) (Wang et al., 2022b).

Moreover, with an increase in the flow rate, the Reynolds number increases, and inertial migration becomes dominant in transporting the proppant (Wang et al., 2022b). Particles within the fracture are more prone to move into the centre of the primary fracture as *Re* increases, and this behaviour is qualitatively represented in Fig. 18. Also, the position of the clustering of the proppants moves up towards the centreline of the fracture as a result of this inertial effect with increasing *Re*. Due to the combined effect of inertial, centrifugal and fluid drag forces, the particle flow rate within the secondary fracture is considerably lower than that in the primary fracture (Zhang et al., 2022b). However, variations in the impacts of these factors depend on the fracture geometry, fluid and particle properties. Particles entering the secondary fracture are subjected to the combined effects of inertial forces of particles and drag forces of the fluid, and due to these effects, an arc-shaped particle-free zone is created at the inlet of the secondary fracture (Fig. 16).

Plug-and-perforation (P-n-P) completion of hydraulic fractures is common during slick water fracturing for horizontal wells. The transport of proppants in multiple fractures (near the heel, middle fracture, and near the fracture toe) at field scale shows uneven distribution and placement of proppants within fractures and their driving mechanism while providing strategies to improve the proppant placement from the perspective of P-n-P treatments (Mao et al., 2021). The results of simulations reveal a heal-biased proppant distribution (most proppants are transported into the first

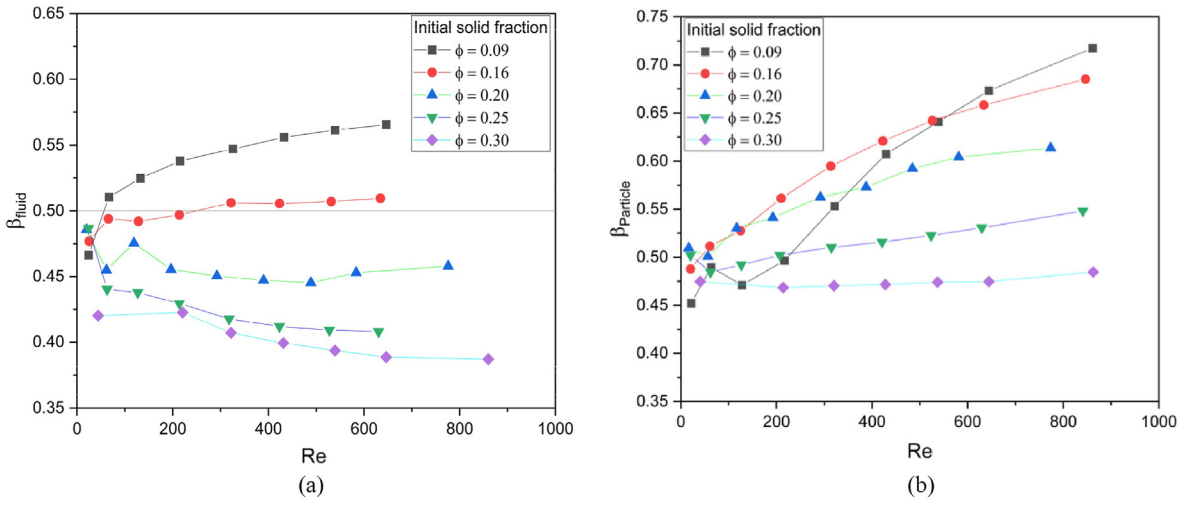

Fig. 15. Component split in a T-channel as a function of *Re* for different inlet solid fractions: (a) Fluid split, and (b) Particle split (replotted from Manoorkar et al. (2018)).

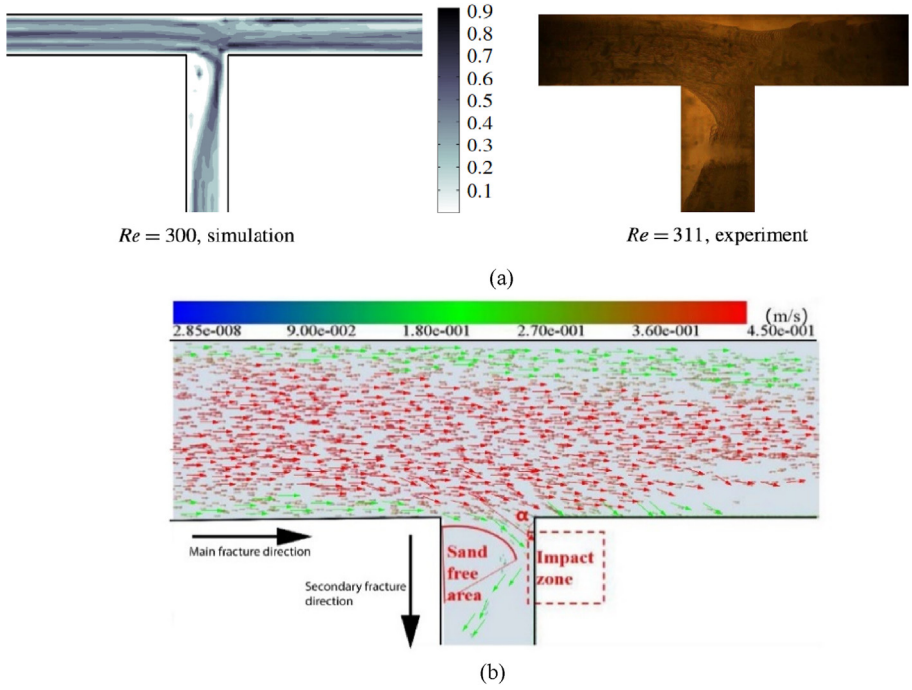

Fig. 16. Comparison of results of experiment and numerical simulation of solid particle distribution at a bifurcation for neutrally buoyant suspensions (Morris, 2020). Formation of the particle-free zone at the fracture intersection (dense particle) (modified from Zhang et al. (2022b)).

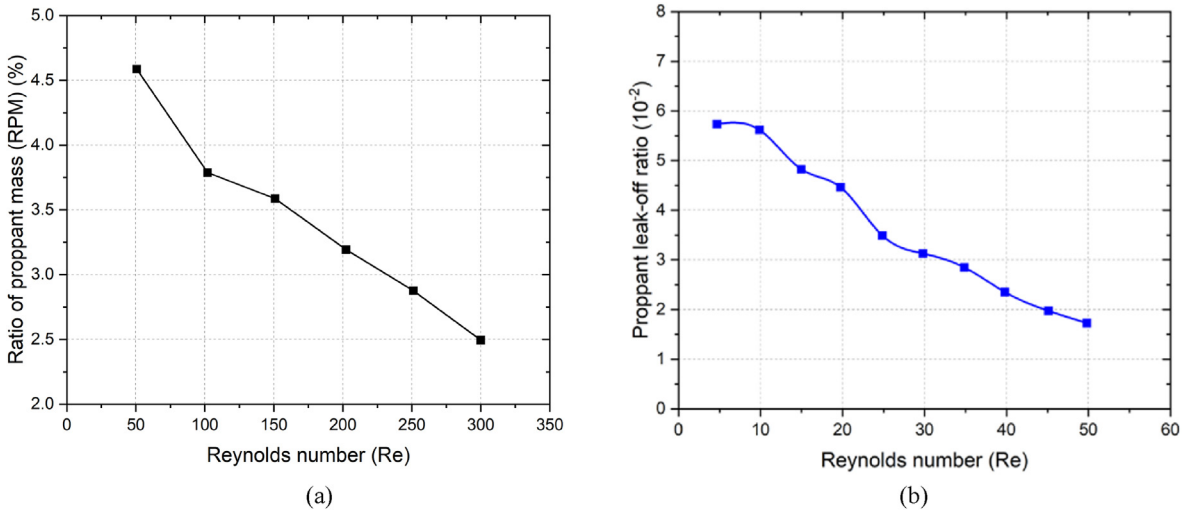

Fig. 17. (a) Variation of the RPM with Reynolds number (replotted from Zhang et al. (2020a)); and (b) Simulation results: Variation of proppant leak-off ratio (α) with the Reynolds number (Re) (replotted from Wang et al. (2022b)).

fracture near the heal), which agrees with several field observations. At the initial stage of injection of the proppants, most of the proppants tend to mobilize into second and third fractures (toe side) due to the inertial fluid effect (Fig. 19). If the fluid velocity near the first fracture (heel) was too large, the fluid flow would not be diverted into the first fracture due to inertial effects. Similarly, much of the proppant will move with the fluid passing the second fracture and forward towards the third fracture (toe side). At a later stage, since the proppant concentration increases near the toe side, injected proppants tend to enter into the first fracture (heel side) (Mao et al., 2021).

In conclusion, many studies have explored the rheology of suspension flows and focused on the flow within the Stokes regime, with limited attention given to the particle dynamics in the inertial regime of channel flow and fractures. Detailed investigations of particle dynamics in inertial and turbulent regimes within complex fracture geometries have rarely been reported. Moreover, the dynamic nature of neutrally buoyant particles within channels is commonly reported, while heavy particle dynamics is seldom found. Caution must be exercised when extrapolating such correlations based on experimental/numerical findings into dense particle dynamics in fracture flow. For higher concentrations of particles, bulk suspension flow is significantly affected by particle-induced rheological effects. While there have been efforts to connect local particle behaviour to the overall flow characteristics within channels in the inertial regime, the complexity of the flow

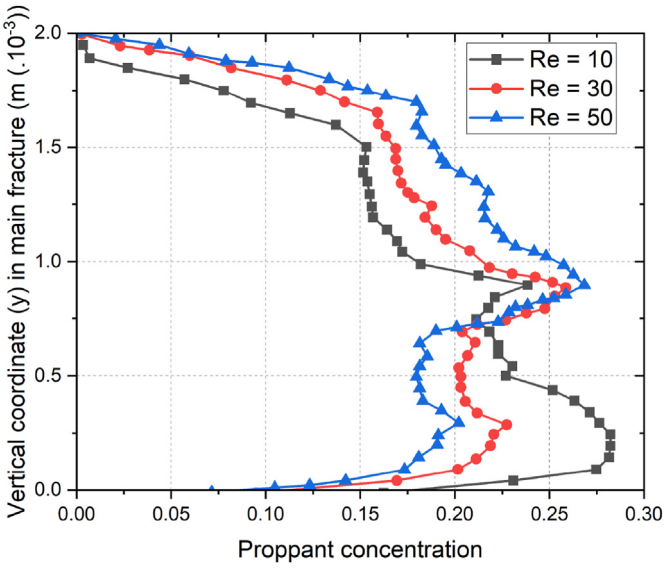

Fig. 18. Simulation results: Variation of proppant concentration with vertical coordinate (y) of the main fracture for different Reynolds numbers (Re) (replotted from Wang et al. (2022b)).

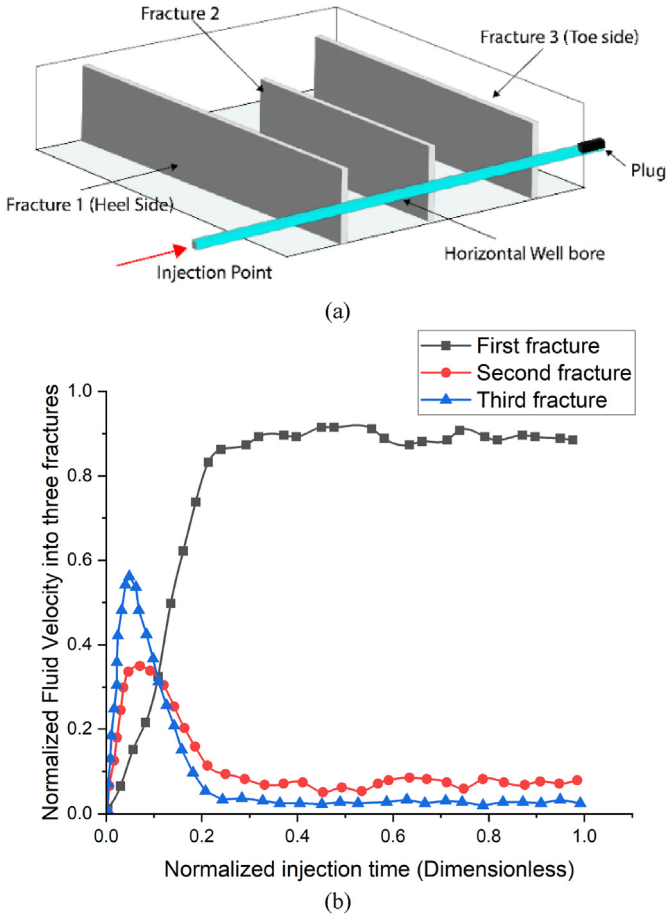

Fig. 19. (a) Computational cell configuration of the wellbore fracture system, and (b) Evolution of normalized fluid velocity flowing into the three fractures during the entire injection (replotted from Mao et al. (2021)).

makes modelling a challenging task. How fluid and particles are distributed into subsidiary fractures and side branches depends on several factors, including *Re*, size and shape of particles, particle volumetric concentration, channel geometry and boundary conditions. In particular, the partitioning of fluid and particles into branching fractures involves fluid inertial effects. However, significant research gaps remain in accurately predicting this dynamic behaviour, which leads to ineffective particle distributions into subsidiary fractures in proppant transport. Laboratory experiments conducted using complex slot configurations have indicated that the complexity of the configuration does not pose a significant limitation on slickwater proppant transport. Instead, proppant transport in subsidiary fractures is primarily influenced by the presence of well-developed proppant dunes in preceding fractures.

7. Summary of particle-fluid modelling approaches

Basically, two approaches available for modelling two-phase flows: the Eulerian-Eulerian approach and the Eulerian-Lagrangian approach (Andrews and O'Rourke, 1996; Prosperetti and Tryggvason, 2009; Barboza et al., 2021; Wen et al., 2022). The primary distinction between these approaches lies in treating the dispersed phase. In the Eulerian-Eulerian method, both the fracturing fluid (continuous phase) and the particles (dispersed phase) are modelled as continuous media that interpenetrate (Barboza et al., 2021; Wen et al., 2022). In contrast, the Eulerian-Lagrangian approach treats the continuous fracturing fluid phase with Navier-Stokes equations, while the dispersed particle phase is modelled using Newton's laws (Barboza et al., 2021). Two primary versions of the Eulerian-Eulerian approach are employed in particle transport modelling in fracture flows: the mixture and the two-fluid models. The mixture model resolves the flow using a single set of Navier-Stokes equations to determine the average properties of the slurry. In contrast, the two-fluid model uses two sets of Navier-Stokes equations to represent the fluid and proppant phases individually (Barboza et al., 2021). Three distinct types of Eulerian-Lagrangian schemes have been utilized: the Dense discrete phase Model (DDPM), coupled Computational Fluid Dynamics-Discrete Element Method (CFD-DEM) and the Multiphase Particle-in-Cell Method (MP-PIC) (Adnan et al., 2021; Wen et al., 2022). DDPM and MP-PIC methods are considered hybrid Eulerian-Lagrangian methods since the particle phase in these models exhibits continuum and discrete properties (Wen et al., 2022). Each proppant particle is individually simulated using the DEM approach in the CFD-DEM framework. On the other hand, the MP-PIC model groups particles sharing similar properties into a single entity, known as a parcel, and tracks these parcels collectively (Barboza et al., 2021). A brief comparison of numerical approaches for particle-fluid flow modelling is given in Table 6.

8. Future directions and improvements

Gaining a deeper insight into particle transport mechanisms in fractures, particularly under fluid inertia and turbulent flows, is paramount. This review underscores several knowledge gaps, and potential research hotspots within this domain warrant further investigation.

Research on the behaviour of particles in inertial and turbulent flows through fractures is still emerging, with most studies focusing on particle settling without considering the complex interactions between particles and their carrier fluid. Although fluid dynamics research has extensively explored particle-laden

Table 6
Comparison of advantages and disadvantages of numerical approaches for particle-fluid flow modelling.

Method	Model	Fluid-particle interaction	Particle-particle interactions	Advantages	Disadvantages	Application in different models
Eulerian-Eulerian	Mixture model			(1) Computationally less intensive, high efficiency and easy implementation; (2) Efficient for simulating large-scale flows where detailed phase interactions are not the primary focus but rather the overall behaviour of the mixture; (3) Well-suited for flows where phases are fully intermingled (where distinguishing between phases on a fine scale is not critical)	(1) Limited information on the interactions between phases; (2) Assumes homogeneous mixing, which may be inaccurate in flows where the distribution of phases is non-uniform or where there is significant phase separation	Adachi et al. (2007), Dontsov and Peirce (2015), Kong et al. (2015), Denison et al. (2018), Hu et al. (2018b), Roostaei et al. (2018)
	Two-fluid model			(1) Treats each phase separately, allowing for a detailed description of phase interactions; (2) Ability to model interfacial forces and momentum transfer between phases more accurately; (3) More versatile for a wide range of multiphase flow situations, including stratified flows, dispersed flows, and flows where phase distribution is non-uniform; (4) Computationally less intensive, high efficiency and easy implementation	(1) Less efficient than the Mixture Model for large-scale simulations; (2) Need for accurate closure models to describe interphase interactions; (3) More susceptible to numerical instability, especially in flows with high phase differences in density and viscosity, requiring careful numerical treatment and possibly more sophisticated solvers; (4) Inaccuracy and lack of physical mechanisms compared to Lagrangian approaches	Boronin and Osiptsov (2014), Shiozawa and McClure (2016)
Eulerian-Lagrangian	DDPM	Empirical models	KTGF (kinetic theory of granular flow)	(1) Efficiently handling dense multiphase flows, where it can be computationally prohibitive to track every particle; (2) Can scale to simulate large systems more effectively than methods requiring individual tracking of each discrete phase entity; (3) Allows for both one-way and two-way coupling between the phases, making it suitable for a broad range of applications; (4) Computationally less expensive compared to other Eu—La methods	(1) For dense particulate flows, where particle-particle interactions are significant, DDPM becomes computationally expensive; (2) The accuracy decreases in dense multiphase flows where particle-particle interactions become dominant	Tong and Mohanty (2016), Hu et al. (2018a), Hwang et al. (2019), Suri et al. (2019), Wen et al. (2020)
	MP-PIC	Empirical models	Solid stress model	(1) Efficiently simulate dense particulate flows by averaging the properties of particles within a computational cell, reducing the computational cost compared to tracking individual particles; (2) Effective for simulations where particle concentrations are high	(1) The averaging process can lead to a loss of detailed information about individual particle dynamics; (2) Uses approximations to represent particle-fluid interactions, which may not capture all the nuances of these interactions in certain conditions	Tsai et al. (2012), Zeng et al. (2019), Zhang et al. (2020c), Mao et al. (2021)
	CFD-DEM	Empirical models	Contact model	(1) Excels in simulating the detailed interactions between particles, including collisions, friction, and cohesion; (2) High accuracy in capturing fluid-particle and particle-fluid interactions; (3) Applicability to the high volume fraction of particles; (4) Allows for two-way and four-way coupling between the phases; (5) Suitable for complex geometries where the detailed behaviour of individual particles needs to be captured	(1) The detailed simulation of fluid phase and discrete particles makes computationally intensive, especially for large-scale systems; (2) Complex to set up and requires significant computational resources, including advanced algorithms for handling particle-fluid and particle-particle interactions	Zhang et al. (2017a), Blyton et al. (2018), Wu and Sharma (2019), Yamashiro and Tomac (2020b), Akhshik and Rajabi (2022), Zhang et al. (2022b), Zhu et al. (2023)
				RANS-DEM: Combines RANS (Reynolds-averaged Navier-Stokes) for fluid flow with DEM for particle tracking. Suitable for statistically steady flows but may not capture all turbulence-particle interactions accurately LES-DEM: Combines LES (large eddy simulation) with DEM, offering improved resolution of turbulence-particle interactions at a higher computational cost DNS-DEM: Combines DNS with DEM, providing the most detailed resolution of fluid-particle interactions but at a prohibitive computational expense for most practical applications		

turbulent flows, it primarily examines neutrally buoyant particles, leaving the dynamics of dense particles in such flows underexplored. This oversight is significant as findings related to neutrally buoyant particles cannot be readily applied to dense particle flows, such as proppant transport in hydraulic fracturing. Bridging this knowledge gap requires a holistic approach that combines experimental research and numerical simulations to enhance our understanding of dense particle dynamics in turbulent inertial flows.

Fluid inertia significantly influences particle-laden flow, particularly at fracture intersections where it partitions the flow, adversely affecting particle distribution in bifurcation flows and leading to suboptimal distribution in subsidiary fractures. The complexity and unpredictability of inertial and turbulent flows hinder understanding these dynamics. Crucially, the interaction with boundaries and the conditions at these boundaries are pivotal, especially for inertial flows at fracture intersections, suggesting that particle inertia effects cannot be fully explained by local conditions alone. This challenges traditional constitutive models. Furthermore, the role of boundary conditions on particle motions, both normal and tangential at solid interfaces, is vital but has not been thoroughly investigated, indicating a significant gap in current research on particle-laden flow dynamics.

The understanding of how solid particles modify the turbulence of a carrier fluid remains limited despite recognising its significance. Various proposed mechanisms and crucial factors contribute to this complex phenomenon. Yet, a consensus is elusive, especially in differentiating direct turbulence modulation effects, like increased viscosity, from other influences such as momentum transfer, particle wake impacts, and particle-induced stresses. The scale-dependent nature of turbulence and the diverse responses from different particle sizes and concentrations compounds the challenge. Advancing our understanding necessitates a nuanced approach integrating experimental research with advanced computational modelling, covering a broad range of scales from microscale particle-fluid interactions to macroscale flow patterns.

Inertial clustering occurs broadly across different parameter spaces, even beyond where preferential sampling is noticeable, particularly in high Reynolds number turbulence, where cluster size varies significantly. The specific processes that lead to cluster formation in such environments, especially under the influence of increased inertial flows and gravity, are still under debate. This situation underscores the necessity for more research to understand the mechanisms behind particle agglomeration in inertial and turbulent flows. Future studies should focus on identifying the conditions favouring different clustering mechanisms and their interactions and how particle characteristics like size, density, and shape affect cluster formation and behaviour.

Turbulence notably increases the settling speed of smaller particles through preferential sweeping, but this effect inversely impacts larger particles over a wide range of parameters due to unsteady and nonlinear forces. The interaction with volume fraction adds complexity, involving hydrodynamic interactions and the obstruction from fluid displacement. This highlights the need for more research into the settling dynamics of particles within turbulent flows and fluid inertia. Future efforts should aim to separate the effects of various forces and interactions, considering different turbulence intensities and particle densities.

Considering the current research findings on fluid inertia and turbulence, as discussed in the review paper, improvements to the proppant process in engineering applications should specifically address the challenges and opportunities these phenomena present.

Accurately modelling fluid inertia is essential for predicting proppant transport and deposition in hydraulic fracturing, with current models often oversimplifying fluid dynamics, resulting in inaccuracies in high flow rates and complex geometries. Advancements could stem from employing sophisticated models that utilise the full Navier-Stokes equations for more precise capture of inertia effects. Research indicates the need for more specific turbulence models beyond generalised ones, suggesting the adoption of LES or DNS for a finer understanding of turbulence and its interaction with proppants. Such detailed models could improve proppant suspension and distribution strategies by identifying zones of significant turbulence or variable fracture roughness, enabling targeted approaches to enhance proppant delivery.

Current models for proppant transport in hydraulic fracturing often do not capture all essential mechanisms, leading to overestimating the propped length of fractures. These models simplify the dynamic nature of proppant settling as fractures expand, which can differ from laboratory observations. Thus, applying laboratory-derived correlations to field scenarios requires caution. Recent experimental research has identified critical factors affecting proppant transport and refined measurements such as drag coefficient, settling velocity, and dune height. Despite these advances, integrating these empirical insights into numerical simulations remains inconsistent, highlighting a gap between experimental findings and their application in modelling efforts.

Optimising proppant characteristics like size, shape, and density is crucial for improving transport efficiency in hydraulic fracturing, considering the effects of fluid inertia and turbulence. Tailoring proppants to minimise the drag and enhance suspension can mitigate the negative impacts of fluid dynamics. Furthermore, adopting innovative fracturing techniques incorporating an advanced understanding of fluid dynamics, such as staged fracturing and variable rate injections, could improve proppant distribution. These strategies might include dynamic adjustments of injection rates and pressures to navigate flow regimes effectively, aiming to extend proppant transport throughout the fracture network and reduce uneven distribution. Research suggests that using smaller or specialised lightweight proppants could facilitate movement into secondary fractures, supported by findings that a certain velocity threshold is necessary for transporting proppants into subsidiary fractures near the wellbore. Cyclic loading of proppants at controlled flow rates has also been identified as beneficial, indicating the importance of fluid dynamics in optimising hydraulic fracturing operations.

In conclusion, the improvements necessary in the field of engineering to optimise the proppant transportation process, considering fluid inertia and turbulent effects, encompass a broad spectrum of research, development, and operational strategies. These strategies range from advanced computational modelling and material science to innovative fracturing techniques and real-time operational adjustments.

9. Conclusions

The preceding comprehensively reviews the state of understanding of the mechanism of particle transport in fractured geo-energy reservoirs, considering the effect of fluid inertia and turbulent flow. Despite considerable research, the mechanisms by which particle transport and distribution within fractured reservoirs are influenced by flows characterised predominantly by fluid inertia and turbulence remain elusive. This gap highlights the necessity for further investigative work in this domain. Such an understanding is critical for optimising hydraulic fracturing techniques and improving resource extraction efficiencies. As this review paper draws to a close, it becomes evident that advancing our knowledge in this area requires dedicated and rigorous future studies.

The traditional lubrication approximation for flow fails to

represent the true complexities of actual fracture morphologies and the impact of nonuniform and unsteady flow behaviours must be fully considered in particle dynamics to account for significant inertial effects. Typically, viscous forces are assumed to govern fluid and particle transport dynamics for low-velocity flows, with fluid inertia considered important only for high-velocity flows. However, resulting from significant gradients in fracture geometry, early onset of fluid inertia can occur even within the laminar flow regime - and its impact on particle dynamics is important and must be considered.

Fluid inertia significantly affects particle-fluid two-phase flow at fracture intersections - that are ubiquitous in fracture networks. These migration phenomena and the mechanics controlling the splitting of streamlines are still not fully comprehended and characterised - response importantly controlled by nuances in Reynolds number, particle volumetric concentration, fracture geometry and boundary conditions. Both fluid inertia and turbulence play a crucial role in controlling particle motion and distribution, with phenomena such as inertial migration, centrifugal instabilities and eddy dynamics impacting transport. The review has elucidated the conditions under which turbulence becomes a dominant factor, emphasising its dual role in promoting mixing and dispersion while potentially trapping particles in low-velocity zones.

The controls of particle volume fraction in defining transport in turbulent flows are complex, involving competing factors such as collective drag, hydrodynamic interactions and hindrance caused by the displaced fluid. Particle clustering and lubrication effects are significant in the transport and settling of concentrated slurries. Understanding these complex particle-fluid interactions is crucial in accurately evaluating slurry flow and settling behaviour.

In conclusion, this review underscores the importance of considering the impacts of fluid inertia and turbulence in studies of particle flow in fractures. It calls for a multidisciplinary approach to tackle the challenges associated with accurately predicting particle transport in fractured media, which is vital for a wide range of applications in geosciences, engineering, and environmental science.

CRediT authorship contribution statement

E.A.A.V. Edirisinghe: Writing – original draft. **M.S.A. Perera:** Conceptualization, Supervision. **D. Elsworth:** Writing – review & editing. **S.K. Matthai:** Writing – review & editing. **E. Goudeli:** Writing – review & editing.

Declaration of competing interest

The authors declare that they have no known competing financial interests or personal relationships that could have appeared to influence the work reported in this paper.

Acknowledgments

This project has been funded by the Australian Research Council Discovery Project (ARC DP 220100851) scheme and would acknowledge that.

References

Abdollahipour, A., Marji, M.F., 2020. A thermo-hydromechanical displacement discontinuity method to model fractures in high-pressure, high-temperature environments. Renew. Energy 153, 1488–1503.
Abdollahipour, A., Marji, M.F., Yarahmadi Bafghi, A., Gholamnejad, J., 2015. Numerical investigation on the effect of crack geometrical parameters in hydraulic fracturing process of hydrocarbon reservoirs. J. Min. Environ.
Abdollahipour, A., Fatehi Marji, M., Bafghi, A.Y., Gholamnejad, J., 2016. A complete formulation of an indirect boundary element method for poroelastic rocks. Comput. Geotech. 74, 15–25.
Abraham, F.F., 1970. Functional dependence of drag coefficient of a sphere on Reynolds number. Phys. Fluids 13 (8), 2194–2195.
Adachi, J., Siebrits, E., Peirce, A., Desroches, J., 2007. Computer simulation of hydraulic fractures. Int. J. Rock Mech. Min. Sci. 44 (5), 739–757.
Adnan, M., Sun, J., Ahmad, N., Wei, J.J., 2021. Verification and validation of the ddpm-emms model for numerical simulations of bubbling, turbulent and circulating fluidized beds. Powder Technol. 379, 69–88.
Agrawal, K., Loezos, P.N., Syamlal, M., Sundaresan, S., 2001. The role of meso-scale structures in rapid gas–solid flows. J. Fluid Mech. 445, 151–185.
Ahmadi, F., Sanders, R.S., Ghaemi, S., 2021. Spatial distribution of particles in turbulent channel flow of dilute suspensions. Int. J. Multiphas. Flow 135, 103538.
Ahmed, G.Y., Singh, A., 2011. Numerical simulation of particle migration in asymmetric bifurcation channel. J. Nonnewton. Fluid Mech. 166 (1–2), 42–51.
Akhshik, S., Rajabi, M., 2022. Simulation of proppant transport at intersection of hydraulic fracture and natural fracture of wellbores using CFD-DEM. Particuology 63, 112–124.
Al-Naafa, M.A., Selim, M.S., 1992. Sedimentation of monodisperse and bidisperse hard-sphere colloidal suspensions. AlChE J. 38 (10), 1618–1630.
Aliseda, A., Cartellier, A., Hainaux, F., Lasheras, J.C., 2002. Effect of preferential concentration on the settling velocity of heavy particles in homogeneous isotropic turbulence. J. Fluid Mech. 468, 77–105.
Alletto, M., Breuer, M., 2012. One-way, two-way and four-way coupled les predictions of a particle-laden turbulent flow at high mass loading downstream of a confined bluff body. Int. J. Multiphas. Flow 45, 70–90.
Alotaibi, M.A., Miskimins, J.L., 2018. Slickwater proppant transport in hydraulic fractures: new experimental findings and scalable correlation. SPE Prod. Oper. 33 (2), 164–178.
Andersson, H.I., Challabotla, N.R., Zhao, L., 2015. Orientation and rotation of inertial disk particles in wall turbulence. J. Fluid Mech. 766, R2.
Andrews, M.J., O'Rourke, P.J., 1996. The multiphase particle-in-cell (mp-pic) method for dense particulate flows. Int. J. Multiphas. Flow 22 (2), 379–402.
Arash Dahi, T., Milad, A., Olson, J.E., 2013. Secondary fractures and their potential impacts on hydraulic fractures efficiency. In: Effective and Sustainable Hydraulic Fracturing. IntechOpen. Ch. 38.
Ardekani, M.N., Asmar, L.A., Picano, F., Brandt, L., 2018. Numerical study of heat transfer in laminar and turbulent pipe flow with finite-size spherical particles. Int. J. Heat Fluid Flow 71, 189–199.
Asmolov, E.S., 1999. The inertial lift on a spherical particle in a plane Poiseuille flow at large channel Reynolds number. J. Fluid Mech. 381, 63–87.
Asmolov, E.S., Osiptsov, A.A., 2009. The inertial lift on a spherical particle settling in a horizontal viscous flow through a vertical slot. Phys. Fluids 21 (6), 063301.
Asmolov, E.S., Lebedeva, N.A., Osiptsov, A.A., 2009. Inertial migration of sedimenting particles in a suspension flow through a hele-shaw cell. Fluid Dynam. 44 (3), 405–418.
Aziz, G.a., 1972. The Flow of Complex Mixtures in Pipes. Van Nostrand Reinhold.
Bagchi, P., Balachandar, S., 2003. Effect of turbulence on the drag and lift of a particle. Phys. Fluids 15 (11), 3496–3513.
Bai, T., Chen, Z., Aminossadati, S.M., Rufford, T.E., Li, L., 2017. Experimental investigation on the impact of coal fines generation and migration on coal permeability. J. Pet. Sci. Eng. 159, 257–266.
Baker, L.J., Coletti, F., 2019. Experimental study of negatively buoyant finite-size particles in a turbulent boundary layer up to dense regimes. J. Fluid Mech. 866, 598–629.
Balachandar, S., Eaton, J.K., 2010. Turbulent dispersed multiphase flow. Annu. Rev. Fluid Mech. 42 (1), 111–133.
Balaramakrishna, P., Chhabra, R., 1992. Sedimentation of a sphere along the axis of a long square duet filled with non-Newtonian liquids. Can. J. Chem. Eng. 70 (4), 803–807.
Banko, A.J., Villafañe, L., Kim, J.H., Eaton, J.K., 2020. Temperature statistics in a radiatively heated particle-laden turbulent square duct flow. Int. J. Heat Fluid Flow 84, 108618.
Barboza, B.R., Chen, B., Li, C., 2021. A review on proppant transport modelling. J. Pet. Sci. Eng. 204, 108753.
Bareš, V., Krupička, J., Picek, T., Brabec, J., Matoušek, V., 2014. Turbulent slurry flow measurement using ultrasonic Doppler method in rectangular pipe. EPJ Web of Conferences.
Barnea, E., Mizrahi, J., 1973. A generalized approach to the fluid dynamics of particulate systems: Part 1. General correlation for fluidization and sedimentation in solid multiparticle systems. Chem.Eng.J. 5 (2), 171–189.
Barnocky, G., Davis, R.H., 1988. Elastohydrodynamic collision and rebound of spheres: experimental verification. Phys. Fluids 31 (6), 1324–1329.
Barree, R.D., Conway, M.W., 1994. Experimental and numerical modeling of convective proppant transport. In: SPE Annual Technical Conference and Exhibition.
Barree, R.D., Conway, M.W., 1995. Experimental and numerical modeling of convective proppant transport (includes associated papers 31036 and 31068). J. Petrol. Technol. 47 (3), 216–222.
Barree, R.D., Conway, M.W., 2001. Proppant holdup, bridging, and screenout behavior in naturally fractured reservoirs. In: SPE Production and Operations Symposium.
Batchelor, G.K., Green, J.T., 1972. The hydrodynamic interaction of two small freely-moving spheres in a linear flow field. J. Fluid Mech. 56 (2), 375–400.
Batchelor, G.K., Wen, C.S., 1982. Sedimentation in a dilute polydisperse system of

interacting spheres. Part 2. Numerical results. J. Fluid Mech. 124, 495–528.
Bec, J., Homann, H., Ray, S.S., 2014. Gravity-driven enhancement of heavy particle clustering in turbulent flow. Phys. Rev. Lett. 112 (18), 184501.
Bec, J., Gustavsson, K., Mehlig, B., 2023. Statistical models for the dynamics of heavy particles in turbulence. arXiv preprint arXiv:2304.01312.
Belhaj, H.A., 2023. Chapter 6 - dynamic modeling of tight unconventional reservoirs. Tight oil reservoirs 1, 157–210 (Gulf Professional Publishing).
Bellani, G., Byron, M.L., Collignon, A.G., Meyer, C.R., Variano, E.A., 2012. Shape effects on turbulent modulation by large nearly neutrally buoyant particles. J. Fluid Mech. 712, 41–60.
Belyadi, H., Fathi, E., Belyadi, F., 2019. Hydraulic Fracturing in Unconventional Reservoirs, second ed. Gulf Professional Publishing.
Blyton, C.A., Gala, D.P., Sharma, M.M., 2015. A comprehensive study of proppant transport in a hydraulic fracture. In: SPE Annual Technical Conference and Exhibition.
Blyton, C.A., Gala, D.P., Sharma, M.M., 2018. A study of proppant transport with fluid flow in a hydraulic fracture. SPE Drill. Complet. 33 (4), 307–323.
Boronin, S.A., Osiptsov, A.A., 2014. Effects of particle migration on suspension flow in a hydraulic fracture. Fluid Dynam. 49 (2), 208–221.
Boronin, S., Osiptsov, A., Desroches, J., 2015. Displacement of yield-stress fluids in a fracture. Int. J. Multiphas. Flow 76, 47–63.
Bragg, A.D., Ireland, P.J., Collins, L.R., 2015. Mechanisms for the clustering of inertial particles in the inertial range of isotropic turbulence. Phys. Rev. E. 92 (2), 023029.
Brandt, L., Coletti, F., 2022. Particle-laden turbulence: progress and perspectives. Annu. Rev. Fluid Mech. 54 (1), 159–189.
Brown, P.P., Lawler, D.F., 2003. Sphere drag and settling velocity revisited. J. Environ. Eng. 129 (3), 222–231.
Burgers, J., 1942. On the influence of the concentration of a suspension upon the sedimentation velocity. Proc. Koninklijke Nederl. Akademie Wetenschappen 45, 126–128.
Capecelatro, J., Desjardins, O., Fox, Rodney O., 2014. Numerical study of collisional particle dynamics in cluster-induced turbulence. J. Fluid Mech. 747, R2. Article R2.
Capecelatro, J., Desjardins, O., Fox, Rodney O., 2015. On fluid–particle dynamics in fully developed cluster-induced turbulence. J. Fluid Mech. 780, 578–635.
Capecelatro, J., Desjardins, O., Fox, R.O., 2018. On the transition between turbulence regimes in particle-laden channel flows. J. Fluid Mech. 845, 499–519.
Cardenas, M.B., Slottke, D.T., Ketcham, R.A., Sharp Jr, J.M., 2009. Effects of inertia and directionality on flow and transport in a rough asymmetric fracture. J. Geophys. Res. Solid Earth 114 (B6).
Chalov, S., Jarsjö, J., Kasimov, N., Romanchenko, A., Pietroń, J., Thorslund, J., Promakhova, E., 2015. Spatio-temporal variation of sediment transport in the Selenga river basin, Mongolia and Russia. Environ. Earth Sci. 73, 663–680.
Chang, O., Kinzel, M., Dilmore, R., Wang, J., 2017. Physics of proppant transport through hydraulic fracture network. J. Energy Resour. Technol. 140.
Cheng, N.-S., 2009. Comparison of formulas for drag coefficient and settling velocity of spherical particles. Powder Technol. 189 (3), 395–398.
Cheng, Y., Yan, C., Han, Z., 2023. Mechanics of Hydraulic Fracturing. Springer Nature Singapore, pp. 213–268.
Chhabra, R.P., Agarwal, S., Chaudhary, K., 2003. A note on wall effect on the terminal falling velocity of a sphere in quiescent Newtonian media in cylindrical tubes. Powder Technol. 129 (1), 53–58.
Chouippe, A., Uhlmann, M., 2015. Forcing homogeneous turbulence in direct numerical simulation of particulate flow with interface resolution and gravity. Phys. Fluids 27 (12), 123301.
Chun, B., Ladd, A., 2006. Inertial migration of neutrally buoyant particles in a square duct: an investigation of multiple equilibrium positions. Phys. Fluids 18 (3), 031704.
Chun, T., Zhu, D., Zhang, Z., Mao, S., Wu, K., 2021. Experimental study of proppant transport in complex fractures with horizontal bedding planes for slickwater fracturing. SPE Prod. Oper. 36 (1), 83–96.
Clark, P.E., Quadir, J.A., 1981. Prop transport in hydraulic fractures: a critical review of particle settling velocity equations. In: SPE/DOE Low Permeability Gas Reservoirs Symposium.
Clark, P.E., Harkin, M.W., Wahl, H.A., Sievert, J.A., 1977. Design of a large vertical prop transport model. In: SPE Annual Fall Technical Conference and Exhibition.
Clift, R., Grace, J., Weber, M., 1978. Bubbles, Drops, and Particles. Dover Publications, Mineola, NY, USA.
Costa, P., Picano, F., Brandt, L., Breugem, W.-P., 2018. Effects of the finite particle size in turbulent wall-bounded flows of dense suspensions. J. Fluid Mech. 843, 450–478.
Crowe, C.T., Schwarzkopf, J.D., Sommerfeld, M., Tsuji, Y., 2011. Multiphase Flows with Droplets and Particles, second ed. CRC Press, Boca Raton, FL, USA.
Cunningham, D., Auradou, H., Shojaei-Zadeh, S., Drazer, G., 2020. The effect of fracture roughness on the onset of nonlinear flow. Water Resour. Res. 56 (11), e2020WR028049.
Daneshy, A.A., 1978. Numerical solution of sand transport in hydraulic fracturing. J. Petrol. Technol. 30 (1), 132–140.
Dang, W., Wu, W., Konietzky, H., Qian, J., 2019. Effect of shear-induced aperture evolution on fluid flow in rock fractures. Comput. Geotech. 114, 103152.
Dang, W., Chen, X., Li, X., Chen, J., Tao, K., Yang, Q., Luo, Z., 2021. A methodology to investigate fluid flow in sheared rock fractures exposed to dynamic normal load. Measurement 185, 110048.
Davis, R.H., Serayssol, J.-M., Hinch, E.J., 1986. The elastohydrodynamic collision of two spheres. J. Fluid Mech. 163, 479–497.
Dayan, A., Stracener, S.M., Clark, P.E., 2009. Proppant transport in slick-water fracturing of shale-gas formations. In: SPE Annual Technical Conference and Exhibition.
Delidis, P., Stamatoudis, M., 2009. Comparison of the velocities and the wall effect between spheres and cubes in the accelerating region. Chem. Eng. Commun. 196 (7), 841–853.
Denison, M.K., Elsworth, D., Wang, J., 2018. Propagation, proppant transport and the evolution of transport properties of hydraulic fractures. J. Fluid Mech. 855, 503–534.
Detournay, E., 2016. Mechanics of hydraulic fractures. Annu. Rev. Fluid Mech. 48 (1), 311–339.
Dey, S., Ali, S.Z., Padhi, E., 2019. Terminal fall velocity: the legacy of Stokes from the perspective of fluvial hydraulics. Proc. R. Soc. A A. 475 (2228), 20190277.
Di Carlo, D., 2009. Inertial microfluidics. Lab Chip 9 (21), 3038–3046.
Di Felice, R., 1994. The voidage function for fluid-particle interaction systems. Int. J. Multiphas. Flow 20 (1), 153–159.
Di Felice, R., 1996. A relationship for the wall effect on the settling velocity of a sphere at any flow regime. Int. J. Multiphas. Flow 22 (3), 527–533.
Di Felice, R., 1999. The sedimentation velocity of dilute suspensions of nearly monosized spheres. Int. J. Multiphas. Flow 25 (4), 559–574.
Di Vaira, N., Leonardi, C., Johnson Jr, R., 2020. Modelling micro-proppant transport in stress-sensitive naturally-fractured reservoirs. SPE Europec.
Dontsov, E., Peirce, A., 2014a. A new technique for proppant schedule design. Hydraul Fract J. 1 (3).
Dontsov, E., Peirce, A., 2014b. Slurry flow, gravitational settling and a proppant transport model for hydraulic fractures. J. Fluid Mech. 760, 567–590.
Dontsov, E., Peirce, A., 2015. Proppant transport in hydraulic fracturing: crack tip screen-out in kgd and p3d models. Int. J. Solid Struct. 63, 206–218.
Doran, P.M., 2013. Chapter 7 - fluid flow. In: Bioprocess Engineering Principles, second ed. Academic Press, pp. 201–254.
Duduković, A.P., Končar-Djurdjević, S.K., 1981. The effect of tube walls on drag coefficients of coaxially placed objects. AIChE J 27 (5), 837–840.
Eaton, J.K., Fessler, J.R., 1994. Preferential concentration of particles by turbulence. Int. J. Multiphas. Flow 20, 169–209.
Eaton, J.K., Fessler, J.R., Kulick, J.D., 1994. Particle response and turbulence modification in fully developed channel flow. J. Fluid Mech. 277, 109–134.
Economides, M.J., Nolte, K.G., 2000. Reservoir Stimulation, third ed. Wiley.
Economides, M.J., Mikhailov, D.N., Nikolaevskiy, V.N., 2007. On the problem of fluid leakoff during hydraulic fracturing. Transport Porous Media 67 (3), 487–499.
Elghobashi, S., Ferrante, A., 2004. On the physical mechanisms of drag reduction in a spatially developing turbulent boundary layer laden with microbubbles. J. Fluid Mech. 503, 345–355.
Elghobashi, S., Ferrante, A., Lucci, F., 2010. Modulation of isotropic turbulence by particles of taylor length-scale size. J. Fluid Mech. 650, 5–55.
Eshghinejadfard, A., Thévenin, D., Zhao, L., 2018. Lattice Boltzmann simulation of resolved oblate spheroids in wall turbulence. J. Fluid Mech. 849, 510–540.
Eshghinejadfard, A., Hosseini, S.A., Thévenin, D., 2019. Effect of particle density in turbulent channel flows with resolved oblate spheroids. Comput. Fluids 184, 29–39.
Fan, M., Chen, C., 2020. Numerical simulation of the migration and deposition of fine particles in a proppant-supported fracture. J. Pet. Sci. Eng. 194, 107484.
Farhan, M., Nicolleau, F.C.G.A., Nowakowski, A.F., 2015. Effect of gravity on clustering patterns and inertial particle attractors in kinematic simulations. Phys. Rev. E. 91 (4).
Fernández, M.E., Sánchez, M., Pugnaloni, L.A., 2019. Proppant transport in a scaled vertical planar fracture: vorticity and dune placement. J. Pet. Sci. Eng. 173, 1382–1389.
Fidleris, V., Whitmore, R., 1961. Experimental determination of the wall effect for spheres falling axially in cylindrical vessels. Br. J. Appl. Phys. 12 (9), 490.
Fjaestad, D., Tomac, I., 2019. Experimental investigation of sand proppant particles flow and transport regimes through narrow slots. Powder Technol. 343, 495–511.
Fornari, W., Formenti, A., Picano, F., Brandt, L., 2016a. The effect of particle density in turbulent channel flow laden with finite size particles in semi-dilute conditions. Phys. Fluids 28 (3), 033301.
Fornari, W., Picano, F., Brandt, L., 2016b. Sedimentation of finite-size spheres in quiescent and turbulent environments. J. Fluid Mech. 788, 640–669.
Fornari, W., Picano, F., Sardina, G., Brandt, L., 2016c. Reduced particle settling speed in turbulence. J. Fluid Mech. 808.
Fornari, W., Zade, S., Brandt, L., Picano, F., 2019. Settling of finite-size particles in turbulence at different volume fractions. Acta Mech. 230 (2), 413–430.
Fourar, M., Lenormand, R., Karimi-Fard, M., Horne, R., 2005. Inertia effects in high-rate flow through heterogeneous porous media. Transport Porous Media 60 (3), 353–370.
Francis, A.W., 1933. Wall effect in falling ball method for viscosity. Physics 4 (11), 403–406.
Fu, W., Savitski, A.A., Damjanac, B., Bunger, A.P., 2019. Three-dimensional lattice simulation of hydraulic fracture interaction with natural fractures. Comput. Geotech. 107, 214–234 [Article].
Gadde, P.B., Liu, Y., Norman, J., Bonnecaze, R., Sharma, M.M., 2004. Modeling proppant settling in water-fracs. In: SPE Annual Technical Conference and Exhibition.
Garagash, I.A., Osiptsov, A.A., Boronin, S.A., 2019. Dynamic bridging of proppant particles in a hydraulic fracture. Int. J. Eng. Sci. 135, 86–101.

Gidaspow, D., 1994. Multiphase Flow and Fluidization: Continuum and Kinetic Theory Descriptions. Academic press.
Goldstein, S., 1929. The steady flow of viscous fluid past a fixed spherical obstacle at small Reynolds numbers. Proc. R. Soc. London, Ser. A 123 (791), 225–235.
Golovin, S., Besov, A., Chebotnikov, A., Ermanyuk, E., 2022. Experimental study of proppant bridging in a model of a hydraulic fracture. SPE J. 27 (2), 1209–1220.
Gong, Y., Mehana, M., El-Monier, I., Viswanathan, H., 2020. Proppant placement in complex fracture geometries: a computational fluid dynamics study. J. Nat. Gas Sci. Eng. 79, 103295.
Good, G., Ireland, P., Bewley, G., Bodenschatz, E., Collins, L., Warhaft, Z., 2014. Settling regimes of inertial particles in isotropic turbulence. J. Fluid Mech. 759.
Gruesbeck, C., Collins, R., 1982. Particle transport through perforations. Soc. Petrol. Eng. J. 22 (6), 857–865.
Gu, H., Desroches, J., 2003. New pump schedule generator for hydraulic fracturing treatment design. In: SPE Latin American and Caribbean Petroleum Engineering Conference..
Guazzelli, É., Morris, J.F., 2011. A Physical Introduction to Suspension Dynamics. Cambridge University Press.
Guo, T., Zhang, S., Qu, Z., Zhou, T., Xiao, Y., Gao, J., 2014. Experimental study of hydraulic fracturing for shale by stimulated reservoir volume. Fuel 128, 373–380 [Article].
Guo, C., Xu, J., Wei, M., Jiang, R., 2015. Experimental study and numerical simulation of hydraulic fracturing tight sandstone reservoirs. Fuel 159, 334–344.
Guo, P., Gao, K., Wang, M., Wang, Y., He, M., 2022. Numerical investigation on the influence of contact characteristics on nonlinear flow in 3d fracture. Comput. Geotech. 149, 104863.
Gupta, A., Clercx, H.J.H., Toschi, F., 2018. Effect of particle shape on fluid statistics and particle dynamics in turbulent pipe flow. Eur.Phys.J.E. 41 (10).
Hampton, R.E., Mammoli, A.A., Graham, A.L., Tetlow, N., Altobelli, S.A., 1997. Migration of particles undergoing pressure-driven flow in a circular conduit. J. Rheol. 41 (3), 621–640.
Han, M., Kim, C., Kim, M., Lee, S., 1999. Particle migration in tube flow of suspensions. J. Rheol. 43 (5), 1157–1174.
Han, J., Yuan, P., Huang, X., Zhang, H., Sookprasong, A., Li, C., Dai, Y., 2016. Numerical Study of Proppant Transport in Complex Fracture Geometry. SPE Low Perm Symposium.
Hangyu, Z., Jianchun, G., Tao, Z., Haoran, G., Chi, C., Shouxin, W., Tang, T., 2023. Numerical study of the wall-retardation effect on proppant transport in rough fractures. Comput. Geotech. 159, 105425.
Hannah, R.R., Harrington, L.J., 1981. Measurement of dynamic proppant fall rates in fracturing gels using a concentric cylinder tester. J. Petrol. Technol. 33 (5), 909–913 (includes associated paper 9970).
Happel, J., Brenner, H., 1983. Low Reynolds Number Hydrodynamics. Kluwer Academic.
Harrington, L.J., Hannah, R.R., Williams, D., 1979. Dynamic experiments on proppant settling in crosslinked fracturing fluids. In: SPE Annual Technical Conference and Exhibition.
Helland, E., Bournot, H., Occelli, R., Tadrist, L., 2007. Drag reduction and cluster formation in a circulating fluidised bed. Chem. Eng. Sci. 62 (1), 148–158.
Homann, H., Bec, J., Grauer, R., 2013. Effect of turbulent fluctuations on the drag and lift forces on a towed sphere and its boundary layer. J. Fluid Mech. 721, 155–179.
Hu, X., Wu, K., Li, G., Tang, J., Shen, Z., 2018a. Effect of proppant addition schedule on the proppant distribution in a straight fracture for slickwater treatment. J. Pet. Sci. Eng. 167, 110–119.
Hu, X., Wu, K., Song, X., Yu, W., Tang, J., Li, G., Shen, Z., 2018b. A new model for simulating particle transport in a low-viscosity fluid for fluid-driven fracturing. AlChE J 64 (9), 3542–3552.
Hu, Y.T., Popeney, C., Gilmer, C., Kurian, P., 2019. Quantification of Dynamic Sand Settling Velocity in High-Viscosity Friction Reducers and Correlation with Rheology. SPE/AAPG/SEG Unconventional Resources Technology Conference.
Hu, X., Yang, Z., Chen, Y.-F., 2021. Fluid-driven particle transport patterns in a confined geometry: effect of flow velocity and particle concentration. J. Nat. Gas Sci. Eng. 92, 103998.
Huang, J., Hao, Y., Settgast, R.R., White, J.A., Mateen, K., Gross, H., 2023. Validation and application of a three-dimensional model for simulating proppant transport and fracture conductivity. Rock Mech. Rock Eng. 56, 7091–7113.
Huilin, L., Gidaspow, D., 2003. Hydrodynamics of binary fluidization in a riser: cfd simulation using two granular temperatures. Chem. Eng. Sci. 58 (16), 3777–3792.
Hwang, I.S., Jeong, H.J., Hwang, J., 2019. Numerical simulation of a dense flow cyclone using the kinetic theory of granular flow in a dense discrete phase model. Powder Technol. 356, 129–138.
Isah, A., Hiba, M., Al-Azani, K., Aljawad, M.S., Mahmoud, M., 2021. A comprehensive review of proppant transport in fractured reservoirs: experimental, numerical, and field aspects. J. Nat. Gas Sci. Eng. 88, 103832.
Iwaoka, M., Ishii, T., 1979. Experimental wall correction factors of single solid spheres in circular cylinders. J. Chem. Eng. Jpn. 12 (3), 239–242.
Kadhim, D., Imqam, A., Dunn-Norman, S., 2017. Ceramic Proppant Transport and Placement in Heterogeneous Fracture Systems. SPE/AAPG/SEG Unconventional Resources Technology Conference.
Kawanisi, K., Shiozaki, R., 2008. Turbulent effects on the settling velocity of suspended sediment. J. Hydraul. Eng. 134 (2), 261–266.
Khan, A., Richardson, J., 1987. The resistance to motion of a solid sphere in a fluid. Chem. Eng. Commun. 62 (1–6), 135–150.
King, G.E., 2010. Thirty years of gas shale fracturing: what have we learned? SPE Annual Technical Conference and Exhibition.
Kirkby, L.L., Rockefeller, H.A., 1985. Proppant settling velocities in nonflowing slurries. In: SPE/DOE Low Permeability Gas Reservoirs Symposium.
Koh, C.J., Hookham, P., Leal, L.G., 1994. An experimental investigation of concentrated suspension flows in a rectangular channel. J. Fluid Mech. 266, 1–32.
Koivisto, J., Durian, D.J., 2017. Effect of interstitial fluid on the fraction of flow microstates that precede clogging in granular hoppers. Phys. Rev. E. 95 (3), 032904.
Kong, B., Fathi, E., Ameri, S., 2015. Coupled 3-d numerical simulation of proppant distribution and hydraulic fracturing performance optimization in marcellus shale reservoirs. Int. J. Coal Geol. 147–148, 35–45.
Kou, R., Moridis, G.J., Blasingame, T.A., 2018. Analysis and modeling of proppant transport in inclined hydraulic fractures. In: SPE Hydraulic Fracturing Technology Conference and Exhibition.
Kou, R., Moridis, G., Blasingame, T., 2019. Bridging criteria and distribution correlation for proppant transport in primary and secondary fracture. In: SPE Hydraulic Fracturing Technology Conference and Exhibition.
Kumar, D., Gonzalez, R.A., Ghassemi, A., 2019. The role of micro-proppants in conductive fracture network development. In: SPE Hydraulic Fracturing Technology Conference and Exhibition.
Lashgari, I., Picano, F., Breugem, W.P., Brandt, L., 2016. Channel flow of rigid sphere suspensions: particle dynamics in the inertial regime. Int. J. Multiphas. Flow 78, 12–24.
Latto, B., Round, G.F., Anzenavs, R., 1973. Drag coefficients and pressure drops for hydrodynamically suspended spheres in a vertical tube with and without polymer addition. Can. J. Chem. Eng. 51 (5), 536–541.
Lecampion, B., Garagash, D.I., 2014. Confined flow of suspensions modelled by a frictional rheology. J. Fluid Mech. 759, 197–235.
Lee, H.P., Olson, J.E., Holder, J., Gale, J.F., Myers, R.D., 2015. The interaction of propagating opening mode fractures with preexisting discontinuities in shale. J. Geophys. Res. Solid Earth 120 (1), 169–181.
Leshansky, A.M., Lavrenteva, O.M., Nir, A., 2003. The weakly inertial settling of particles in a viscous fluid. Proc. R. Soc. London, Ser. A 459 (2040), 3079–3098.
Li, N., Li, J., Zhao, L., Luo, Z., Liu, P., Guo, Y., 2017. Laboratory testing on proppant transport in complex-fracture systems. SPE Prod. Oper. 32 (4), 382–391.
Li, P., Zhang, X., Lu, X., 2018. Numerical simulation on solid-liquid two-phase flow in cross fractures. Chem. Eng. Sci. 181, 1–18.
Li, Q., Abbas, M., Morris, J.F., 2020. Particle approach to a stagnation point at a wall: Viscous damping and collision dynamics. Physical Review Fluids 5 (10), 104301.
Li, Q., Abbas, M., Morris, J.F., Climent, E., Magnaudet, J., 2020. Near-wall dynamics of a neutrally buoyant spherical particle in an axisymmetric stagnation point flow. J. Fluid Mech. 892, A32.
Li, M., Guo, J., Zhang, T., Zeng, X., Yang, R., Gou, H., 2022. Quantitative experimental study on the rule of fluid flow and its influencing factors in hydraulic fractures. J. Pet. Sci. Eng. 214, 110505.
Liang, S.C., Hong, T., Fan, L.S., 1996. Effects of particle arrangements on the drag force of a particle in the intermediate flow regime. Int. J. Multiphas. Flow 22 (2), 285–306.
Liu, Y., 2006. Settling and Hydrodynamic Retardation of Proppants in Hydraulic Fractures. The university of Texas at Austin.
Liu, Y., Sharma, M.M., 2005. Effect of fracture width and fluid rheology on proppant settling and retardation: an experimental study. SPE Annual Technical Conference and Exhibition.
Liu, R., Id, Y., Jiang, Y., Jing, H., Yu, L., 2018. Nonlinear flow characteristics of a system of two intersecting fractures with different apertures. Processes 6, 94.
Liu, X., Li, M., Zeng, N., Li, T., 2020. Investigation on nonlinear flow behavior through rock rough fractures based on experiments and proposed 3-dimensional numerical simulation. Geofluids 2020, 1–34.
Liu, C., Li, M., Zhang, G., Zhang, Y., 2021. Quantitative study on bed load proppant transport during slickwater hydraulic fracturing. Lithosphere 2021 (Special 1).
Liu, W., He, Y., Li, M., Huang, C., Liu, Y., 2022. Effect of drag models on hydrodynamic behaviors of slurry flows in horizontal pipes. Phys. Fluids 34 (10).
Lu, C., Ma, L., Li, Z., Huang, F., Huang, C., Yuan, H., Tang, Z., Guo, J., 2020. A novel hydraulic fracturing method based on the coupled cfd-dem numerical simulation study. Appl. Sci. 10 (9), 3027.
Luo, L., Tomac, I., 2018a. Experimental investigation of particle agglomeration effects on slurry settling in viscous fluid. Transport Porous Media 121 (2), 333–352.
Luo, L., Tomac, I., 2018b. Particle image velocimetry (PIV) analysis of particle settling in narrow fracture experiments. Geotech. Test J. 41 (2), 354–370.
Ma, W., Perng, J., Tomac, I., 2022. Experimental investigation of proppant flow and transport dynamics through fracture intersections. Geomech. Energy Environ. 30, 100232.
Machac, I., Lecjaks, Z., 1995. Wall effect for a sphere falling through a non-Newtonian fluid in a rectangular duct. Chem. Eng. Sci. 50 (1), 143–148.
Mack, M.G., Warpinski, N.R., 2000. Mechanics of hydraulic fracturing. Reservoir Stimulation 6, 1.
Mack, M., Sun, J., Khadilkar, C., 2014. Quantifying proppant transport in thin fluids - theory and experiments. In: SPE Hydraulic Fracturing Technology Conference.
Malhotra, S., Sharma, M.M., 2012. Settling of spherical particles in unbounded and confined surfactant-based shear thinning viscoelastic fluids: an experimental study. Chem. Eng. Sci. 84, 646–655.
Mallouppas, G., van Wachem, B., 2013. Large eddy simulations of turbulent particle-laden channel flow. Int. J. Multiphas. Flow 54, 65–75.
Manoorkar, S., Morris, J.F., 2021. Particle motion in pressure-driven suspension flow

through a symmetric t-channel. Int. J. Multiphas. Flow 134, 103447.
Manoorkar, S., Sedes, O., Morris, J.F., 2016. Particle transport in laboratory models of bifurcating fractures. J. Nat. Gas Sci. Eng. 33, 1169–1180.
Manoorkar, S., Krishnan, S., Sedes, O., Shaqfeh, E.S.G., Iaccarino, G., Morris, J.F., 2018. Suspension flow through an asymmetric t-junction. J. Fluid Mech. 844, 247–273.
Manouchehrian, A., Marji, M.F., 2012. Numerical analysis of confinement effect on crack propagation mechanism from a flaw in a pre-cracked rock under compression. Acta Mech. Sin. 28 (5), 1389–1397.
Mao, S., Zhang, Z., Chun, T., Wu, K., 2021. Field-scale numerical investigation of proppant transport among multicluster hydraulic fractures. SPE J. 26 (1), 307–323.
Marchioli, C., Soldati, A., Zonta, F., 2012. Modulation of turbulence in forced convection by temperature-dependent viscosity. J. Fluid Mech. 697, 150–174.
Marji, M.F., 2014. Numerical analysis of quasi-static crack branching in brittle solids by a modified displacement discontinuity method. Int. J. Solid Struct. 51 (9), 1716–1736.
Matas, J.-P., Morris, J.F., Guazzelli, É., 2004. Inertial migration of rigid spherical particles in Poiseuille flow. J. Fluid Mech. 515, 171–195.
Matas, J.P., Morris, J.F., Guazzelli, É., 2009. Lateral force on a rigid sphere in large-inertia laminar pipe flow. J. Fluid Mech. 621, 59–67.
Matthäi, S.K., Mezentsev, A., Belayneh, M., 2007. Finite element–node-centered finite-volume two-phase-flow experiments with fractured rock represented by unstructured hybrid-element meshes. SPE Reservoir Eval. Eng. 10 (6), 740–756.
Maude, A.D., Whitmore, R.L., 1958. A generalized theory of sedimentation. Br. J. Appl. Phys. 9 (12), 477.
Maxey, M.R., 1987. The gravitational settling of aerosol particles in homogeneous turbulence and random flow fields. J. Fluid Mech. 174, 441–465.
Maxey, M.R., Corrsin, S., 1986. Gravitational settling of aerosol particles in randomly oriented cellular flow fields. J. Atmos. Sci. 43 (11), 1112–1134.
Mays, D.C., 2005. Hydrodynamics of Particle Clogging in Saturated Granular Media: Analysis and Experiments. University of California, Berkeley.
McCaffery, S., Elliott, L., Ingham, D.B., 1998. Enhanced sedimentation in inclined fracture channels. Computational Mechanics Publications.
McClure, M., 2018. Bed load proppant transport during slickwater hydraulic fracturing: insights from comparisons between published laboratory data and correlations for sediment and pipeline slurry transport. J. Pet. Sci. Eng. 161, 599–610.
McClure, M., Kang, C., 2017. A three-dimensional reservoir, wellbore, and hydraulic fracturing simulator that is compositional and thermal. In: Tracks Proppant and Water Solute Transport, Includes Non-darcy and Non-newtonian Flow, and Handles Fracture Closure.
McCullough, J.W.S., Aminossadati, S.M., Leonardi, C.R., 2020. Transport of particles suspended within a temperature-dependent viscosity fluid using coupled lbm–dem. Int. J. Heat Mass Tran. 149, 119159.
McLaughlin, J.B., 1994. Numerical computation of particles-turbulence interaction. Int. J. Multiphas. Flow 20, 211–232.
McLennan, J.D., Green, S.J., Bai, M., 2008. Proppant placement during tight gas shale stimulation: literature review and speculation. In: The 42nd U.S. Rock Mechanics Symposium (USRMS).
McMechan, D., Shah, S., 1991a. Static proppant-settling characteristics of non-Newtonian fracturing fluids in a large-scale test model. SPE Prod. Eng. 6 (3), 305–312.
McMechan, D.E., Shah, S.N., 1991b. Static proppant-settling characteristics of non-Newtonian fracturing fluids in a large-scale test model. SPE Prod. Eng. 6 (3), 305–312.
Mei, R., Adrian, R.J., Hanratty, T.J., 1997. Turbulent dispersion of heavy particles with nonlinear drag. J. Fluid Eng. 119 (1), 170–179.
Métais, O., Vázquez, M.S., 2002. Large-eddy simulation of the turbulent flow through a heated square duct. J. Fluid Mech. 453, 201–238.
Meyers, M.A., 1994. Dynamic Behavior of Materials. John Wiley & Sons.
Mikhailov, M.D., Freire, A.P.S., 2013. The drag coefficient of a sphere: an approximation using shanks transform. Powder Technol. 237, 432–435.
Miri, R., Haftani, M., Nouri, A., 2021. A review of fines migration around steam assisted gravity drainage wellbores. J. Pet. Sci. Eng. 205, 108868.
Moradi, A., Tokhmechi, B., Rasouli, V., Fatehi Marji, M., 2017. A comprehensive numerical study of hydraulic fracturing process and its affecting parameters. Geotech. Geol. Eng. 35 (3), 1035–1050.
Morris, J.F., 2020. Toward a fluid mechanics of suspensions. Physical Review Fluids 5 (11), 110519.
Morris, J.F., Boulay, F., 1999. Curvilinear flows of noncolloidal suspensions: the role of normal stresses. J. Rheol. 43 (5), 1213–1237.
Morrison, F.A., 2013. An Introduction to Fluid Mechanics. Cambridge University Press.
Mortimer, L., Fairweather, M., 2019. Effect of Particle Diameter on Agglomeration Dynamics in Multiphase Turbulent Channel Flows.
Munroe, H.S., 1889. The English versus the Continental System of Jigging: Is Close Sizing Advantageous? Nabu Press.
Nevskii, Y.A., Osiptsov, A., 2011. Slow gravitational convection of disperse systems in domains with inclined boundaries. Fluid Dynam. 46 (2), 225–239.
Nielsen, P., 1993. Turbulence effects on the settling of suspended particles. J. Sediment. Res. 63 (5), 835–838.
Nott, P.R., Brady, J.F., 1994. Pressure-driven flow of suspensions: simulation and theory. J. Fluid Mech. 275, 157–199.
Novotny, E., 1977. Proppant transport. In: SPE Annual Fall Technical Conference and Exhibition.
Oseen, C.W., 1910. Uber die stokes' sche formel und uber eine verwandte aufgabe in der hydrodynamik. Arkiv Mat., Astron. och Fysik. 6, 1.
Osiptsov, A.A., 2017. Fluid mechanics of hydraulic fracturing: a review. J. Pet. Sci. Eng. 156, 513–535.
Osiptsov, A.A., Asmolov, E.S., 2008. Asymptotic model of the inertial migration of particles in a dilute suspension flow through the entry region of a channel. Phys. Fluids 20 (12), 123301.
Palisch, T.T., Vincent, M.C., Handren, P.J., 2008. Slickwater fracturing - food for thought. In: SPE Annual Technical Conference and Exhibition.
Pan, L., Zhang, Y., Cheng, L., Lu, Z., Kang, Y., He, P., Dong, B., 2018. Migration and distribution of complex fracture proppant in shale reservoir volume fracturing. Nat. Gas. Ind. B. 5 (6), 606–615.
Panfilov, M., Fourar, M., 2006. Physical splitting of nonlinear effects in high-velocity stable flow through porous media. Adv. Water Resour. 29 (1), 30–41.
Peker, S.M., Helvaci, S.S., 2011. Solid-liquid Two Phase Flow. Elsevier.
Peng, H., Fan, Y., Peng, J., Han, H., Gao, X., Wang, L., Gou, X., Yin, Y., Zhou, Y., 2022. Research and application of a proppant transport experimental device for complex fractures in the unconventional reservoir. Geofluids 2022, 8356470.
Picano, F., Breugem, W.-P., Brandt, L., 2015. Turbulent channel flow of dense suspensions of neutrally buoyant spheres. J. Fluid Mech. 764, 463–487.
Poiseuille, J., 1836. Observations of blood flow. Ann Sci Nat STrie 5 (2).
Prosperetti, A., Tryggvason, G., 2009. Computational Methods for Multiphase Flow. Cambridge university press.
Proudman, I., Pearson, J., 1957. Expansions at small Reynolds numbers for the flow past a sphere and a circular cylinder. J. Fluid Mech. 2 (3), 237–262.
Pu, L., Xu, P., Xu, M., Zhou, J., Li, C., Liu, Q., 2023. Numerical simulation on particle-fluid flow in fractured formations: evolution law of plugging layers. Energy 274, 127450.
Qu, H., Hu, Y., Liu, Y., Wang, R., Tang, S., Xue, L., 2021a. The study of particle-fluid flow in narrow, curved slots to enhance comprehension of particle transport mechanisms in complex fractures. J. Nat. Gas Sci. Eng. 92, 103981.
Qu, H., Tang, S., Liu, Z., McLennan, J., Wang, R., 2021b. Experimental investigation of proppant particles transport in a tortuous fracture. Powder Technol. 382, 95–106.
Qu, H., Liu, Y., Lin, H., Tang, S., Wang, R., Xue, L., Hu, Y., 2022. 3d cfd-dem simulation and experiment on proppant particle-fluid flow in a vertical, nonplanar fracture with bends. Int. J. Multiphas. Flow 146, 103873.
Ravi-Chandar, K., Knauss, W.G., 1984. An experimental investigation into dynamic fracture: III. On steady-state crack propagation and crack branching. Int. J. Fract. 26, 141–154.
Ray, B., Lewis, C., Martysevich, V., Shetty, D.A., Walters, H.G., Bai, J., Ma, J., 2017. An investigation into proppant dynamics in hydraulic fracturing. In: SPE Hydraulic Fracturing Technology Conference and Exhibition.
Reeks, M.W., 1983. The transport of discrete particles in inhomogeneous turbulence. J. Aerosol Sci. 14 (6), 729–739.
Richardson, J.F., Zaki, W.N., 1954. The sedimentation of a suspension of uniform spheres under conditions of viscous flow. Chem. Eng. Sci. 3 (2), 65–73.
Richardson, J.F., Zaki, W.N., 1997. Sedimentation and fluidisation: Part i. Chem. Eng. Res. Des. 75, S82–S100.
Rong, G., Cheng, L., He, R., Quan, J., Tan, J., 2021. Investigation of critical non-linear flow behavior for fractures with different degrees of fractal roughness. Comput. Geotech. 133, 104065.
Roodhart, L.P., 1985. Proppant settling in non-Newtonian fracturing fluids. In: SPE/DOE Low Permeability Gas Reservoirs Symposium.
Roos, F.W., Willmarth, W.W., 1971. Some experimental results on sphere and disk drag. AIAA J. 9 (2), 285–291.
Roostaei, M., Nouri, A., Fattahpour, V., Chan, D., 2018. Numerical simulation of proppant transport in hydraulic fractures. J. Pet. Sci. Eng. 163, 119–138.
Roostaei, M., Nouri, A., Fattahpour, V., Chan, D., 2020a. Coupled hydraulic fracture and proppant transport simulation. Energies 13 (11), 2822.
Roostaei, M., Nouri, A., Hosseini, S.A., Soroush, M., Velayati, A., Mahmoudi, M., Ghalambor, A., Fattahpour, V., 2020b. A concise review of experimental works on proppant transport and slurry flow. In: SPE International Conference and Exhibition on Formation Damage Control.
Rowe, P.N., 1987. A convenient empirical equation for estimation of the richardson-zaki exponent. Chem. Eng. Sci. 42 (11), 2795–2796.
Saffman, P.G., 1965. The lift on a small sphere in a slow shear flow. J. Fluid Mech. 22 (2), 385–400.
Sahai, R., 2012. Laboratory Evaluation of Proppant Transport in Complex Fracture Systems. Colorado School of Mines.
Sahai, R., Moghanloo, R.G., 2019. Proppant transport in complex fracture networks – a review. J. Pet. Sci. Eng. 182, 106199.
Sahai, R., Miskimins, J., Olson, K., 2014. Laboratory results of proppant transport in complex fracture systems. In: Society of Petroleum Engineers - SPE Hydraulic Fracturing Technology Conference.
Sahu, A.K., Tripathy, A., Biswal, S.K., 2013. Study on particle dynamics in different cross sectional shapes of air dense medium fluidized bed separator [Article]. Fuel 111, 472–477.
Saieed, A., Rahman, M.M., Hickey, J.-P., 2022. Role of viscosity in the preferential concentration of heated, bidispersed particles. Int. J. Multiphas. Flow 155, 104185.
Schiller, L., Naumann, A., 1935. A Drag Coefficient Correlation, vol. 77, pp. 51–86.
Schonberg, J.A., Hinch, E.J., 1989. Inertial migration of a sphere in Poiseuille flow. J. Fluid Mech. 203, 517–524.

Segre, G., Silberberg, A., 1962. Behaviour of macroscopic rigid spheres in Poiseuille flow part 2. Experimental results and interpretation. J. Fluid Mech. 14 (1), 136–157.
Shah, S.N., Lord, D.L., 1990. Hydraulic fracturing slurry transport in horizontal pipes. SPE Drill. Eng. 5 (3), 225–232.
Shah, S.N., El Fadili, Y., Chhabra, R.P., 2007. New model for single spherical particle settling velocity in power law (visco-inelastic) fluids. Int. J. Multiphas. Flow 33 (1), 51–66.
Shiozawa, S., McClure, M., 2016. Simulation of proppant transport with gravitational settling and fracture closure in a three-dimensional hydraulic fracturing simulator. J. Pet. Sci. Eng. 138, 298–314.
Sievert, J.A., Wahl, H.A., Clark, P.E., Harkin, M.W., 1981. Prop transport in a large vertical model. In: SPE/DOE Low Permeability Gas Reservoirs Symposium.
Song, X., Zhu, Z., Xu, Z., Li, G., Faustino, M.A., Chen, C., Jiang, T., Xie, X., 2019. Experimental study on the wall factor for spherical particles settling in parallel plates filled with power-law fluids. J. Pet. Sci. Eng. 179, 941–947.
Squires, K.D., Eaton, J.K., 1991. Preferential concentration of particles by turbulence. Phys. Fluid. Fluid Dynam. 3 (5), 1169–1178.
Staben, M.E., Zinchenko, A.Z., Davis, R.H., 2003. Motion of a particle between two parallel plane walls in low-Reynolds-number Poiseuille flow. Phys. Fluids 15 (6), 1711–1733.
Suri, Y., Islam, S.Z., Hossain, M., 2019. A new cfd approach for proppant transport in unconventional hydraulic fractures. J. Nat. Gas Sci. Eng. 70, 102951.
Syamlal, M., O'Brien, T., 1989. Computer simulation of bubbles in a fluidized bed. AICHE Symp. Ser. 85, 22–31.
Terfous, A., Hazzab, A., Ghenaim, A., 2013. Predicting the drag coefficient and settling velocity of spherical particles. Powder Technol. 239, 12–20.
Ting, D.S.K., 2016. Chapter 8 - vortex dynamics. In: Ting, D.S.K. (Ed.), Basics of Engineering Turbulence. Academic Press, pp. 165–186.
Tomac, I., Gutierrez, M., 2013. Numerical study of horizontal proppant flow and transport in a narrow hydraulic fracture. In: 47th U.S. Rock Mechanics/Geomechanics Symposium.
Tomac, I., Gutierrez, M., 2014. Fluid lubrication effects on particle flow and transport in a channel. Int. J. Multiphas. Flow 65, 143–156.
Tomac, I., Gutierrez, M., 2015. Micromechanics of proppant agglomeration during settling in hydraulic fractures. J. Pet. Explor. Prod. Technol. 5 (4), 417–434.
Tomac, I., Tartakovsky, D.M., 2018. Experimental evaluation of turbulent flow and proppant transport in a narrow fracture. In: Proceedings of the 43rd Workshop on Geothermal Reservoir Engineering. Stanford University. SGP-TR-213.
Tong, S., Mohanty, K.K., 2016. Proppant transport study in fractures with intersections. Fuel 181, 463–477.
Tong, S., Mohanty, K., 2017. Proppant Placement in Secondary Fractures. SPE/AAPG/SEG Unconventional Resources Technology Conference.
Tooby, P.F., Wick, G.L., Isaacs, J.D., 1977. The motion of a small sphere in a rotating velocity field: a possible mechanism for suspending particles in turbulence. J. Geophys. Res. 82 (15), 2096–2100.
Toschi, F., Bodenschatz, E., 2009. Lagrangian properties of particles in turbulence. Annu. Rev. Fluid Mech. 41 (1), 375–404.
Tsai, K., Degaleesan, S., Fonseca, E., Lake, E., 2012. Advanced computational modeling of proppant settling in water fractures for shale gas production. SPE J. 18.
Tsuji, Y., 2007. Multi-scale modeling of dense phase gas–particle flow. Chem. Eng. Sci. 62 (13), 3410–3418.
Tsuji, Y., Tanaka, T., Yonemura, S., 1994. Particle induced turbulence. Appl. Mech. Rev. 47 (6S), S75–S79.
van der Vlis, A.C., Haafkens, R., Schipper, B.A., Visser, W., 1975. Criteria for proppant placement and fracture conductivity. In: Fall Meeting of the Society of Petroleum Engineers of AIME.
Voth, G.A., Soldati, A., 2017. Anisotropic particles in turbulence. Annu. Rev. Fluid Mech. 49 (1), 249–276.
Wang, L.-P., Maxey, M.R., 1993. Settling velocity and concentration distribution of heavy particles in homogeneous isotropic turbulence. J. Fluid Mech. 256, 27–68.
Wang, X., Yao, J., Gong, L., Sun, H., Yang, Y., Zhang, L., Li, Y., Liu, W., 2019. Numerical simulations of proppant deposition and transport characteristics in hydraulic fractures and fracture networks. J. Pet. Sci. Eng. 183, 106401.
Wang, D., You, Z., Johnson, R.L., Wu, L., Bedrikovetsky, P., Aminossadati, S.M., Leonardi, C.R., 2021. Numerical investigation of the effects of proppant embedment on fracture permeability and well production in queensland coal seam gas reservoirs. Int. J. Coal Geol. 242, 103689.
Wang, D., Bai, B., Wang, B., Wei, D., Liang, T., 2022a. Impacts of fracture roughness and near-wellbore tortuosity on proppant transport within hydraulic fractures. Sustainability 14 (14), 8589.
Wang, D., You, Z., Wang, M., Li, Q., Wu, L., 2022b. Numerical investigation of proppant transport at hydraulic-natural fracture intersection. Powder Technol. 398, 117123.
Warpinski, N., Teufel, L., 1987. Influence of geologic discontinuities on hydraulic fracture propagation (includes associated papers 17011 and 17074). J. Petrol. Technol. 39 (2), 209–220.
Wen, C.Y., Yu, Y.H., 1966. A generalized method for predicting the minimum fluidization velocity. AlChE J 12 (3), 610–612.
Wen, Q., Wang, S., Duan, X., Li, Y., Wang, F., Jin, X., 2016. Experimental investigation of proppant settling in complex hydraulic-natural fracture system in shale reservoirs. J. Nat. Gas Sci. Eng. 33, 70–80.
Wen, H., Yang, R., Huang, Z., Zheng, Y., Wu, X., Hu, X., 2020. Numerical simulation of proppant transport in liquid nitrogen fracturing. J. Nat. Gas Sci. Eng. 84, 103657.
Wen, Z., Zhang, L., Tang, H., Zeng, J., He, X., Yang, Z., Zhao, Y., 2022. A review on numerical simulation of proppant transport: Eulerian–Lagrangian views. J. Pet. Sci. Eng. 217, 110902.
Wu, C.-H., Sharma, M.M., 2019. Modeling proppant transport through perforations in a horizontal wellbore. SPE J. 24 (4), 1777–1789.
Wu, K., Olson, J., Balhoff, M.T., Yu, W., 2016. Numerical analysis for promoting uniform development of simultaneous multiple-fracture propagation in horizontal wells. SPE Prod. Oper. 32 (1), 41–50.
Wu, Z., Cui, C., Jia, P., Wang, Z., Sui, Y., 2022. Advances and challenges in hydraulic fracturing of tight reservoirs: a critical review. Energy Geosci 3 (4), 427–435.
Xiao, H., Li, Z., He, S., Lu, X., Liu, P., Li, J., 2021. Experimental study on proppant diversion transportation and multi-size proppant distribution in complex fracture networks. J. Pet. Sci. Eng. 196, 107800.
Xiong, F., Wei, W., Xu, C., Jiang, Q., 2020. Experimental and numerical investigation on nonlinear flow behaviour through three dimensional fracture intersections and fracture networks. Comput. Geotech. 121, 103446.
Xu, C., Xie, Z., Kang, Y., Yu, G., You, Z., You, L., Zhang, J., Yan, X., 2020. A novel material evaluation method for lost circulation control and formation damage prevention in deep fractured tight reservoir. Energy 210. Article 118574.
Yamashiro, B., Tomac, I., 2020a. Particle clustering mechanisms and influence on proppant flow and transport. In: 54th US Rock Mechanics/Geomechanics Symposium.
Yamashiro, B.D., Tomac, I., 2020b. Proppant slurry flow and transport within fractures with rough surfaces. In: 54th U.S. Rock Mechanics/Geomechanics Symposium.
Yamashiro, B.D., Tomac, I., 2021. Particle clustering dynamics in dense-phase particle-fluid slurries. Comput. Geotech. 132, 104038.
Yamashiro, B.D., Tomac, I., 2022. A numerical study of neutrally buoyant slickwater proppant flow and transport in rough fractures. Geomech. Energy Environ. 29, 100266.
Yan, Y., Koplik, J., 2009. Transport and sedimentation of suspended particles in inertial pressure-driven flow. Phys. Fluids 21 (1), 013301.
Yan, X., Kang, Y., Xu, C., Shang, X., You, Z., Zhang, J., 2020. Fracture plugging zone for lost circulation control in fractured reservoirs: multiscale structure and structure characterization methods. Powder Technol. 370, 159–175.
Yang, T., Shy, S., 2003. The settling velocity of heavy particles in an aqueous near-isotropic turbulence. Phys. Fluids 15 (4), 868–880.
Yang, T., Shy, S., 2005. Two-way interaction between solid particles and homogeneous air turbulence: particle settling rate and turbulence modification measurements. J. Fluid Mech. 526, 171–216.
Yang, R., Guo, J., Zhang, T., Zhang, X., Ma, J., Li, Y., 2019. Numerical Study on Proppant Transport and Placement in Complex Fractures System of Shale Formation Using Eulerian Multiphase Model Approach. International Petroleum Technology Conference.
Yao, S., Chang, C., Hai, K., Huang, H., Li, H., 2022. A review of experimental studies on the proppant settling in hydraulic fractures. J. Pet. Sci. Eng. 208, 109211.
Zade, S., Costa, P., Fornari, W., Lundell, F., Brandt, L., 2018. Experimental investigation of turbulent suspensions of spherical particles in a square duct. J. Fluid Mech. 857, 748–783.
Zeng, J., Li, H., Zhang, D., 2016. Numerical simulation of proppant transport in hydraulic fracture with the upscaling cfd-dem method. J. Nat. Gas Sci. Eng. 33, 264–277.
Zeng, J., Li, H., Zhang, D., 2019. Numerical simulation of proppant transport in propagating fractures with the multi-phase particle-in-cell method. Fuel 245, 316–335.
Zhang, G.-D., Li, M.-Z., Xue, J.-Q., Wang, L., Tian, J.-L., 2016. Wall-retardation effects on particles settling through non-Newtonian fluids in parallel plates. Chem. Pap. 70 (10), 1389–1398.
Zhang, G., Gutierrez, M., Li, M., 2017a. A coupled cfd-dem approach to model particle-fluid mixture transport between two parallel plates to improve understanding of proppant micromechanics in hydraulic fractures. Powder Technol. 308, 235–248.
Zhang, G., Gutierrez, M., Li, M., 2017b. Numerical simulation of transport and placement of multi-sized proppants in a hydraulic fracture in vertical wells. Granul. Matter 19.
Zhang, G., Li, M., Gutierrez, M., 2017c. Numerical simulation of proppant distribution in hydraulic fractures in horizontal wells. J. Nat. Gas Sci. Eng. 48, 157–168.
Zhang, G., Gutierrez, M., Chao, K., 2019. Hydrodynamic and mechanical behavior of multi-particle confined between two parallel plates. Adv. Powder Technol. 30 (2), 439–450.
Zhang, Y., Lu, X., Zhang, X., Li, P., 2020a. Proppant transportation in cross fractures: some findings and suggestions for field engineering. Energies 13 (18), 4912.
Zhang, Z., Mao, S., Shang, Z., Chun, T., Wu, K., 2020b. Numerical study of proppant transport in field-scale fractures for slickwater fracturing. In: 54th U.S. Rock Mechanics/Geomechanics Symposium.
Zhang, Z., Zhang, S., Ma, X., Guo, T., Zhang, W., Yushi, Z., 2020c. Experimental and numerical study on proppant transport in a complex fracture system. Energies 13, 6290.
Zhang, Z., Legendre, D., Zamansky, R., 2021. Fluid inertia effects on the motion of small spherical bubbles or solid spheres in turbulent flows. J. Fluid Mech. 921.
Zhang, B., Pathegama Gamage, R., Zhang, C., Wanniarachchi, A., 2022a. Hydrocarbon recovery: optimized cfd-dem modeling of proppant transport in rough rock fractures. Fuel 311, 122560.
Zhang, T., Li, C., Shi, Y., Mu, K., Wu, C., Guo, J., Lu, C., 2022b. Numerical simulation of proppant directly entering complex fractures in shale gas. J. Nat. Gas Sci. Eng.

107, 104792.
Zhang, T., Zeng, X., Guo, J., Zeng, F., Li, M., 2022c. Numerical simulation on oil-water-particle flows in complex fractures of fractured-vuggy carbonate reservoirs. J. Pet. Sci. Eng. 208, 109413.
Zhou, Z., Abass, H., Li, X., Teklu, T., 2016. Experimental investigation of the effect of imbibition on shale permeability during hydraulic fracturing. J. Nat. Gas Sci. Eng. 29, 413–430.
Zhou, H.-Y., Zhang, T., Guo, J.-C., Sun, K., Yang, R.-Y., 2022. Drag coefficient modification for proppant transport in fractures considering wall retardation. Chem. Eng. Res. Des. 178, 478–487.
Zhou, H., Guo, J., Zhang, T., Li, M., Tang, T., Gou, H., 2023. Eulerian multifluid simulations of proppant transport with different sizes. Phys. Fluids 35 (4).
Zhu, G., Zhao, Y., Zhang, T., Khalid, M.S.U., Liu, M., Zhang, S., Zhang, Z., 2023. Micro-scale reconstruction and cfd-dem simulation of proppant-laden flow in hydraulic fractures. Fuel 352, 129151.
Zigrang, D.J., Sylvester, N.D., 1981. An explicit equation for particle settling velocities in solid-liquid systems. AlChE J. 27, 1043–1044.
Zimmerman, R., 2003. Fluid flow in rock fractures. AGU Fall Meeting Abstracts.
Zimmerman, R.W., Yeo, I.-W., 2000. Fluid flow in rock fractures: from the Navier-Stokes equations to the cubic law. In: Dynamics of Fluids in Fractured Rock, pp. 213–224.
Zimmerman, R.W., Al-Yaarubi, A., Pain, C.C., Grattoni, C.A., 2004. Non-linear regimes of fluid flow in rock fractures. Int. J. Rock Mech. Min. Sci. 41 (3), 163–169.

E.A.A.V. Edirisinghe holds a BSc degree in Mining Engineering from the Department of Earth Resources Engineering, University of Moratuwa, Sri Lanka. He is currently a PhD candidate in the Department of Infrastructure Engineering at the University of Melbourne, Australia. His research primarily focuses on the dynamics of fluid and particle movement within subsurface fracture flows. Edirisinghe is conducting laboratory experiments utilizing advanced particle image velocimetry (PIV) techniques, complemented by numerical analysis, to investigate particle-laden two-phase flows under turbulent conditions. In addition to his current research, he has expertise in various aspects of mining engineering and has garnered significant industrial experience in this field.